The Jbel Saghro Au(–Ag, Cu) and Ag–Hg Metallogenetic Province: Product of a Long-Lived Ediacaran Tectono-Magmatic Evolution in the Moroccan Anti-Atlas

Johann Tuduri, Alain Chauvet, Luc Barbanson, Jean-Louis Bourdier, Mohamed Labriki, Aomar Ennaciri, Lakhlifi Badra, Michel Dubois, Christelle Ennaciri-Leloix, Stanislas Sizaret, et al.

minerals

MDPI

Review

The Jbel Saghro Au(–Ag, Cu) and Ag–Hg Metallogenetic Province: Product of a Long-Lived Ediacaran Tectono-Magmatic Evolution in the Moroccan Anti-Atlas

Johann Tuduri [1,2,*], Alain Chauvet [3], Luc Barbanson [2], Jean-Louis Bourdier [2], Mohamed Labriki [4], Aomar Ennaciri [4], Lakhlifi Badra [5], Michel Dubois [6], Christelle Ennaciri-Leloix [4], Stanislas Sizaret [2] and Lhou Maacha [4]

1 BRGM, F-45060 Orléans, France
2 ISTO, UMR7327, Université d'Orléans, CNRS, BRGM, F-45071 Orléans, France; luc.barbanson@univ-orleans.fr (L.B.); jean-louis.bourdier@univ-orleans.fr (J.-L.B.); stanislas.sizaret@univ-orleans.fr (S.S.)
3 Géosciences Montpellier, cc. 060, Université de Montpellier 2, CEDEX 5, 34095 Montpellier, France; alain.chauvet@univ-montp2.fr
4 MANAGEM, Twin Center, BP 5199, Casablanca 20100, Morocco; m.labriki@managemgroup.com (M.L.); a.ennaciri@managemgroup.com (A.E.); cleloix@yahoo.fr (C.E.-L.); l.maacha@managemgroup.com (L.M.)
5 Faculté des Sciences, Université Moulay Ismaïl, BP 11201 Zitoune, Meknes 50 000, Morocco; badra_lakhlifi@yahoo.fr
6 Laboratoire de Génie Civil et géo-Environnement–Lille Nord de France, EA 4515, Département des Sciences de la Terre, Université de Lille, Bât. SN5, 59655 Villeneuve d'Ascq, France; michel.dubois@univ-lille1.fr
* Correspondence: j.tuduri@brgm.fr; Tel.: +33-238-644-790

Received: 31 August 2018; Accepted: 10 December 2018; Published: 13 December 2018

Abstract: The Jbel Saghro is interpreted as part of a long-lived silicic large igneous province. The area comprises two lithostructural complexes. The Lower Complex consists of folded metagreywackes and N070–090°E dextral shear zones, which roughly results from a NW–SE to NNW–SSE shortening direction related to a D_1 transpressive tectonic stage. D_1 is also combined with syntectonic plutons emplaced between ca. 615 and 575 Ma. The Upper Complex is defined by ash-flow caldera emplacements, thick and widespread ignimbrites, lavas and volcaniclastic sedimentary rocks with related intrusives that were emplaced in three main magmatic flare ups at ca. 575, 565 and 555 Ma. It lies unconformably on the Lower Complex units and was affected by a D_2 trantensive tectonic stage. Between 550 and 540 Ma, the magmatic activity became slightly alkaline and of lower extent. Ore deposits show specific features, but remain controlled by the same structural setting: a NNW–SSE shortening direction related to both D_1 and D_2 stages. Porphyry Au(–Cu–Mo) and intrusion-related gold deposits were emplaced in an earlier stage between 580 and 565 Ma. Intermediate sulfidation epithermal deposits may have been emplaced during lull periods after the second and (or) the third flare-ups (560–550 Ma). Low sulfidation epithermal deposits were emplaced late during the felsic alkaline magmatic stage (550–520 Ma). The D_2 stage, therefore, provided extensional structures that enabled fluid circulations and magmatic-hydrothermal ore forming processes.

Keywords: structural control; silicic large igneous province; ignimbrite flare-ups; ash-flow caldera; epithermal; porphyry; IRGD; Anti-Atlas

1. Introduction

In northwest Africa, the Anti-Atlas, Ougarta and Hoggar domains consist of pericratonic terranes located at the margin of the West African Craton (WAC, Figure 1a) and that were mostly amalgamated from Palaeoproterozoic to Phanerozoic times [1–5]. These terranes were the site of recurring tectonic activity and periods of intense magmatic activity. The most important magmatic pulses occurred during the Mesoproterozoic [6–8] and at the end of Triassic when the Central Atlantic Magmatic Province (CAMP) was emplaced [9–11]. According to Ernst [12] and Ernst and Bleeker [13], both events have been related to large igneous provinces (LIPs). Indeed LIPs consist of large volumes of mainly mafic magma (>0.1 Mkm^3) in provinces whose areal extent might exceed 0.1 Mkm^2. LIPs are thought to emplace in a short duration pulse or multiple pulses (less than 1–10 Myr each) with a whole maximum duration of ca. 50 Myr. Intense felsic magmatism may also occur as silicic large igneous provinces (SLIPs) [12,14]. Dacite–rhyolite pyroclastic rocks (ignimbrites), along with transitional calc-alkaline I-type [15] to A-type granites, mainly characterise these SLIPs [16]. Further, LIPs are commonly related to a wide variety of metal deposits [17] including world-class deposits such as magmatic sulfide ore deposits associated with mafic and ultramafic magmatism (Ni, Cu, PGE, Cr, Ti, Fe [18,19]), with carbonatite and peralkaline complexes (Nb, Ti, REE, Zr [20,21]), or with diamondiferous kimberlites [22]. Iron oxide copper gold (IOCG) deposit types [23] and epithermal deposits of mostly low and intermediate sulfidation gold-based metal types [24–26] may be also related to more silicic LIPs. Another magmatic event described in peri-Gondwanan terranes of, e.g., Avalonian and Cadomian types, is mostly characterised by huge volumes of pyroclastic flows and was emplaced at the end of the Neoproterozoic era [27–30]. Conditions and geodynamical environment at the origin of such a silicic province remain insufficiently understood, although Moume et al. [31] recently proposed that this event might be related to the Central Iapetus Magmatic Province event (CIMP) of Ediacaran-Cambrian age [13,32]. In the Moroccan Anti Atlas, world-class deposits occur in an area mostly dominated by rhyolitic ignimbrites such as the giant Ag–Hg Imiter deposit, the Ag-Hg Zgounder deposit and the Co–Ni–Fe–As(–Au–Ag) Bou Azzer district (Figure 1b).

In fact, the Moroccan Anti-Atlas hosts several precious and base-metal deposits affected by at least four major tectonic phases: i.e., the Palaeoproterozoic, the Neoproterozoic, the Variscan and the Alpine cycles [29,33–35]. Until recently, most of the ore deposits from the Anti-Atlas were considered as Neoproterozoic in age due to their occurrence within Proterozoic inliers. One exception was the vein and stratabound copper deposits hosted within the early Palaeozoic cover, which were assumed to be syn-sedimentary or epigenetic and Variscan in age [36,37]. However, recent studies have reassessed the age and origin of numerous metal deposits, assigning younger ages than previously admitted. The arguments are essentially two-fold: (i) absolute dating and (ii) fluid chemistry by isotopic and fluid inclusion study methods. Indeed geochronological methods (e.g., Re/Os, Ar/Ar) frequently give younger ages than expected though possible resetting of dating materials and (or) ore remobilisation are rarely discussed. For instance, the Imiter deposit would coincide with the Permo-Triassic boundary [38]. Similarly, a late Carboniferous age has been proposed for ore enrichment at BouAzzer with a possible earlier pre-mineralising stage [39]. The strong association of mineral deposits with fluids of moderate to high salinities, suggests interpretations favouring the influence of basinal brines in the ore-forming processes [40,41]. Indeed, processes involving basin-related and(or) surface-related brines resulting from evaporation of seawater in Triassic basins in the formation of ore deposits, up to now interpreted as, deposits related to the late Neoproterozoic felsic magmatic event [42–48] have been defended by several recent works [40,41,49] although the debate is still open [50]. This controversy mainly concerns the Bou Azzer (Co–Ni–), Imiter (Ag–Hg) and Zgounder (Ag–Hg) mines that represent the main three world-class ore deposits of the Moroccan Anti-Atlas after the Akka gold mine was closed few years ago. The Imiter concentration has been proposed to be associated with the 550 $\pm$ 3 Ma rhyolitic magmatism [51], a hypothesis recently controverted by Ar-Ar geochronology [38] and palaeo-fluid geochemistry investigations [41]. The Zgounder deposit is supposed to be emplaced around 564 $\pm$ 5 Ma at the same time as rhyolitic intrusions [46,52] although fluid geochemistry would suggest a Triassic

fluid contribution [41,49] sedimentary. The Bou Azzer Co–Ni–Fe–As(–Au–Ag) district hosts the only mine in the world where Co is produced as a primary commodity directly from Co- and As-bearing arsenide minerals [53]. It is interpreted as having experienced many ore remobilisations from Late Neoproterozoic, Variscan to Triassic magmatic-hydrothermal stages [39,40,44,54,55].

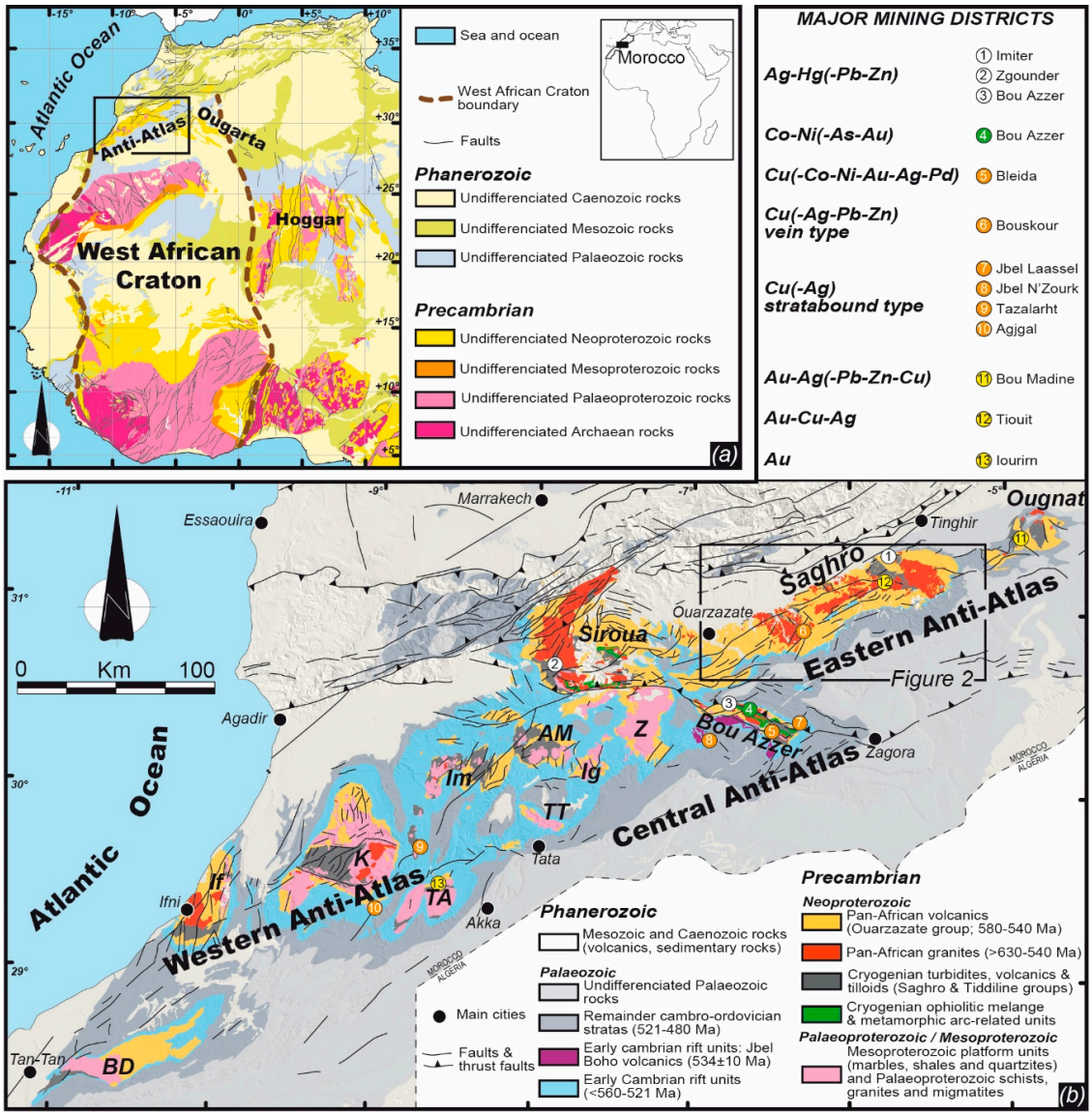

Figure 1. (**a**) Location of the Anti-Atlas belt at the northern limit of the West African Craton, after Thiéblemont et al. [56]. (**b**) Main geological units and major mining districts of the Moroccan Anti-Atlas [5,7,29,48,57–59]. Inliers–BD: Bas Drâa; If: Ifni; K: Kerdous; TA: Tagragra d'Akka; Im: Igherm; TT: Tagragra de Tata; Ig: Iguerda; AM: Agadir-Melloul; Z: Zenaga.

The debate as to whether the Anti-Atlas ore deposits are mostly Neoproterozoic in age and magmatic-related, or Phanerozoic and disconnected from any magmatic input, is similar to the one that exists between the orogenic and intrusion-related gold deposit models [60–65]. For instance, as applied to the Variscan gold ore deposits in the French Massif Central and beyond, this debate is focused on the involvement of magmatic fluids in the formation of mineralised systems. Arguments supporting the orogenic model are mostly based on fluid inclusion studies and isotopic data on quartz-bearing veins and highlight the meteoric and/or metamorphic signatures of the fluids [66,67]. In such cases, heat production from possible synchronous granitoids is supposed to generate only thermal convection cells. Arguments in favour of an intrusion-related model highlight the systematic spatial association

between granite and hydrothermal systems, while fluid compositions and metal source are interpreted as showing a magmatic signature [68–70].

Therefore, it may be relevant to clarify whether most of the ore deposits of the Moroccan Anti-Atlas are linked to a Neoproterozoic magmatic input (the magmatic-related alternative), or to a more recent stage related to the penetration and circulation of sedimentary brines and (or) metamorphic fluids into the basement (the orogenic alternative). Indeed, as the Anti-Atlas domain may be considered as an important Neoproterozoic magmatic province with respect to the abundance of plutonic and volcanic rocks, evidences for a major Neoproterozoic metallogenetic province need to be deciphered. In this work, we present a review of the global geology and metallogeny of the Jbel Saghro in the Eastern Anti-Atlas with a specific emphasis on the formation, styles and tectonic controls of different ore deposit occurrences in order to assess and discuss a tectono-magmatic evolution of the studied area and a metallogenetic and geodynamic model. The world-class Bou Azzer deposit is not concerned in this study because of its location far from the Jbel Saghro. Its characterisation will be the subject of work currently in progress.

2. Geological Overview of the Anti-Atlas Mountains

The Moroccan Anti-Atlas belt, located in the northern part of the WAC (Figure 1a), constitutes an important segment of the Pan-African orogeny, also known as the Cadomian orogeny, that occurred from the Middle Neoproterozoic to Early Cambrian. This area is currently elevated at altitudes exceeding 1000 m in large areas due to a Caenozoic uplift [35,71,72] although they basically represent a Variscan intra-cratonic, thick-skinned basement inversion belt [34]. Consequently, the Anti-Atlas mountains present significant exposures of WSW–ENE trending inliers, (aka *boutonnières*), which consist of Proterozoic rocks in core of Phanerozoic, mainly Palaeozoic, sedimentary sequences (Figure 1b).

During Precambrian times, the Anti-Atlas domain has recorded two major orogenic cycles: the Eburnean, a Palaeoproterozoic cycle from about 2.1 to 2.0 Ga and the Pan-African/Cadomian cycle from about 885 to 540 Ma [5,33,73–75]. The Pan-African orogeny is characterised by three main tectono-magmatic events [29,73,75–77]. (i) The first event corresponds to an oceanic basin closure, oceanic subduction and arc-craton accretion, coeval with calc-alkaline magmatism and ophiolite obduction. This event is supposed to have occurred between 770 and 630 Ma and related formations are mainly observable in the Central Anti-Atlas [29,59,78–80]. (ii) Then, the development of an active margin along the amalgamated West African Craton was responsible for an intense high-K calc-alkaline magmatism and transpressive tectonics between ca. 615 and ca. 560 Ma [29,48,59,74,75,77,81,82]. (iii) Finally, late to post-orogenic granites with cogenetic volcanic and volcaniclastic cover are emplaced between ca. 560 and 550 Ma together with subsequent transtensional tectonics [5,29,47,74]. The transition from transpressive to transtensive tectonics remains the subject of debate but it likely occurred between 580 and 560 Ma [29,48,74]. There is still also an ongoing debate on the origin of the two late magmatic events, which are either described as arc-related [29] or as post-orogenic related to an asthenospheric rise beneath the West African Craton, without any active subduction [74,83]. Then, the Ediacaran–Cambrian transition is recognised as a carbonate-dominated succession (the Adoudou formation) that unconformably overlies the late Ediacaran plutonic and volcaniclastic rocks [84–86]. This sedimentation period shows dramatic and rapid thickness changes, consistent with an active extensional faulting related to incipient continental rifting [86,87]. Intercalated alkaline volcanic ash and flows dated between 550 and 520 Ma confirm that deposition of the Adoudou formation took place during the Early Cambrian and is in tectono-magmatic continuity with the Ediacaran volcano-tectonism [74,88–90].

In the Eastern Anti-Atlas of interest here, Jbel Saghro, Palaeoproterozoic terranes are not exposed (Figures 1b and 2), so, the oldest rocks outcropping consist of Middle Neoproterozoic (Cryogenian) metasedimentary rocks [91,92]. These are slightly deformed and unconformably overlain by a thick and widespread upper Neoproterozoic (Ediacaran) volcanic and volcaniclastic sequence (Figure 2). Both Cryogenian and Ediacaran units are intruded by Pan-African plutons (Figure 2).

Prior to the Variscan compression, the Palaeozoic sedimentary cover reaches an overall thickness of 8–10 km in the western Anti-Atlas and only 4 km in the eastern part of the Anti-Atlas, being mainly characterised by shallow marine sedimentary rocks [34,86,93–95]. Subsidence is assumed to be regular and characterised by two main steps [34,96]. The first step occurs during the Cambrian, from the Terreneuvian to the Miaolingian. It corresponds to a rifting episode [84,86,97,98]. The Adoudou formation and related alkaline volcanic rocks mentioned above belong to this step. The second step occurs during the Upper Devonian and is characterised by a multi-directional extension mainly controlled by NNW–SSE and ENE–WNW faults inherited from the Pan-African basement [93]. Fission track dating on zircon [99] yields a peak temperature affecting the basement around 328 ± 30 Ma (Carboniferous, Upper Mississipian). It is interpreted as the age of maximum burial. The subsequent uplift is attributed to the Variscan compression [34,100] during the Upper Carboniferous (early Pennsylvanian). It results in the inversion tectonics of these palaeofaults as thrusts and strike-slip–reverse faults. The main shortening directions are assumed to be NW–SE to N–S in the Western Anti-Atlas [34,100], and NE–SW in the Eastern Anti-Atlas [93]. The Precambrian basement is actually uplifted and folded into huge antiformal culminations probably at the origin of the present days inliers which characterise the Anti-Atlas fold belt. Thus, many authors e.g., [34,86,93,100] suggest that brittle deformations related to the Variscan compression occur in the whole Anti-Atlas and reactive structures from the Precambrian basement. Ductile deformation related to the Variscan tectonics has not yet been described in the Anti-Atlas. It might be suggested in the Western Anti-Atlas because the overall Palaeozoic rock thickness reaches 10 km making it possible a ductile–brittle transition. However, with a maximum thickness of only 4 km such ductile deformations seem precluded in the Eastern Anti-Atlas. Consequently, how and to what extent the Palaeozoic tectono-hydrothermal events may have an influence on the main ore deposits of the Eastern Anti-Atlas remains an important topic. For this reason, we focus our work below on the re-examination of the model of formation and structural control of different ore-bearing deposits of the Jbel Saghro. We highlight the relevance of a pluri-disciplinary approach involving analyses of regional tectonics, vein geometry, internal texture and mineralogy of ore deposits in order to decipher the mode of formation for each deposits. The ore-forming processes are specifically adressed with the view of their possible relationships with the Precambrian magmatism, in order to better assess whether they could have been mainly formed during the Neoproterozoic times, or mostly formed and remobilised during the Phanerozoic. We also stress that conventional approaches of ore deposits involving kinematic criteria on slip surfaces of faults and palaeostress reconstructions in the brittle regime are here excluded, since the whole Anti-Atlas is still an active seismic area [94]. So, the Precambrian or Palaeozoic features should be erased by recent tectonic reactivations.

The Jbel Saghro hosts numerous precious and base metal deposits (Figure 2). The most famous are: the giant Ag Imiter mine (8.5 Mt @ 700 g/t Ag; [41,45,51,101,102]) and the Cu Bouskour mine (21 Mt @ 1.3% Cu; [103]) and also the now closed Cu–Ag Tizi Mouddou (1.5 Mt @ 2% Cu, 250 g/t Ag; [43]) and Cu–Au–Ag Tiwit (1.06 Mt @ 8 g/t Au, 65 g/t Ag, ~0.4% Cu; [43]) mines. Mining activity in the Jbel Saghro area dates back a very long time as suggested for the Imiter and Bouskour mining sites [101,103]. Although no precise dating is available, some historical texts suggest that workings occurred since the beginning of medieval times. These sites were subsequently abandoned and forgotten and were rediscovered under the French Protectorate between 1912 to 1956, leading to subsequent intensive exploration and mining. Since the mid 1990s and after reinterpreting the regional geology of the Anti-Atlas area, the BRPM (Bureau de Recherches et de Participation Minière, currently ONHYM: Office National des HYdrocarbures et des Mines) and Reminex (a subsidiary of the Managem Group) conducted several exploration campaigns. Indeed, before the 1990s, the Anti-Atlas was mainly interpreted as a collisional belt and the formation of ore deposits was related to orogenic processes, e.g., [43,73,76]. Then, the geology and the ore forming processes were related to the complex evolution of active margin(s) in a subduction and accretion setting, e.g., [29,45,47,48,51,77,82]. This led to the discovery of new Au–Ag occurrences such as those of the Issarfane (0.5 Mt @ 1.8 g/t Au), Qal'at Mgouna and Thaghassa (Figure 2).

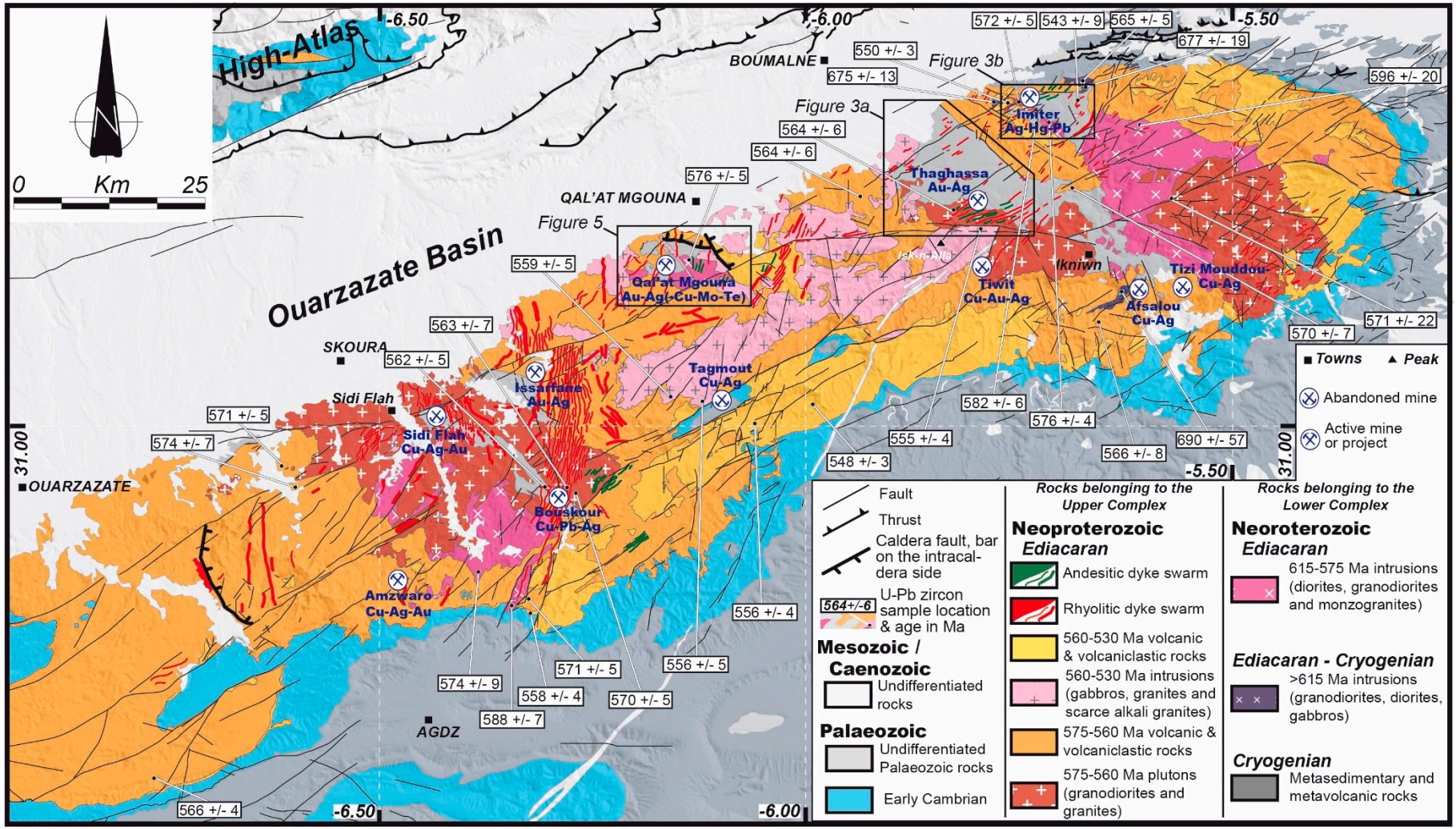

Figure 2. Simplified geologic map of the Jbel Saghro, after Hindermeyer et al. [104], Tuduri [47] and Tuduri et al. [48]. U-Pb radiometric ages obtained on zircon [29,48,51,78,105–108].

3. Tectono-Magmatic Evolution of the Jbel Saghro

Until the early 2000s, the Precambrian terranes in Morocco were traditionally subdivided into 3 main epochs: the PI for the Palaeoproterozoic era or Archaean aeon; PII for the Tonian and Cryogenian; and PIII for the Ediacaran periods [73,109–112]. These periods have been further subdivided into various units (e.g., P.II[1], P.II-III, P.IIsup, P.III3m-1a . . .) in order to take into account the extraordinary complexity of the different areas [77,109,113]. Geologists then used a lithostratigraphic approach in which rocks were correlated based on their lithological characteristics and grouped in Supergroups, Groups, Subgroups, Formations and Members for layered sedimentary and volcanic sequences, and in Suites for plutonic and metamorphic rocks [5,29,59,107]. However, these lithostratigraphic schemes confuse the geological and tectonic messages and the resulting legends on geological maps. Indeed, showing the cogenetic relationships in a volcano-plutonic setting where plutonic, hypabyssal and volcanic rocks coexist as in the Anti-Atlas, remains a challenge, especially when tectonic controls are combined. For the seek of consistency, we propose below a tectono-lithostratigraphic framework that groups the sedimentary, plutonic and volcanic rocks of the Saghro area in Lower and Upper Complexes with regard to the tectono-magmatic evolution of the eastern Anti-Atlas. Such a complex corresponds to the definition of the ICS (International Commission on Stratigraphy), that is, a lithostratigraphic unit composed of diverse types of any classes of rocks (sedimentary, igneous and metamorphic) and characterised by irregularly mixed lithology or by complicated structural relationships. The definition of the two complexes and rationale behind are given below.

3.1. The Lower Complex and the D_1 Transpressive Tectonics

The Lower Complex is composed of a thick succession of slightly deformed volcano-sedimentary rocks intruded by broadly coeval high-K calc-alkaline plutons (Figure 2). Volcano-sedimentary rocks are deformed and tightly upright folded (Figure 3a,b). They are also affected by a metamorphism below the amphibolite facies with hornfels around plutons [48,91,111]. Elsewhere, cleavage is well expressed in the vicinity of the large-scale, regional, strike-slip faults that mainly trend N070°E (Figure 2). The general structure is characterised by steeply dipping bedding (Figure 3a–c), large-scale folds (Figure 3a,b) and intense fracturing (see below).

3.1.1. The Earlier Arc-Related Metagreywackes and Metavolcanic Rocks

These oldest formations belong to the Anti-Atlas supergroup, Saghro Group or MGouna Group of Thomas et al. [5] or Habab Group of O'Connor et al. [107] and consist of metaturbidites with intercalated thin mafic metavolcanic layers, exposed, from west to east, near the cities of Sidi Flah, Qal'at Mgouna, Boumalne and Imiter (Figure 2). The metasedimentary sequences, hereafter, called metagreywackes, are dominated by sandstones and silty mudstone [91,92,114–118]. Although slightly deformed (Figures 3 and 4), they consist of 2000 to 6000 m of flysh-like turbiditic rocks [83,91,118] that locally alternate with basaltic flows, volcanic breccias, hyaloclastite and pillow structures (Figure 3a,b). Based on geochemical analyses, the interbedded mafic lava rocks may have a transitional character between tholeiites and alkali basalts and may be related to a back-arc environment formed in an extensional setting or correspond to the remnants of a passive-margin [91,115,118,119]. These rocks have a mean Nd depleted mantle model age (T_{DM}) of 650 ± 30 Ma, the ε_{Nd} range from +7.63 to +8.08, and the initial $^{87}Sr/^{86}Sr$ from 0.704 to 0.706 that have been interpreted as indicating a mantle origin without any old crust contribution [83,119]. These sedimentary sequences are considered to be Cryogenian [91,115,116]. However, Liégeois et al. [120] in Gasquet et al. [83], using U/Pb geochronology on detrital zircons from similar metagreywacke sequences in the Qal'at Mgouna area, have shown that zircon grains become younger towards the top of the metasedimentary sequences. They suggest that basins infilling were active until more recently than previously suspected, i.e., until 630–610 Ma. This corresponds to the onset of the Ediacaran Period and Pan-African magmatism that culminated during the next stages (see below).

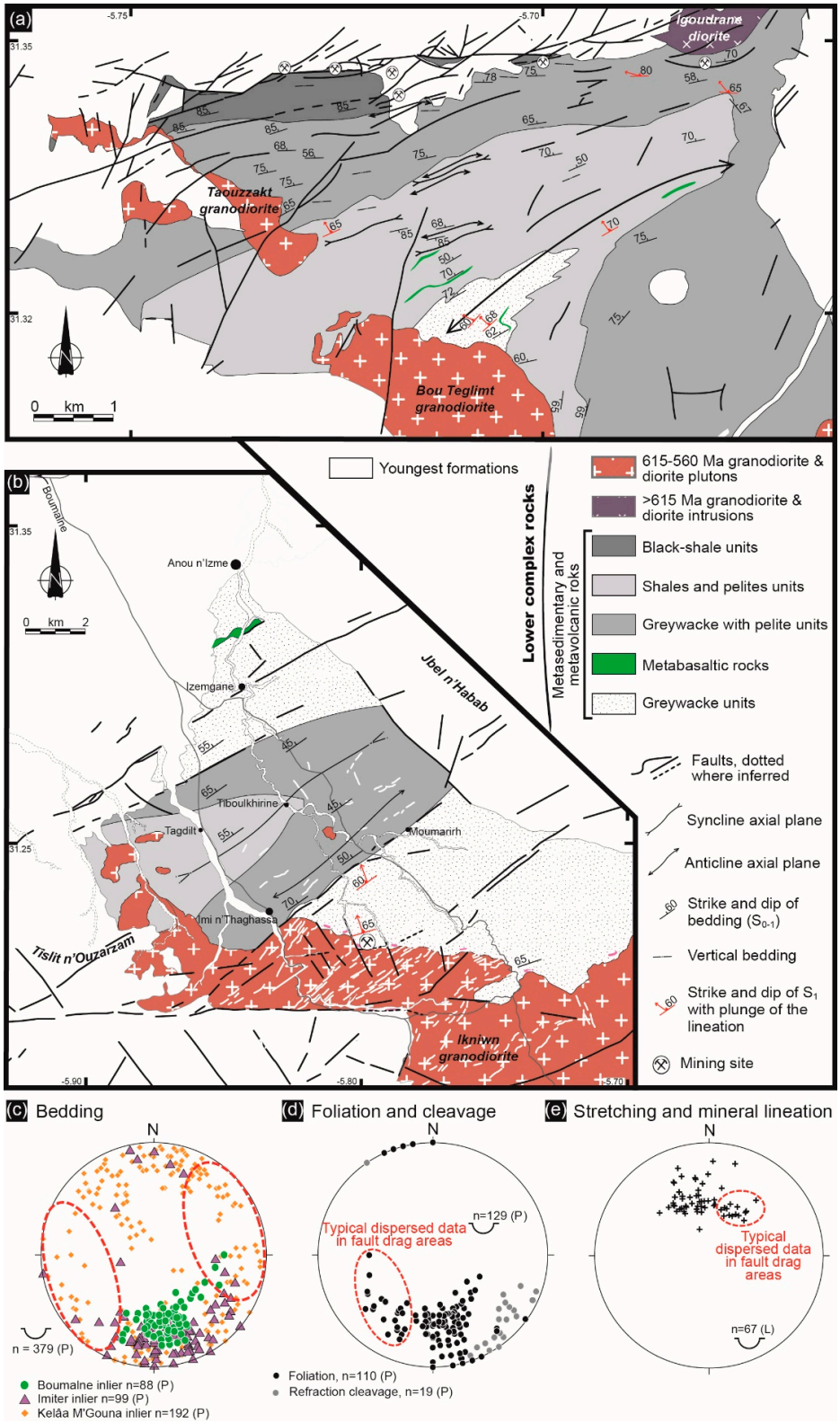

Figure 3. Structural maps of the (**a**) Imiter inlier modified from SMI (Société Métallurgique d'Imiter) data and Ighid et al. [121] and (**b**) Boumalne inlier (from Tuduri et al. [48]). Note that metabasaltic rocks with pilloid structures have never been observed in the Imiter inlier. Sills have been described and discussed as possibly syn-sedimentary in origin [100]. Stereoplots of structural orientation data: (**c**) bedding, (**d**) foliation and refraction cleavage, and (**e**) lineation. Bedding data are from the Qal'at

MGouna, Boumalne and Imiter Lower Complex inliers whereas foliation, refraction cleavage and lineation data are mainly from the Boumalne and Imiter Lower Complex inliers [47,48]. The dotted red lines in the bedding stereoplot highlight zones where data are locally reoriented because of drag fault zones and disturbance upon pluton emplacement.

3.1.2. The Intrusive Rocks

Diorites, granodiorites with minor gabbros and monzogranites [29,47,48,105,122–124], intrude these metaturbiditic and metavolcanic sequences (Figures 2 and 3a,b). The most representative are granodiorite and diorite intrusions that belong to the Ouarzazate Supergroup "precursor rocks" and Bardouz suite of Thomas et al. [5]. They are composed of plagioclase ($An_{20–56}$), biotite, amphibole (Mg-hornblende to Fe-tschermakite and pargasite to Fe-edenite), rare pyroxene and accessory minerals such as titanite, zircon, apatite and magnetite [47,119,123]. K-feldspar and quartz abundances vary depending on pluton compositions. At the contact with the country rocks, cordierite, andalusite and biotite related to contact metamorphism are observed [47,48,121,125].

Rock geochemistry shows that most plutons have moderate to high-K calc-alkaline affinities with trends that are consistent with formation in an active continental margin [29,119]. Available ages range from 677 ± 19 and 576 ± 4 Ma for this event, although most of the data are bracketed between 615 and 575 Ma in the Jbel Saghro [29,51,59,78,81,105–108]. With regard to the oldest intrusions, their age and emplacement conditions remain unclear and debated in the Jbel Saghro [48] and are only evidenced by poorly defined U-Pb zircon geochronology (i.e., >615 Ma) on calc-alkaline tonalite, diorite and granodiorite intrusions [107,108,126]. However, in the Central Anti-Atlas, similar plutons are widespread and were emplaced continuously between 660 and 615 Ma in a supra-subduction setting [29,78]. One can therefore question on a possible diachronism of magmatic activity between the Central Anti-Atlas and the Eastern Anti-Atlas during this period especially if we consider that some rare ages reported in the Eastern Anti-Atlas are inherited (677 ± 19, 675 ± 13, 645 ± 12 Ma, [108,126]). However, the following magmatic period spanning from 615 to 575 Ma is well expressed in both the Central and Eastern Anti-Atlas. This is mostly plutonic in the Eastern Anti-Atlas and both volcanic and plutonic in the Central Anti-Atlas.

3.1.3. The Main Pan-African D_1 Deformation Event

At map-scale (Figure 3a,b), the overall style of the deformation suggests that steep bedding and folds are the most conspicuous features of the metaturbiditic terranes [47,48,77,125–129]. Two types of folds are observed. (i) At the regional scale, first-order folds are easily discernible such as in the Imiter and Boumalne areas (Figure 3a,b). They are tight (Figure 3c) and the majority of the ENE–WSW axial surfaces are moderately to steeply inclined (50–60°), with a predominance of dips to the NNW suggesting that folds roughly verges toward the SE [125,127,128]. Their hinge lines gently plunge toward the ENE. (ii) At local scale, higher-order folds are metric and open to tight (Figure 4a). They are asymmetric and probably unrelated to lower-order folds as they always show a right-verging (dextral wrenching, [47]). Indeed, they are observed in shear zones where cleavage is well developed. These folds are interpreted as drag folds below. Their axial surfaces are upright (NE–SW to ENE–WSW) with a hinge line that steeply plunges toward the ENE or WSW [47]. In Figure 3c, most of the poles to bedding falling in the NNW and SSE quadrants are related to the regional scale, first-order folds. Gentle poles falling in the SW and NE quadrants are related to drag folds. However, these plots and more generally the ones comprised within the dotted red lines (Figure 3c) highlight areas where data are locally reoriented because of drag fault zones and plutonic interferences. Such interferences are abundant in the Qal'at MGouna area where folds may be also interpreted as open and upright (Figure 3c, [47]).

In detail, metaturbiditic rocks show finite strain markers including foliation and stretching and mineral lineation [47,48,77,81,128–130]. Foliation that usually consists in a slaty cleavage is evident throughout the entire inlier. It is noteworthy that both metamorphic planar fabrics and lineations have

been only observed in the eastern part of the Jbel Saghro, in the Boumalne and Imiter areas. Indeed, these fabrics (Figures 3 and 4b) remain difficult to observe except in the hornfels zone surrounding the diorite and granodiorite intrusions described above (Figure 4b). Foliations show a constant ENE strike and dip toward the NW (N075°E 60°N, Figure 3d), except when reoriented in fault drag areas (i.e., NW–SE strikes) or when refracted (NE–SW strikes). Such foliation is axial planar and, thus, is generally parallel to the bedding of the metaturbiditic rocks when localised along the limbs of the first-order tight folds. It is called herein $S_{0–1}$. A S_2 cleavage refraction (Figure 4c) may also occur in specific areas, that define an obliquity with respect to the $S_{0–1}$. It is caused by localised shear developed in incompetent layers usually associated with the drag fold structures. Stretching and mineral lineations (L_1) are always carried by the $S_{0–1}$ foliation. They are discrete and their orientation (Figure 3e) also appear fairly constant with a rather low dispersion from NW–SE to N–S trending directions (average: N170°E 55°N). According to mineralogic and micro-structural evidences, at least 2 distinct metamorphic assemblages are observed but appear to be related to the same tectonic event defined as a hornfels assemblage and a regional chlorite to amphibole assemblage. (i) The hornfels zone is observed in the contact metamorphic aureoles caused by the diorite and granodiorite intrusions within the Cryogenian greywackes [48,121,130]. It consists of a spotted phyllite zone in which foliation (phyllitic cleavage to gneissic foliation) and lineation are easily discernable. Rocks are mostly characterised by K-feldspar, muscovite, biotite and small spots of retrogressed andalusite and/or cordierite (Figure 4b). The latter frequently highlights the lineation and, therefore, suggests a probable relationship between pluton emplacement and the D_1 tectonics. Garnet-amphibole assemblage and spessartine occurrences are associated with skarns and skarnoids as reported by Benziane [130] and Tuduri [47]. (ii) When observable far from intrusions, foliation (slaty to phyllitic cleavage) is defined by a planar-linear fabric mainly formed by phyllosilicates such as chlorite, sericite to biotite [48]. In both assemblages, rolling structures and S-C fabrics (Figure 4d) define unambiguous south- to southeast-verging noncoaxial shear criteria, parallel to the average lineation trending direction. These structures indicate reverse sense top-to-the-south deformation in the Boumalne and Imiter areas [47,48,77,82,121,123].

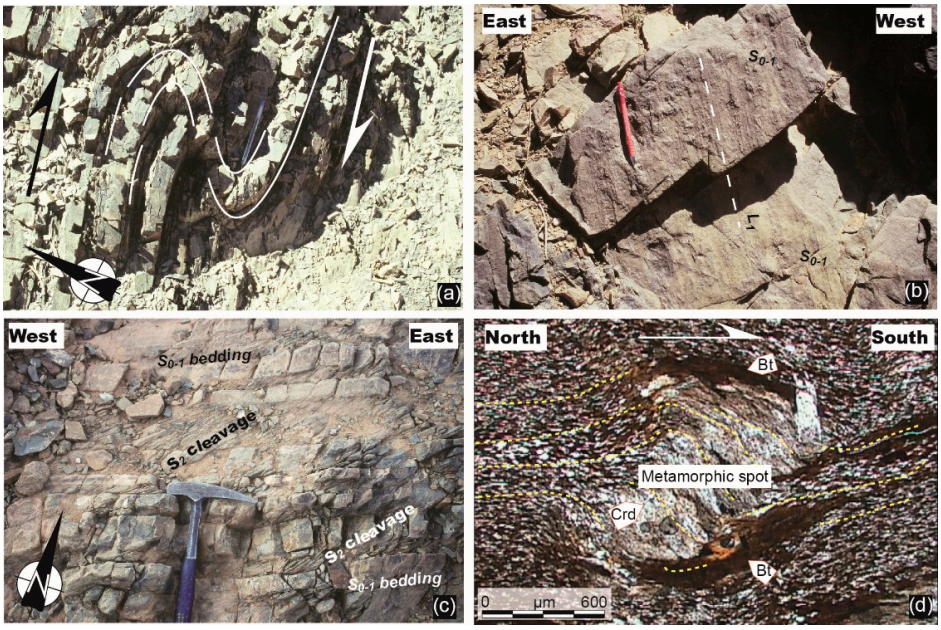

Figure 4. (**a**) Drag fold from the Qal'at Mgouna metagreywacke inlier. (**b**) Regional $S_{0–1}$ metamorphic foliation and related lineation marked by elongate contact metamorphic minerals that affect the metagreywacke sequence. (**c**) S_2 cleavage refraction, from the Imiter metagreywacke inlier, consistent with a dextral shearing. (**d**) Microphotograph showing syn- to late kinematic metamorphic mineral, a probable cordierite (Crd) showing rolling structure consistent with a top-to-the-south shearing sense. Note the asymmetric tails composed of biotite (Bt), plane polar light.

The D_1 deformation is also well-expressed along the large-scale N070–090°E trending strike slip faults, about 100 to 150 km long that occur in the northern and central part of the Jbel Saghro (Figures 2 and 3a,b). On both sides of these shear zones, deformation appears more intense especially in the slaty to phyllitic cleavage domains where the S_2 refraction cleavage oriented N040–050°E 80°N is formed (Figure 4c) synchronously with drag-folds (Figure 4a). These structures are consistent with a dextral sense of shearing [47]. Where plutons are emplaced within shear zones, they develop both magmatic foliation and lineation (e.g., the Igoudrane pluton). There, the foliation is parallel to the fault (N075–090°E 80°N) and the lineation roughly horizontal. All structures linked with the D_1 events and the geometry of the associated intrusions indicate that this first Pan-African event developed in response to a NW–SE to WNW–ESE trending shortening.

3.2. The Upper Complex or the Inception of a Silicic Large Igneous Province

3.2.1. Generalities

Rocks of the Upper Complex cover nearly 80% of the surface of the Jbel Saghro (Figure 2). This complex, only affected by very low-grade metamorphism and weak deformation, consists of thick and regionally extensive felsic volcaniclastic sequences that are non-conformably above the more deformed and metamorphosed rocks of the Lower Complex [29,30,47,112,131–133]. Related dykes and plutons intrude both the rocks of the Lower and Upper Complexes. These rocks belong to the Ouarzazate Supergroup that includes the lower Mançour Group and the upper Imlas Group [5,107]. Plutonic suites are attributed to the Tanghourt Suite. These plutonic and volcanic rocks were emplaced between ca. 575 and 540 Ma [29,51,74,78,106–108,112,134,135]. Most of the volcanic rocks are ash-flow tuffs, felsic lavas, resedimented volcaniclastic deposits with some andesitic lavas and rare mafic intrusions [29,30,47,112,133] that cover an area of approximately 2000 km^2 and reach a maximum thickness of 1000–1500 m.

3.2.2. The Qal'at Mgouna Ash-Flow Caldera

In the vicinity of Qal'at Mgouna (Figures 2 and 5), the association of lava flows (rhyodacites, rhyolites and andesites), pyroclastic rocks (ash-flow tuffs and ash falls), re-deposited volcaniclastics and reworked volcanic rocks is consistent with an ash-flow caldera environment [47]. The pre-caldera formations mostly consist of metagreywacke basement rocks and diorite and granodiorite intrusion dated at 576 ± 5 Ma [29], all belonging to the Lower Complex. Related to the caldera formation stage, plutonic rocks are mostly represented by monzogranites and coeval porphyries (Figure 5). Volcaniclastic rocks are not deformed, but only tilted when localised inside the caldera (Figure 5). The structural limit of the proposed Qal'at Mgouna caldera can be traced over 5–6 km. Tuduri [47] interprets the near vertical arcuate lineament located at the margin of the caldera as a potential ring-fault that trends E–W to NW–SE (Figures 5 and 6a). Evidence is given because this boundary separates the near vertical Cryogenian metagreywacke bedding to the South from the NNW dipping (50° to 80°) monocline intra-caldera sequences, to the North (Figures 5 and 6b). Numerous rhyolite dykes, 10 to 20 meters wide are located along this lineament (Figures 5 and 6a,b). Dykes are vertical or near-vertical and intrude the Lower Complex rocks as well as the plutonic and volcaniclastic rocks of the Upper Complex. Because these rhyolitic dykes are emplaced along the proposed structural limit and generally present an arcuate shape, they are interpreted as ring dykes.

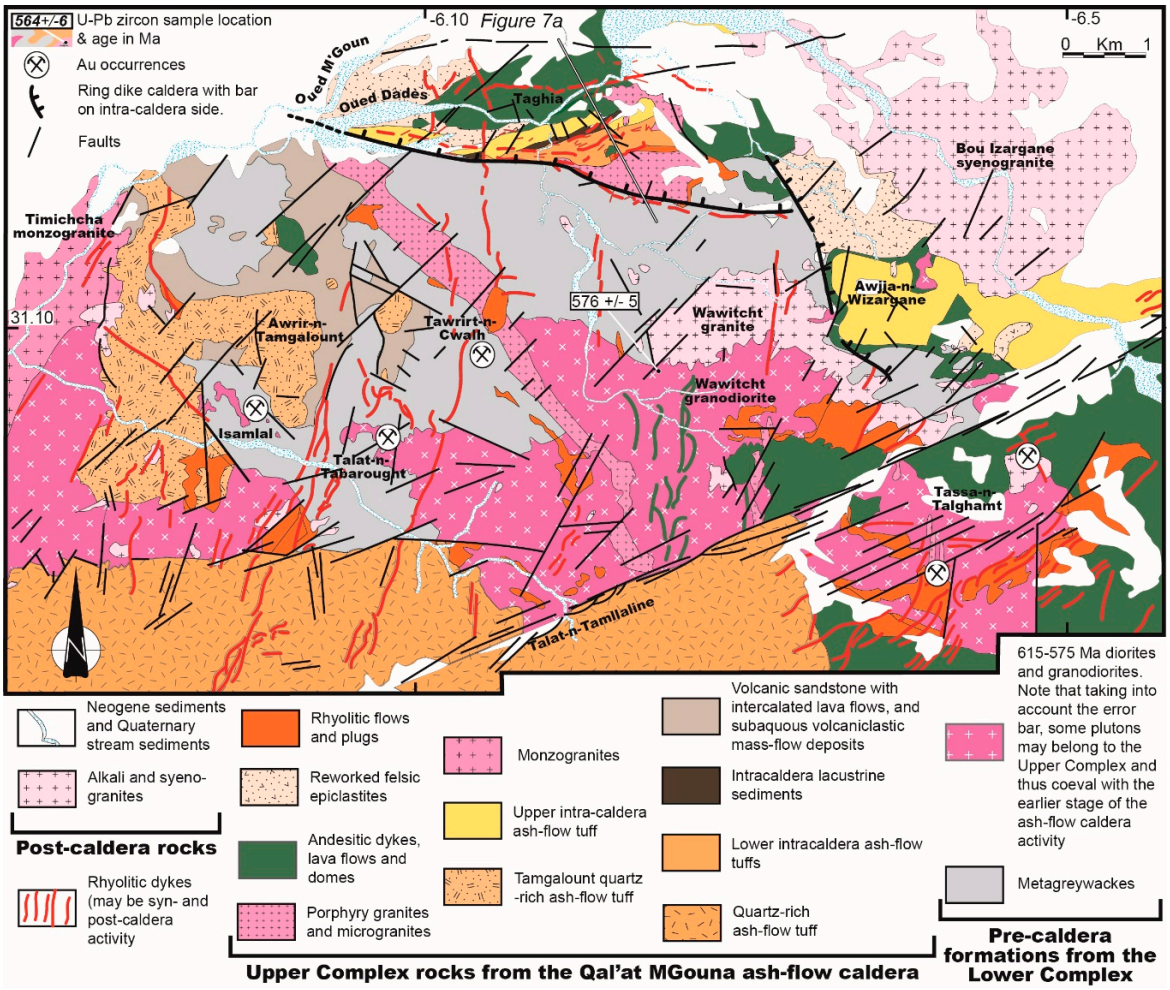

Figure 5. Detailed geologic map of the Qal'at MGouna district showing the extra- and intra-caldera rock units (from Benharref [132], Derré and Lécolle [113] and Tuduri [47]).

All the data presented above argue for the existence of a collapse caldera structure as shown on Figure 5 [136–139]. The peripheral structure of the ash-flow caldera where ring dykes occur is herein interpretated as having accommodated both subsidence (caldera collapse and intra-caldera sequences deposition) as well as subsequent uplift and tilting (magmatic resurgence and ring dykes injections). The geometry given by the NW–SE trending structural limit favours an elliptic shape rather than a sub-circular one for the caldera [41,140,141]. The consequence of such a shape will be discussed further. From bottom to top and according to Tuduri [47], the intra-caldera volcaniclastic sequence is detailed below (Figures 5–7):

(i). A lowermost pyroclastic layer consists of a 400–500 m thick, unwelded to slightly welded, moderately crystal-rich dacitic lapilli tuff (Figure 6c,d and Figure 7a,b) interpreted as an ash-flow deposit [142,143]. Internal stratification of the ash-flow tuff is crude, oriented N060–080°E 80°NW, as highlighted by discrete layers which are either pumice-richer, lithic-richer or entirely devitrified with spherulites. In a specific layer 40 m thick, greenish fibrous pumices displaying silicified tubular micro-vesicles and a silky/fibrous fabric can reach up to 5 cm long. Lithic clasts up to 20 cm in size are common throughout and consist mainly of basement greywackes, lavas and quartz-rich ignimbrite fragments. Phenocrysts are mostly broken plagioclase and K-feldspar, in various ratios with minor amounts of chloritised ferro-magnesian crystals (biotite and probable amphibole) and very scarce quartz.

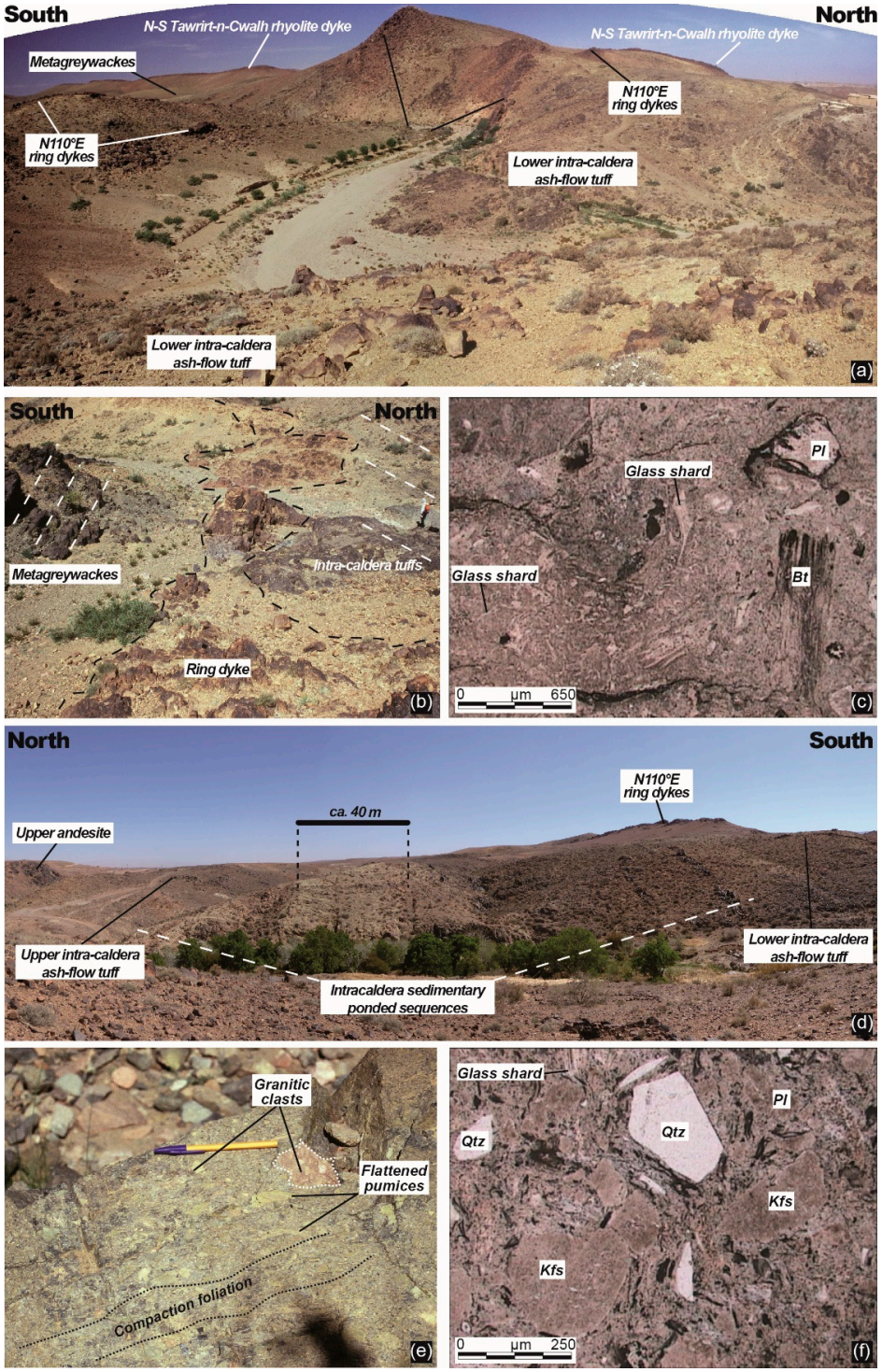

Figure 6. (**a**) View of the structural limit of the caldera showing the contact between the intra-caldera sequence, rhyolite ring dykes and basement, Taghia area (see location on Figure 5). (**b**) Detailed view of the structural limit showing the ring dykes and the unconformity between the basement to the south and the intra-caldera sequences to the north. (**c**) Microphotograph of the lower intra-caldera ash-flow tuff. Slight compaction and welding of shards are characteristics of this tuff, Plane Polar Light. (**d**) View towards the east showing the relationships between the lower and upper intra-caldera tuffs and interbedded sedimentary ponded rock sequences Taghia area (see location on Figure 5). (**e**) Close-up view of the upper intra-caldera tuff characterised by compacted fiammes (flattened pumices) and lithic fragments of K-feldspar-rich granite. (**f**) In thin section, the upper ignimbrite shows strong compaction and welding of shards, Plane Polar Light. Bt: biotite, Kfs: K-feldspar, Pl: plagioclase, Qtz: quartz.

(ii). Above the ash-flow unit lies a ca. 200 m thick volcano-sedimentary (epiclastic) unit with very thin bedding (Figures 6d and 7a,b). The lower part (100 m thick) is made of layered tuffaceous breccias containing ignimbrites fragments. The upper part consists of laminated reddish and greenish mudstones and sandstone oriented N070°E 70°NW. When preserved from important silicification, the identifiable components are microscopic broken crystals and lithic fragments. Beds are broadly continuous laterally, being only sometimes disrupted by syn-sedimentary normal faults and slump-like structures. Faults are roughly oriented NW–SE. Fluid escape textures are common and allow assessment of the polarity of the intra-caldera sequence. All sedimentological features argue for a subaqueous emplacement, at least for the upper part of the epiclastic unit. In our model, and as no marine sediments have been hitherto recognised in the entire Jbel Saghro in the Ediacaran formations, such subaqueous environment may be reasonably related to a caldera lake.

(iii). Above the volcano-sedimentary unit lies a ca. 200–300 m thick crystal-rich rhyolitic ash-and-lapilli tuff (Figures 6d and 7a–c). Plastic deformation due to significant compaction is evidenced by reddish flattened pumices (Figure 6e). Glass shards and broken phenocrysts are visible under the microscope (Figure 6f). Phenocrysts are quartz, plagioclase, K-feldspar, and scarce amounts of chloritised Fe–Mg minerals (biotite and amphibole). Up to 2 m-sized lithic clasts are abundant, especially in the basal part, and consist of metagreywacke, ash-flow tuff fragments, jasperoids and monzogranite (Figure 6e). This voluminous quartz- and pumice-rich unit is readily interpreted here as a welded ignimbrite.

(iv). The top of the sequence is dominated by massive andesite lava flows and epiclastic polylithologic breccias (Figures 5, 6d and 7a,b). The bottom of this whole sequence is intruded by a monzogranite porphyry (Figures 5 and 7a,b). Plugs of similar porphyry facies also locally intrude the upper parts of the sequence. Such porphyry is here interpreted as a resurgent pluton [137,144] that tilted the intra-caldera sequence upon emplacement [47]. Because of the tilting, the thickness of the intra-caldera sequence is exposed over 1500–2000 m, of which 800–1000 m consists of ash-flow tuffs and epiclastic rocks. To the north, the intra-caldera sequence disappears beneath the young sedimentary rocks of the Dadès valley (Figure 5).

Volcanic and pyroclastic rocks also occur outside the caldera structure to the south and west. They form a broadly stratified pile up to 500 m thick with moderate dips toward the W–NW (Figure 5). In the vicinity of the Awrir-n-Tamgalount (Figure 5), the extra-caldera sequences are made up of two units overlain by the Tamgalount tuff (Figure 7d,e). The lower unit is dominated by hundreds of meters of well bedded, normally graded crystal-rich sandstones and siltstones (Figure 7e). Under the microscope some of the silt-sized layers are formed of formerly vitric, now devitrified, material and might be primary ash fall deposit. The stratified lower unit dips towards the west at variable angles (Figure 5), perhaps due to palaeo-topography effects and(or) syn-tectonic deposition. The upper unit is dominated by rhyo-dacitic lavas that display distinctive spherulitic devitrification microtexture and pilloïd texture in the field that suggests emplacement under water. The Tamgalount tuff (Figures 5 and 7d,e) is a porphyritic porphyritic rhyo-dacitic ash-flow tuff (ca. 25% phenocryst) with eutaxitic texture. Broken phenocrysts consist of quartz, plagioclase, K-feldspar and chloritised Fe-Mg minerals. Lithic fragments are abundant and composed of greywackes, ash-flow tuff fragments and jasperoids. all extra-caldera units lie unconformably on the Lower Complex and are pervasively affected to various degrees by hydrothermal alteration and/or silicification. The importance of this unconformity will be discussed later.

Numerous intrusions are related to the Upper Complex (Figures 2 and 5). They have been mapped according to their mineralogy, texture and geochemical features. Two types are distinguished: (i) gabbros and biotite- and amphibole-rich, pink-coloured coarse-grained granites (monzo- to syenogranites), which are calc-alkaline to highly potassic, abd coeval porphyries emplaced at shallower levels (e.g., the intra-caldera resurgent granite and its apophyses); and (ii) Si-rich alkali (K-rich, i.e., shoshonitic in composition) granites and related aplitic bodies (sills, dykes), which frequently appear as late magmatic events in the Upper Complex history. The pink mozogranites contain

quartz, albite-oligoclase, Fe-edenite, annite, K-feldspar and accessory minerals such as thorite, zircon, allanite, apatite, magnetite, sulphides and W and Mo-rich minerals. By analogy with the Isk-n-Alla monzogranite in the central part of the Jbel Saghro (Figure 2), they may have been emplaced around 555 Ma [29,106]. The alkali granites are mainly composed of quartz, albite and K-feldspar displaying granophyric intergrowths. Accessory minerals include tourmaline (fluor-schorl) and metamict zircon [47]. They are associated with late N–S rhyolitic dykes that also display shoshonitic compositions (Figure 5). We assume they may have emplaced later, between 550 and 530–520 Ma [74,107,108].

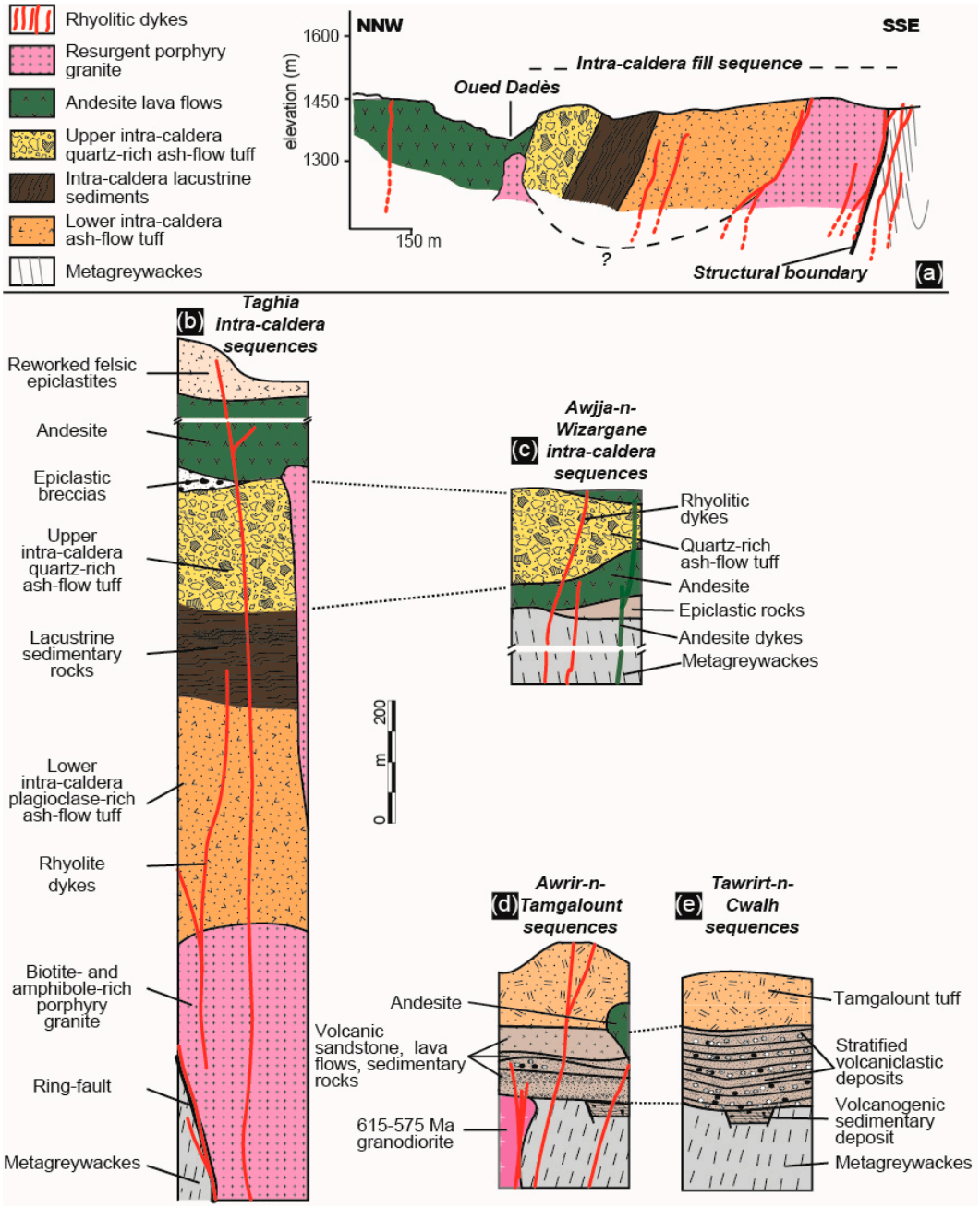

Figure 7. Simplified cross section and graphic logs of the Qal'at Mgouna volcanic sequences according to Tuduri [47]. (**a**) Schematic N–S cross section across the Qal'at MGouna ash-flow caldera. Summary stratigraphic sections for the (**b**) Taghia and (**c**) Awjja-n-Wizargane intra-caldera sequences, and extra-caldera sequences from (**d**) Awrir-n-Tamgalount and (**e**) Tawrirt-n-Cwalh (See location on Figure 5).

According to the relative and absolute chronology of both volcanic and plutonic rocks in both the Jbel Saghro and in the Qal'at MGouna area, three main ignimbrites flare-ups are herein evidenced. The earliest flare-up corresponds to the lower intra-caldera ash-flow tuff emplacement. It is mostly dacitic and may coeval with granodiorite plutons emplaced around 575 Ma [29,74]. Ignimbrites from the Oued Dar'a caldera described by Walsh et al. [29] are herein interpreted as belonging to this earliest flare-up. Then, the emplacement of the Tamgalount ash-flow tuff with rhyo-dacitic affinities, may correspond to a second high-volume magmatic event emplaced around 565 Ma [78,107]. Such an event would have produced similar tuffs that are coeval with the huge rhyo-dacitic dyke swarm [29] observed in the western and southern parts of the Jbel Saghro (Figure 2). The later ignimbrite flare-up corresponds to the upper intra-caldera rhyolitic ash-flow tuff and to the numerous rhyolitic lava flows and domes reported in the literature [29,74,106], coeval with pink monzogranite plutons around 555 Ma.

3.2.3. The D_2 Deformation Event

D_2 is interpreted as a strike-slip faulting event [29,47] that is also controlled by a WNW–ESE direction of shortening [47]. Tectonic features are faint, belong to the brittle regime, and affect both the Lower and Upper Complex units. Indeed, large-scale structures (except faults) and intense folding as observed in the Lower Complex are absent. It may be noted that some authors [29,78] described gentle folds that only affect the lower ignimbritic sequences (i.e., the 575 and 565 Ma ones) mainly in the western part of the Jbel Saghro and the Central and Western Anti-Atlas. Field works document: (i) ca. NNW–SSE normal faulting emplaced perpendicular to the extensional direction (i.e., NNE–SSW); and (ii) N070°E strike slip fault systems and associated veining. In the Qal'at Mgouna area, D_2-related normal faults control the emplacement and development of extra-caldera basins filled by the volcaniclastic rocks (Figures 5 and 7d,e). In contrast to the D_1-related ones, structures related to the D_2 event are characterised by dominant opening and extensional features [47]. Some specific locations (see below) demonstrate the re-activation of previously formed faults (i.e., the regional strike-slip faults trending N070°E) and fractures under the state of stress link with D_2. Others structures were formed, mainly in the Upper Complex. As fractures are favourable sites for fluid circulations and fluid trapping, intense veining occur within domains were intense fracturing is coeval of significant magmatic activity and related hydrothermal events. All these factors lead to the establishment of a general D_2-related extensional/transtensional setting that is particularly favourable for the emplacement of fluid-filled structures and, consequently, to the formation of the numerous ore deposits concerned by this study.

In the Qal'at Mgouna area, the structural map of the volcanic complex points to a control by a combination between E–W to NW–SE faults and NNE–SSW normal faults (Figure 5). Both structural direction controlled block-faulting, collapse and caldera formation. Because E–W to NW–SE faults are more developed and have a longer extent, they are assumed to represent the structural limit of the Qal'at Mgouna caldera (Figure 5). The orientation of these faults is consistent with a caldera formed under the control of a transtensional regime with a WNW–ESE shortening direction and a NNE–SSW extensional direction. Similar tectonic features have been described in the Oued Dar'a caldera which is localised 60 km to the WSW [29]. Few examples of ash-flow calderas developed in strike-slip and(or) extensional tectonic regimes have been documented [145–150].

4. Characteristics of Ore Deposits

Au–Ag showings and/or mines occur in several areas of the studied area (Figure 2). Four zones were selected. These showings are hosted in rocks of the Lower Complex (i.e., Thaghassa), the Upper Complex (i.e., Zone des Dykes area), or both (i.e., Imiter and Qal'at Mgouna) depending upon the depth of their formation. Mineralisation formed during the D_2 tectonic event within the four localities herein described in detail.

4.1. The Thaghassa Intrusion-Related Gold Deposit

The Thaghassa intrusion-related gold deposit (IRGD) is an exploration project with drill core data showing the presence of several intersects of 1–2 m at 5 g/t Au, and up to 400 g/t Ag. It is hosted in hornfelsed metagreywacke rocks (Figure 8a) that are adjacent to a large granodioritic pluton [47,48,151], while the metagreywackes belong to the Lower Complex, the intrusion may correspond to the earlier development of the Upper Complex. Two main tectono-magmatic stages control the formation of the deposit. (i) The first stage corresponds to the top-to-the-south asymmetry and the syn-kinematic Ikniwn pluton emplacement controlled by a transpressional strain regime. Zircon U-Pb dating yields a Concordia age of 564 ± 6 Ma for the intrusion [48]. (ii) The second stage (Figure 8b) is characterised, from older to younger and further away from the intrusion, by: metatexite with leucocratic stromatic bands, aplo-pegmatite sills (Figure 8c), intermediate veinlets composed of quartz, K-feldspar and muscovite (Figure 8d), and then gold-bearing striped foliation-veins (Figure 8e). All these are assumed to have been emplaced under large-scale ENE–WSW dextral shearing that results from an ESE–WNW shortening during transtensive tectonics (Figure 8b). Tuduri et al. [48] suggested that the progressive and continuous shearing was initiated at the aplo-pegmatite stage and achieved during the hydrothermal phase (Figure 8b–f). The existence of intermediate veins characterised by quartz-rich core and apatite-muscovite-feldspar-rich rims demonstrates a progressive evolution from a magmatic to a hydrothermal stage and the persistence of the magmatic character, at least until the onset of the hydrothermal process. The main Au-mineralization was concentrated at the end of such a magmatic-hydrothermal evolution. The ore paragenesis is characterised by arsenian pyrite with refractory gold (<5 μm) arsenopyrite, sphalerite and scarce grains of chalcopyrite, loellingite, pyrrhotite, tetraedrite, freibergite, argentite and cassiterite. Galena is abundant but always in the form of microscopic inclusions within pyrite. Fluid inclusion characterisation, based on the concept of fluid inclusion assemblages (FIA, [152]) as in all the cited references, combined with mineral geothermometry [48] suggests that the system evolved from hot fluids (~550 °C) dominated by N_2 and CH_4 to intermediate temperature (~300–450 °C) and low salinity aquo-carbonic fluids in the system (H_2O-NaCl-CO_2) + CH_4. Salinities are low to intermediate, being lower than 11.5 wt. % NaCl equiv. Gold precipitation is related to intermediate temperature mineralising fluids that have strongly interacted with the hornfelsed country rocks. According to Tuduri et al. [48], such a metallogenetic system is assumed to have developed due to migmatisation and partial melting of metagreywackes country rocks in response to heat transfer from the underlying Ikniwn intrusion. Fluid and metal sources may originate from magmatic processes (i.e., magmatic exsolution of incompatible elements from newly formed peraluminous melts and perhaps from the Ikniwn intrusion) and from the devolatilisation of the metamorphic host rocks. (iii) A third, later tectono-magmtic stage in the area developed a large volcanic dyke swarm and brittle faulting and is assumed to belong to the Upper Complex.

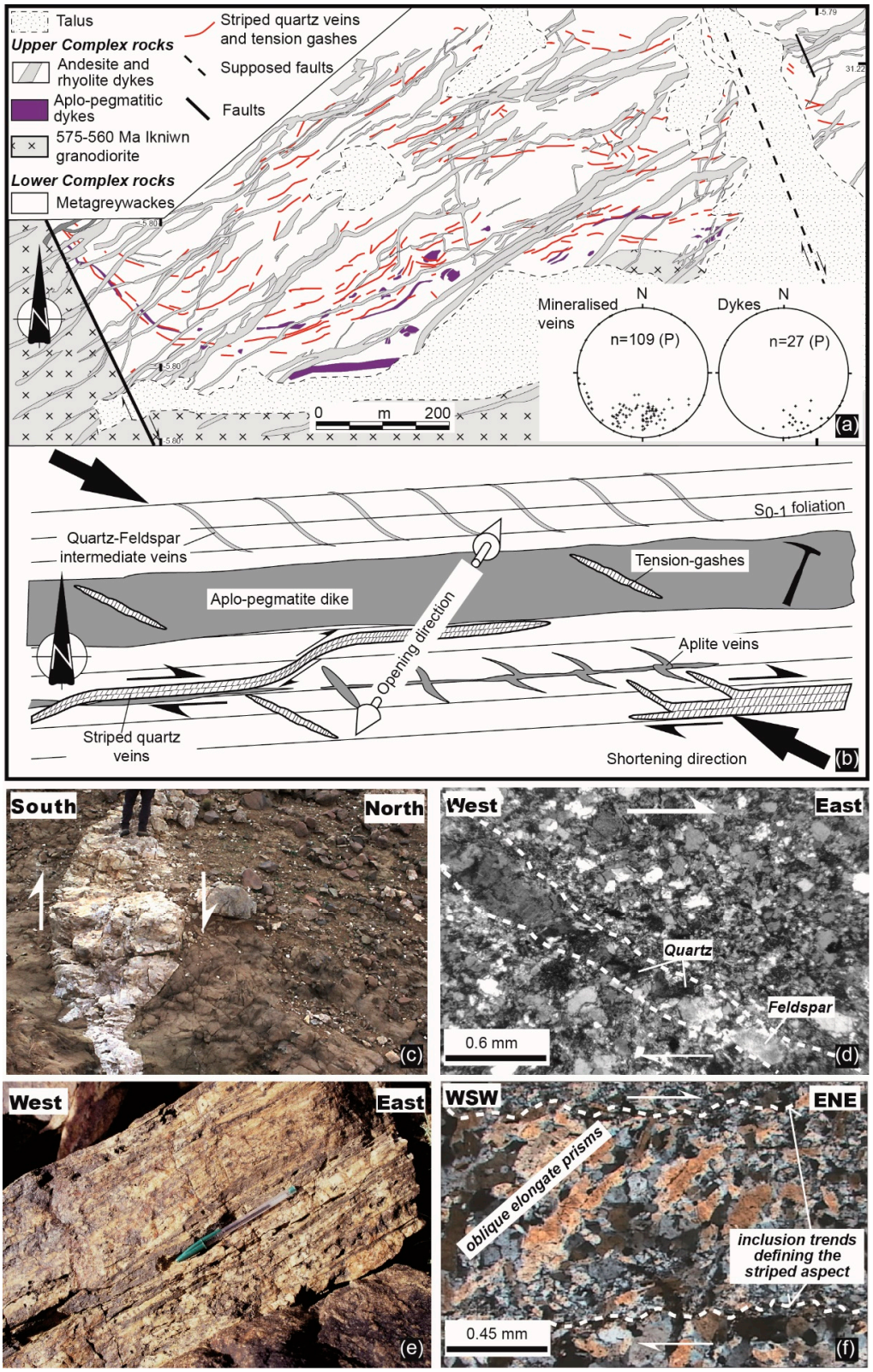

Figure 8. Main features of the Taghassa intrusion-related gold deposit (IRG) [47,48]. (**a**) General map and stereoplots of structural orientation data of the Au–Ag Thaghassa intrusion-related gold deposit. These reveal the high density of veins developed north of the 575–560 Ma Ikniwn granodiorite. (**b**) Interpretative sketch illustrating the magmatic-hydrothermal model that involved a progressive and continuous tectonic event including the aplo-pegmatitic dykes and sills emplacement, then the intermediate veins and the hydrothermal and gold-rich striped quartz veins. (**c**) Pegmatite dyke

showing a dextral pull-apart geometry. (**d**) N120°E trending intermediate veins filled by quartz, muscovite and feldspar assemblage, cross polar light. (**e**) Macrostructure illustrating the gold-bearing quartz vein stage. The layering texture defined the striped aspect of veins. (**f**) Microtextural characteristics of gold-bearing quartz veins. The internal texture shows elongate quartz grains with obliquity with respect to vein walls suggesting a dextral shearing, cross polar light.

4.2. The Qal'at Mgouna Au–Ag (Cu, Mo, Bi, Te) District

The Qal'at Mgouna district is composed of three main exploration projects: the Isamlal, Talat-n-Tabarought and Tawrirt-n-Cwalh districts, all of which located outside of the caldera structure (Figures 5 and 9). Based on mineralogical, chemical, textural and structural constraints, two distinct ore deposit types have been identified: an older porphyry ore deposit on which a younger epithermal system is superimposed [47,113,153,154].

4.2.1. The Isamlal Porphyry Au(–Cu–Mo) Deposit

The porphyry Au(–Cu–Mo) deposit type is related to high-temperature hydrothermal system observed in the Isamlal and Talat-n-Tabarought areas (Figure 9a–e). The Isamlal project appears as being the most promising [47,154–157]. Ore emplacement is assumed to be synchronous to slightly late with respect to the emplacement of diorite and granodiorite stocks [158]. Most of these intrusive stocks, that display porphyritic textures in drill cores (Figure 9e), present a preferential NW–SE orientation in map (Figure 9a,b). Their age of emplacement is still unknown. However, a large pluton, the Wawitcht granodiorite, displaying similar mineralogy and located ca. 4 km east of the Isamlal deposit, has been dated at 576 ± 5 Ma (U-Pb radiometric ages on zircon, [29]). Alterations are mostly observed within the Lower Complex and affect both the metagreywackes and diorite-granodiorite intrusions. The deposit is characterised by a Au mineralisation hosted by the metagreywackes that is also elongated along a ca. NW–SE trending direction (Figure 9b). Cu and Mo occurrences are additionally associated. In paragenetic order, the mineralisation includes magnetite, K-feldspar and late forming and less pervasive quartz veins that form a well developed stockwork. The stockwork occurs along a ca. N120°E preferred orientation, highlighting a strong structural control (Figure 9c). It is localised in the vicinity of the granodiorite intrusion or related apophyses but seems more developed within the metagreywackes at the hanging-wall (Figure 9d). Veins range in size from 0.5 to 30 cm in width and are ≤10 m in length except for the largest veins which are more than 30 m long. Such an important structural control on the stockwork may suggest that the main opening direction (i.e., NE–SW) is controlled by an ESE–WNW shortening direction. In drill cores, the central part of the mineralised zone is characterised by potassic-altered rocks. K-feldspar mostly occurs in highly reactive igneous rocks (Figure 9e). Biotite may coexist with K-feldspar but also occurs around the central zone whereas the propylitic alteration is more distal [158] In the Isamlal area, the quartz-rich stockwork is characterised by K-feldspar, magnetite, F-Cl-rich amphibole, Cl-F-rich biotite with scarce F-rich tourmaline, brannerite and rutile in the central part of the deposit, and muscovite with scarce iron oxides more externally. Note that such a stockwork has never been reported in rocks belonging to the Upper Compex [47]. Sulfides mostly occur in the central zone and mainly consist of pyrite, chalcopyrite, with scarce molybdenite, pyrrhotite, electrum, galena and tetradymite [47,155,157,158]. Fluid inclusions from the quartz-rich stockwork veinlets were used to constrain the palaeohydrothermal conditions [154,155,159]. Primary multiphase fluid inclusions are composed of liquid, vapour and halite cubes, as well as other salts such as sylvite, and $CaCl_2$. In addition, uncommon mineral inclusions that may be abundant have been identified, such as calcite, brookite–titanite, haematite, magnetite, and a solid phase with a very high refringence identified as andradite.

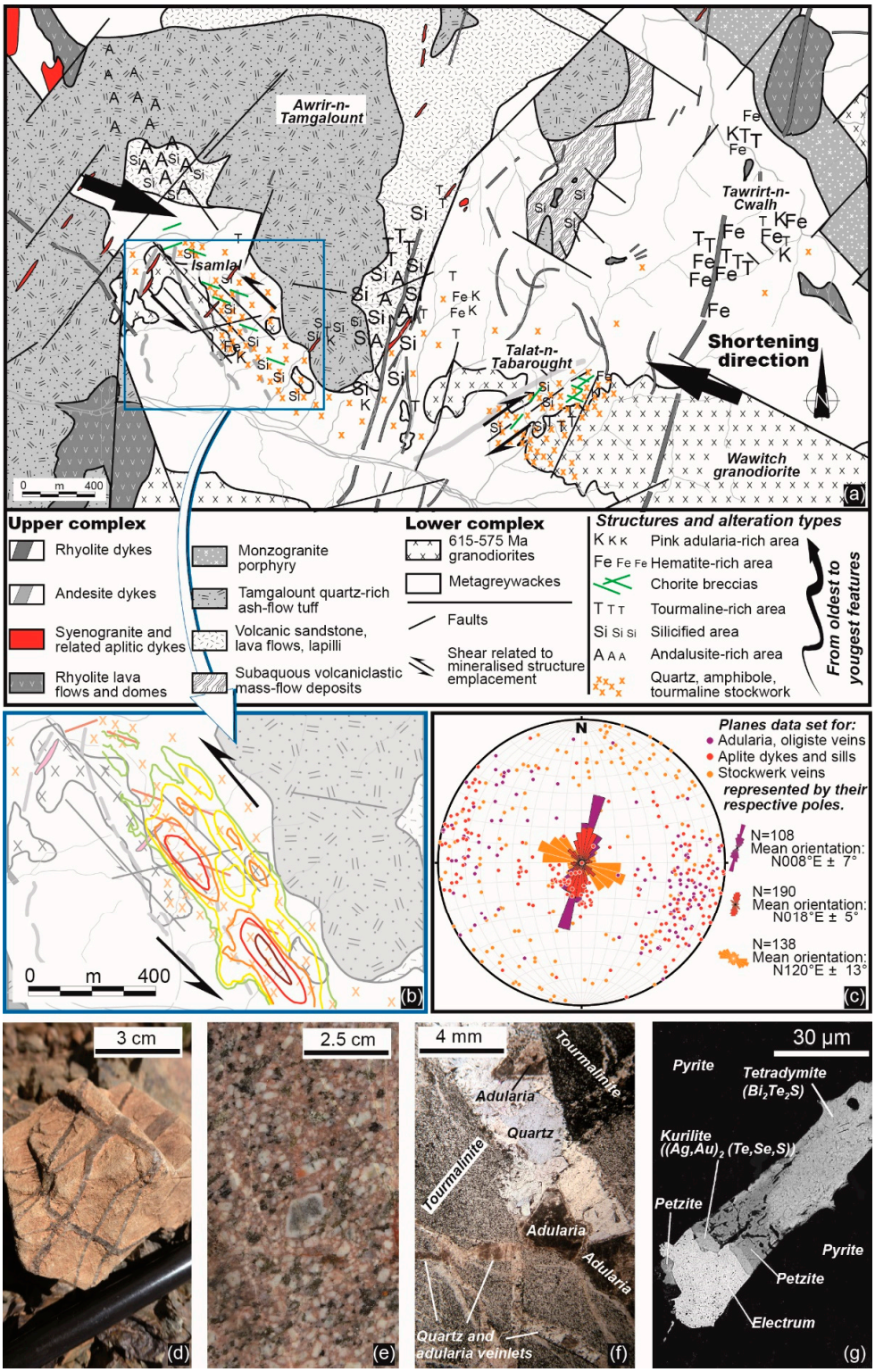

Figure 9. Main features of the Qal'at Mgouna deposit types [47,158]. (**a**) Detailed map of the Au(–Cu–Mo–Ag–Te–Bi) Qal'at Mgouna district (from Tuduri [47]). Note that the kinematics shown by shear zones are consistent with a WNW–ESE direction of shortening. (**b**) Kriging interpolation revealed that gold anomalies are correlated with both the quartz stockwork and the NW–SE faulted corridor in the Isamal porphyry deposit. The red colour is indicative of the highest Au grades [158]. (**c**) Stereoplots of structural orientations data for: the quartz stockwork related to the porphyry stage (mean orientation N120°E); the aplitic dykes and sills related to the alkali–syeno–granite stocks (mean

orientation N018°E); and the adularia-specularite-quartz veins from the epithermal stage (mean orientation N008°E). (**d**) Quartz stockwork from the Isamlal porphyry Au(–Cu–Mo) system. (**e**) Typical potassic alteration (pink coloured zones) of a porphyritic granodiorite (the Isamlal porphyry Au(–Cu–Mo) system). (**f**) Typical alteration and vein development of the epithermal stage: pervasive tourmalinites are cut by quartz and adularia-rich veins in the vicinity of the Tawrirt-n-Cwalh deposit, plane polar light. (**g**) Economic paragenesis of the epithermal stage characterised by Au-Ag tellurides, electrum and Bi-telluride veinlets within pyrite; Tawrirt-n-Cwalh deposit, SEM back scattered picture.

Chalcopyrite and gold were also observed in multiphase inclusions. Multiphase inclusions have a high though variable salinity (30 to 45 wt. % NaCl equiv.) and are characterised through homogenization by halite-disappearance. The large range of homogenization temperatures (160–460 °C) combined with a zoned potassic to propylitic alteration, stockwork structures and with an Au(–Cu–Mo) paragenesis is interpretated as characteristic of Au(–Cu–Mo) porphyry environments. This porphyry Au(–Cu–Mo) system is herein described as a vein-dominated deposit (stockwork) that is consistent with the emplacement of a porphyry stock, then exsolution and cooling of a magmatic-derived hydrothermal fluid. The overall system appears as mostly controlled by a ca. WNW–ESE trending direction. Indeed, this pattern suggests that the stockwork structure both reflects the magmatic stress associated with the porphyry emplacement and fluid exsolution, and also, a ca. NNE–SSW-oriented minimum principal stress (i.e., extensional direction) associated with a regional deformation that may be consistent with a WNW–ESE shortening direction although no clear tectonic regime has been proposed for the hydrothermal stage.

4.2.2. The Qal'at Mgouna Au–Ag(–Bi–Te) Epithermal System

In contrast to the porphyry deposit type, this low sulfidation epithermal deposit type appears more atypical (Figure 9a,c,f,g). From west (Timicha) to east (Isamlal then Tawrirt-n-Cwalh), the Qal'at Mgouna area (Figure 5) displays a progressive and continuous tectono-magmatic activity initiated as the plutonic stage (mostly observed to the west) and ending with a volcanic and hydrothermal stage observed from west to east [47]. The magmatic stage produced small pink-coloured Si-rich alkali granites, and sill and dyke intrusions with a typical fine-grained aplitic texture. Rhyolitic K-feldspar-phyric dykes are also assumed to belong to this stage. Such intrusive bodies may intrude rock units from both the Lower and Upper Complexes. The transition to hydrothermal stage is characterised by fluid exsolutions from the alkali granites and the formation of (i) quartz, Fe- and F-rich tourmaline with scarce F-rich muscovite miarolitic cavities; (ii) quartz, K-feldspar with scarce tourmaline stockscheider; (iii) tourmaline-rich quartz veins and NW–SE chlorite-rich transtensive cataclasites; and (iv) quartz, adularia, specularite veins with magnetite, fluorite, sulphides and gold (Figure 9f,g; [47,158–160]). The magmatic-hydrothermal processes strongly affected rocks especially the highly reactive volcaniclastic ones from the Upper Complex. These alterations correspond to a strong pervasive silicification. In addition to quartz, andalusite, diaspore pyrophyllite, Mg- F-rich tourmaline, F-rich phlogopite, F-rich muscovite, Cl-F-rich apatite occur along with rutile, haematite, monazite, xenotime, thorite and uranothorite as well as pyrite with inclusions of galena, coloradoite, hessite and altaite [47,113,153]. In some locations close to the Isamlal porphyry, the association of andalusite, pyrophyllite and diaspore with phlogopite and muscovite may be associated with the late epithermal or earlier porphyry stages [47,113,153]. Tourmalinisation is noteworthy and well developed along pervasive axes. Chlorite appears later in the paragenesis and mostly occurs in fault breccias. Ore concentration occurs during the hydrothermal stage with the quartz-adularia veins by crystallisation of As- and Co-rich pyrite, minor chalcopyrite and precious metal (Au–Ag telluride, electrum, Ag-telluride and Bi-telluride, Figure 9f) in the core of previously formed quartz–adularia–chlorite veins. Except for the chloritic breccias, which are strongly oriented along the NW–SE trending direction, all sills, dykes and veins related to the hydrothermal stage are roughly N–S with a maximum of 20° of dispersion toward the NNW and NNE (Figure 9c). The structural control of this event remains poorly evidenced as both extensional and transtensional features have been reported [47]. Paragenetic and

microthermometric studies show the mineralising system is characterised by decreasing temperature of formation [154,160]. Indeed quartz from the miarolitic and stockscheider stages are characterised by high temperature of formation (400–600 °C), multiphase highly saline fluid inclusions (22–32 wt. % NaCl + $CaCl_2$ equiv.), while the intermediate stages related to massive tourmalinisation show temperatures of homogenization of 200–250 °C. The system then evolves toward lower salinity fluids probably belonging to the H_2O–NaCl–$CaCl_2$ (11–27 wt. % NaCl equiv.) system, with the absence of multiphase inclusions, and temperature around 180 ± 20 °C for the quartz-adularia veins. This hydrothermal stage corresponds to the formation of Au–Ag(–Te–Bi) epithermal showings in this part of the Jbel Saghro [47]. The issue whether this system belongs to an alkaline, low sulfidation or intermediate epithermal deposit remains open. The age of formation is unclear, although it may be coeval with the slightly alkaline N–S rhyolitic dykes dated between 550 and 530–520 Ma in the eastern Saghro [74,107,108].

4.3. The Zone des Dykes Intermediate Sulfidation Epithermal Au-Base Metal Deposit

The Zone des Dykes, also known as the Issarfane area, is located in the western part of the Jbel Saghro inlier (Figure 2) in the vicinity of a huge N–S rhyolitic dyke swarm emplaced around 565 Ma [29]. The Zone des Dykes ore district consists of quartz veins systems hosted by two ash-flow tuff units belonging to the Upper Complex (Figure 10). Therein, three mineralised systems, called the F1, F5 and Bou Issarfane structures, respectively (Figure10a), are identified [47]. The F1 structure consists of a 2 km long and 2 m width vein system that trends N180–160°E and dips about 50–60° to the east. The vein system shows several step-over zones showing a left lateral pull-apart geometry (Figure 10b) with a faint vertical component. The F5 structure also consists of a vein system, 1 km long and 2 m width, that is roughly oriented N080°E 60–70°S and is characterised by right-lateral shear structures (Figure 10c). The F1 and F5 structures are both interpreted as developed as conjugate pairs (Figure 10d). Because cross-cutting relationships are observed, we interpret the N080°E direction trend (i.e., F5) as the dominant direction. The F1 shear structures is herein interpreted as emplaced along a pre-existing NNW–SSE fracture analogous to the ones occuring between the Bouskour and Issarfane areas (Figure 2). The F5 structure is also emplaced along an important pre-existing fracture set that corresponds to a main ENE–WSW regional fault. This may explain why the F1 and F5 shear fractures are almost orthogonal yet conjugated, but also why the F1 pull-apart structures are always brecciated. The Bou Issarfane structure has a ca. N–S orientation like the F1 system, but unlikely lies at dip angles of 20–40° to the east. It consists of a 1.5 km long and 5 to 10 m thick silicified breccia system hosted by ignimbrites and rhyolitic tuff that is affected by E–W brittle faults (Figure 10a). While an unsilicified rhyodacitic lava flow occurs at the hanging wall, the footwall is made up of a 5–10 m thick anastomosed quartz stockwork. All veins are mostly filled in by quartz (Figure 10e,g–i) with scarce amount of adularia, sericite, chlorite, calcite and rare fluorite [47]. Sulphides are also common and mainly consist of arsenian pyrite (Figure 10f). Chalcopyrite, sphalerite, Pb–Cu–Bi assemblages (aikinite group) and electrum are accessory minerals and appear as inclusions within the As-rich pyrites (Figure 10f). Chlorite has a pycnochlorite composition and a Fe/Fe + Mg ratio close to 0.48 which is consistent with temperature of crystallisation bracketed between 210 and 280 °C [47]. All veins are characterised by internal textures typical of epithermal deposits according to Dong et al. [161]. The most representative quartz textures are those showing a partial replacement of a silica gel precursor characterised by colloform and moss texture (Figure 10g). Such textures are specific of siliceous sinters in active geothermal systems [161]. Ghost-bladed calcite textures [162] are also observed (Figure 10h,i). The occurrence of platy calcite (ghost-bladed calcite) demonstrates that boiling processes were active during vein formation [163–165]. Veins also show complex texture reflecting several stages of crystallisation, replacement and re-crystallisation occur. Within this complex process of vein formation, Tuduri [47] suggests that sulphides crystallised after the second stage of quartz replacement while electrum is mostly located within fissures of the pyrite. While the structural control of the F1 and F5 structures is clearly evidenced, the emplacement of the Bou Issarfane breccia remains

unclear and needs to be discussed. Fragments from the Bou Issarfane breccia are silicified, sub-angular and of dimensions lower than 1 cm. Their probable volcanic origin suggest minor distance of transport. The matrix is highly silicified and seems composed by detritus of rock fragments (host rocks), and (or) by comminuted gangue minerals.

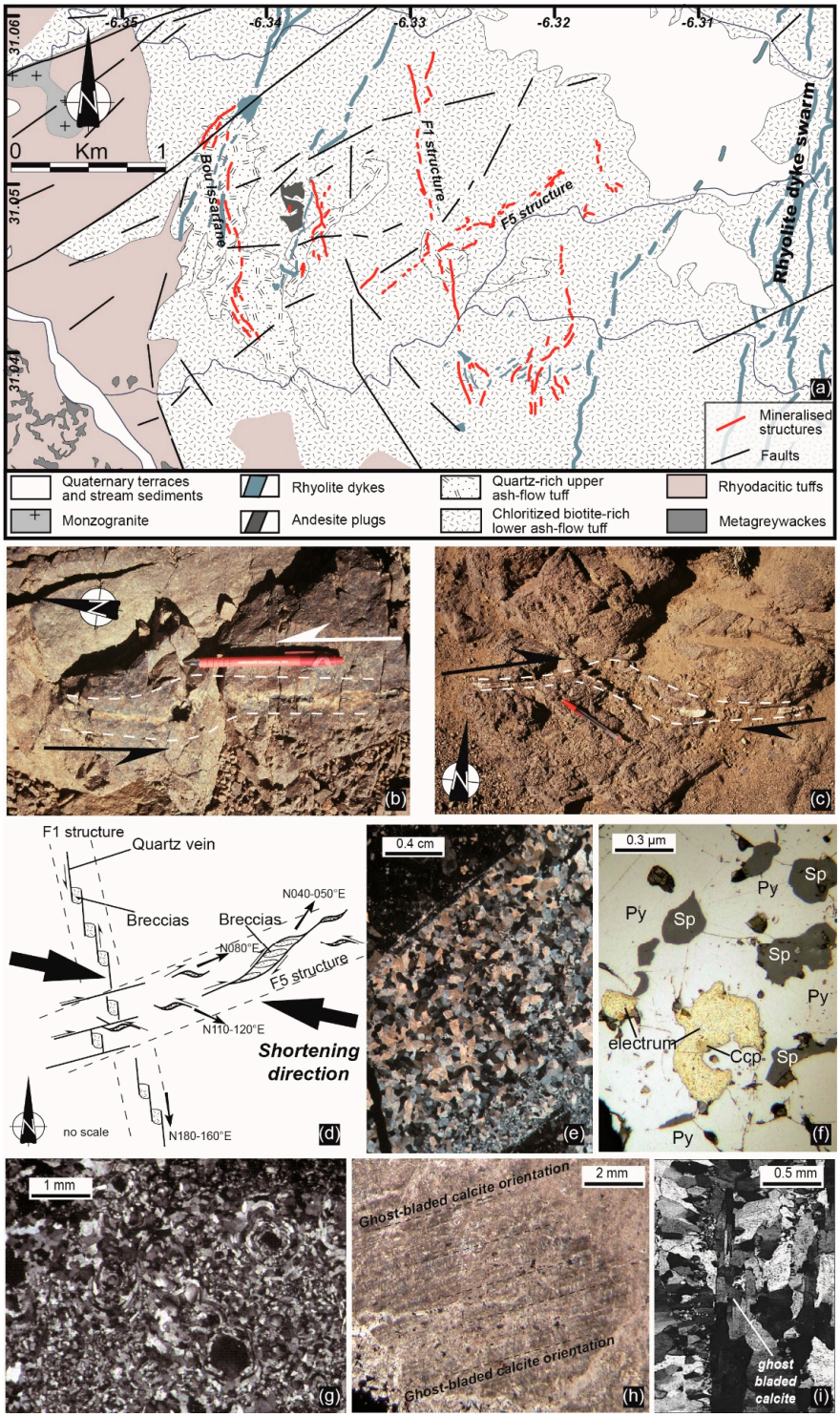

Figure 10. Main features of the Zone des Dykes deposits [47]. (**a**) General map of the Zone des Dykes Au-Ag deposit at the crossing between the F1 and F5 vein systems and Bou Issarfane area (after Tuduri [47]). (**b**) Pull-apart texture indicative of a left-lateral shearing movement along the F1 structure.

The filling is composed by quartz. (**c**) Pull-apart geometry of the F5 structure mainly filled by quartz and formed by dextral kinematics. (**d**) Global kinematic interpretation for the F1 and F5 structures integrating all the structural features observed in the field. (**e**) Microphotograph showing internal microtexture of the F1 structure characterized by a saccharoidal layout of quartz grains, cross polar light. (**f**) Typical gold-rich paragenesis of the F5 structure. Py: pyrite, Sp: sphalerite, Ccp: chalcopyrite. (**g**) Microphotograph of silica spheroid aggregates displaying moss texture, cross polar light. (**h**) Microphotograph of parallel ghost bladed calcites replaced by quartz, cross planar light and (**i**) plane polarized light microscopy.

The origin of this breccia may be therefore compared with phreatic or phreatomagmatic breccia pipes, although we cannot exclude a tectonic origin corresponding to a silicified cataclasite. According to salinity and homogenization temperatures, two type of fluids are assumed to be at the origin of the mineralised system [166]. The Bou Issarfane stockwork is characterised by primary multiphase fluid inclusions composed of liquid, vapour and halite cubes. Values obtained using the FIA concept indicate homogenization temperatures between 210 and 230 °C and moderate salinities (14–17 wt. % eq. NaCl). Secondary inclusions have lower homogenization temperatures between 130 and 180 °C. The F1–F5 veins consist of primary multiphase inclusions composed of liquid, vapour and halite cube with $CaCl_2$ assemblages.

Homogenization temperatures are bracketed between 160 and 180°C. Salinities are variable from 6% to 29% (wt. % NaCl + $CaCl_2$ equiv.) and may reflect the effects of boiling processes. Such textural, mineralogical and fluid characteristics suggest this hydrothermal Au–Ag(–Cu–Zn–Pb–Bi) system is comparable with intermediate sulfidation epithermal deposits as the ones reported in the Sierra Madre Occidental in Mexico [25,26,167]. The age of this ore deposit is still unknown. Considering the N–S trending direction of the F1 and Bou Issarfane structures, and the N–S trending direction of the rhyolitic dyke swarm, the mineralisation may have been formed coevally with this volcanic pulse around 565 Ma, i.e., after the emplacement of the ash-flow tuffs, that host the mineralisation dated, at 574 ± 7 and 571 ± 5, respectively [29]. However, we cannot exclude that the mineralisation is related to a later magmatic-hydrothermal period (e.g., the 550 or 530–520 Ma event) whilst no study has so far evidenced such later activity in the Bou Isserfane area.

4.4. The Giant Ag–Hg Imiter Deposit

The world-class Ag–Hg mining distirct of Imiter (Figures 2 and 11a) with 8.5 Mt of ore at a concentration of 700 g/t Ag consists of mineralised quartz–carbonate veins hosted by metagreywackes and more seldomly by the lower volcaniclastic units of the Upper Complex. The ore is located along a major E–W faulted corridor (Figure 11a) and results from a two-stage model of formation [47,102]. The main economic stage 1 developed within a N070–090°E 75–90°N trending dextral vein system filled by grey quartz, adularia and minor pink dolomite (Figure 11b,c, [102]). Satellite veins are common (e.g., F0 South, F0 North, R7 and R6, Figure 11b) and were formed synchronously with the main ones (e.g., F0 and B3, Figure 11b) within a global model of formation that involves double restraining bends along a strike-slip system. Indeed, such a push-up geometry results from irregular trends and stepovers developed along the N070–090°E dextral regional-scale faults (Figures 2 and 11a,b). The system also includes steeply-dipping, listric reverse faults and veins that flatten with depth (N065°E 50°SE, Figure 11b,d,e) and therefore that become flat-lying faults/veins in deeper parts of mine (N065°E 20–30°SE, Figure 11b). Reverse motions are clearly observed along all these structures (Figure 11d,e) and are assumed to have been formed during transpression. They serve as receptacles for the late emplacement of the high-grade silver deposit defined by Ag–Hg and Ag-rich minerals (Figure 11f, [102]). The main economic paragenesis is characterised by massive deposition of Ag–Hg amalgam (luanheite, eugenite), polybasite–pearceite, acanthite, stephanite, pyrargyrite-proustite and imiterite [47,168–170]. Sphalerite and galena are abundant while no silver was detected. Arsenopyrite is well represented but always as small euhedral crystals of a few hundred micrometers [47].

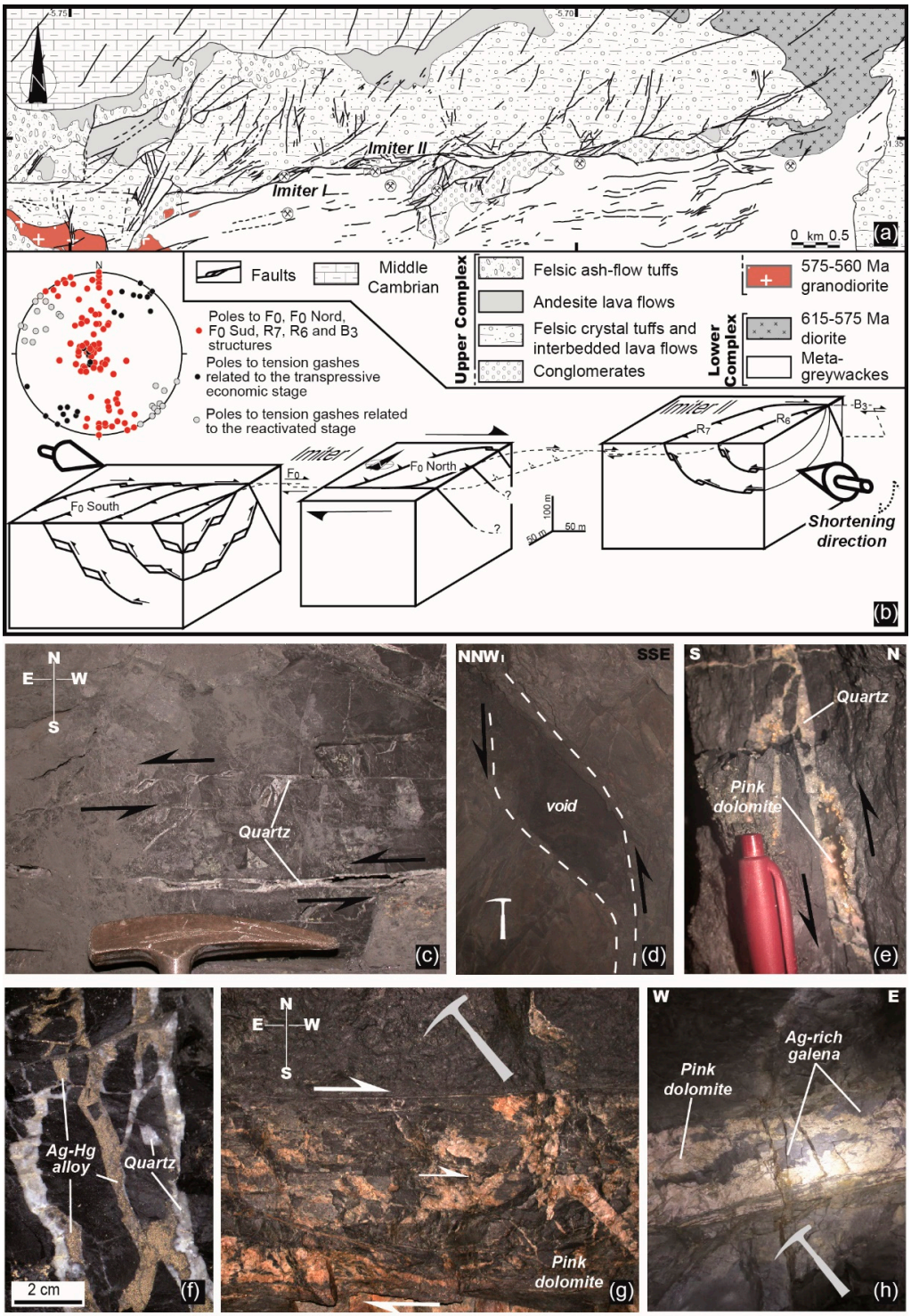

Figure 11. Main features of the world-class Ag–Hg Imiter mining district [47,102]. (**a**) General map of the giant Ag–Hg Imiter mine (after Leistel and Qadrouci [127] and Tuduri [47]) and (**b**) stereoplots of structural orientations and interpretative block diagram explaining the formation of the main ore-bearing vein system. Thrusts are formed in core of transpressive push-up structures. Note that the mineralised structures were everywhere controlled by a ESE–WNW direction of shortening. (**c**) Pull-apart and tension-gashes structures of the economic stage filled by geodic quartz and formed

during dextral kinematics, F_0 North vein systems, view realised towards the top of the mining gallery, Imiter I. (**d**) Pull-apart geometry of the economic stage indicative of a reverse shearing towards the north and showing void formations, R_6 structure, Imiter II. (**e**) Pull-apart texture of the F_0 South vein systems, thrusting towards the NW–NNW. The filling is composed by quartz (economic stage) and scarce pink dolomite in core of pull-apart texture. (**f**) Typical paragenesis of the economic stage 1 composed by quartz veins and huge concentration of Ag–Hg alloys, Imiter I, F_0 south. (**g**) Tension gashes and left lateral pull-apart structures filled with pink dolomite of the stage 2, F_0 structure, Imiter I. (**h**) Typical features of the stage 2 pink dolomite stage with large patches of Ag-rich galena, F_0 structure, Imiter I. Since photographs c and h were taken towards the top of exploration galleries, kinematics interpretation must be inverted.

Tuduri et al. [102] further demonstrated that a stage 2 reactivated the transpression-related structures in the opposite sense, and developed normal left-lateral motions associated with massive pink dolomite crystallisation, as well as prismatic quartz and variable amounts of Ag-rich galena and sphalerite, pyrite, chalcopyrite, arsenopyrite and freibergite (Figure 11g,h). Note that these two economic stages were preceded by a barren quartz vein network stage associated with sericite, illite-chlorite and base-metal sulphide minerals such as pyrite, galena, sphalerite with chalcopyrite exsolutions [45,47,51,127,169–171].

The main driving mechanism for silver ore deposition is assumed to be the dilution of ore-bearing fluids that were $CaCl_2$-dominated. Values obtained using the FIA concept [172,173] point to a general temperature decrease from stage 1 (280–100 °C) to stage 2 (110–60 °C). Note that the deepest levels of the mine workings (−220 m below the surface) record temperature in excess of 60 °C (i.e., lowest temperatures >160 °C) with respect to the shallow levels (−100 m) where the lowest temperatures are around 100°C. During stage 1, fluid salinities are moderate to high (8.4 to 26.1 wt. % NaCl + $CaCl_2$ equiv.), whereas they are very high when stage 2 dolomite precipitates (24.6 to 30 wt. % NaCl + $CaCl_2$ equiv.). Such value ranges are in agreement with data published by previous authors whether or not they used the FIA concept [41,45,101,171]. At shallower levels, additional supergene enrichment has been responsible for massive formation of native silver (1500 g/t Ag) associated with cerusite and mimetite [164].

Work in progress shows that Ag–Hg sulfohalides could also be related to the supergene processes [174]. Two opposing ore-forming models are strongly debated at Imiter. Some authors taking into account halogen composition of fluid inclusions, stable (C, O, S) and radiogenic (Pb, Re/O) isotope data together with noble gas (He) isotope compositions, suggest that the deposit is consistent with an epithermal model related to the felsic volcanic event at the Precambrian–Cambrian transition [45,47,51,101,127,170,175]. In that way, the huge Ag–Hg deposit would be comparable with the ones from the Mexican Sierra Madre Occidental Ag–Pb–Zn–Au belt, and should be considered as an intermediate sulfidation epithermal deposit [167,175]. On the other hand, a lithogene model [176] has been alternatively proposed in which fluids, according to laser ablation inductively coupled plasma-mass spectrometry (LA-ICP-MS) data on fluid inclusions, halogen signatures, and stable isotopes (H, C, O), are the products of diagenetic brine–evaporite interactions within a sedimentary basin [41]. The ore deposit might also be the result of basin inversion that expelled deep Ag-rich brines during, or at the end, of the Palaeozoic orogeny [41,175]. Recent $^{40}Ar/^{39}Ar$ age measured at 255 ± 3 Ma on adularia from stage 1 quartz vein supports the late Palaeozoic brine model [38].

5. Discussion

5.1. A Simplified Tectono-Magmatic Evolution Model of the Eastern Anti-Atlas

The evolution and transition between two main tectono-magmatic events is of importance in the Eastern Anti-Atlas and deserves to be discussed extensively and integrated with metallogenetic issues.

5.1.1. The Lower Complex and the D_1 Deformation

The D_1 deformation affects metagreywackes and metavolcanics and is associated with the syntectonic emplacement of calc-alkaline diorite and granodiorite plutons (Figure 12a). It is consistent with a NW–SE to WNW–ESE trending horizontal shortening. Structural studies have highlighted several important deformation structures related to that D_1 stage, i.e., upright tight folds with large-scale anticline and syncline, development of an axial planar S_{0-1} foliation, regional-scale N070–090°E trending dextral wrenching shear-zones, contact metamorphic minerals defining a stretching lineation (L_1) and rare S–SE-verging thrusts; Figures 2–4. Some plutons are inferred to be coeval with the D_1 deformation. Indeed, some of them are emplaced within the N070–090°E dextral shear-zones where they develop penetrative magmatic foliation and lineation. Elsewhere, other plutons seem to be emplaced in the core of folded sequences [47,121]. Furthermore, a tectonically-controlled fabric is best expressed in the thermal metamorphic aureoles developed around such plutons. There, foliations, lineations and related shear sense indicators show top-to-the-SSE–SE thrusting (Figure 4b,d) and dextral shearing depending on the distance from major shear-zones [47,121]. For those reasons, such diorite and granodiorite intrusions are herein interpreted as syntectonic and emplaced under the control of a NW–SE to WNW–ESE trending shortening [47,48,121]. This is consistent with the model of Saquaque et al. [77] who proposed that the main regional deformation results in top-to-the-SE thrusting, right-lateral wrenching along ca. E–W to ENE–WSW shear zones and syn-tectonic plutons. Since we herein combine strike-slip and shortening that is roughly perpendicular to the shear-zones, we infer a global transpressive tectonic regime as dominant in the D_1 stage. The characteristics of this tectonic stage that associates transpressive tectonics, pluton emplacement, strike-slip and rare thrusts explain the heterogeneity of the deformation observed within the entire Jbel Saghro.

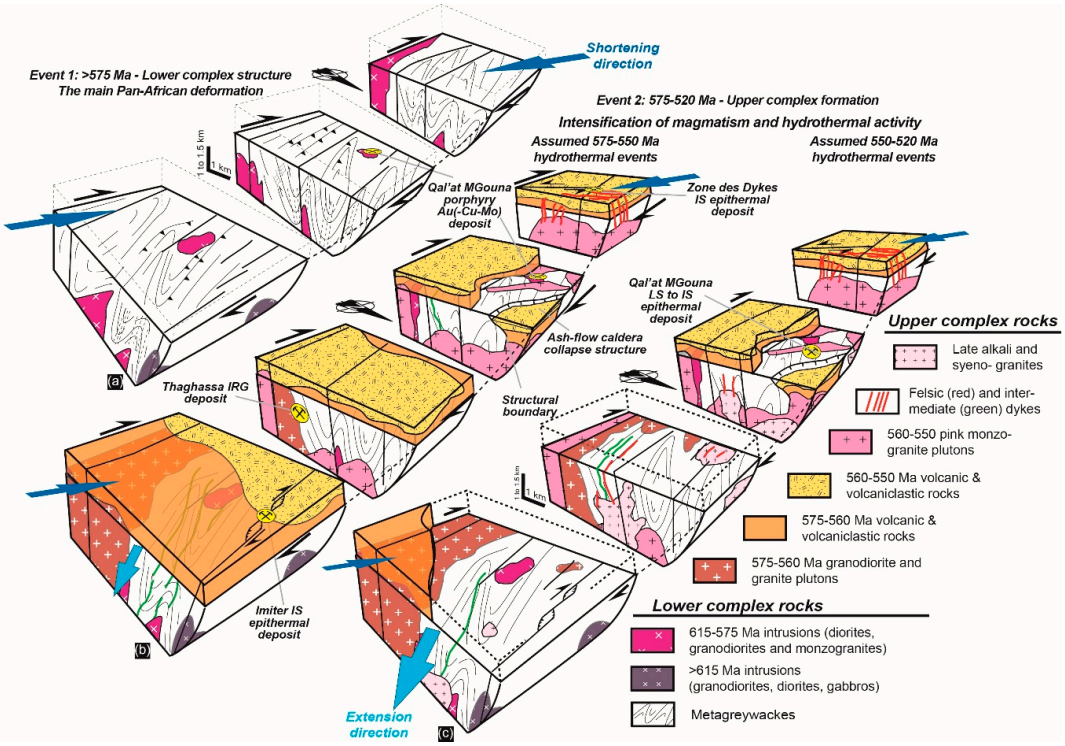

Figure 12. Interpretative three-phase model (**a**–**c**) explaining the tectono-magmatic evolution as well as the Lower and Upper Complexes definition of the Jbel Saghro and the formation of the ore-bearing vein systems of the Zone des Dykes, Qal'at MGouna, Thaghassa and Imiter districts. The size of the blue arrow relates with the inferred intensity of regional stress. See text for explanation. Note that the Qal'at MGouna porphyry deposit may belong to either the late stage of event 1 or the earlier stage of event 2 as the related porphyry stock emplaced at the transition between the two at 576 ± 5 Ma [29].

Previous interpretations tried to link each type of structures or pluton emplacement to one distinct tectonic event, increasing the complexity. From this study, it appears more appropriate to interpret all these features by the occurrence of a single and unique D_1 tectono-magmatic event. According to Gasquet et al. [83], as basins infilling with greywacke sequences was active until the onset of the Ediacaran period between 630 and 610 Ma; we suggest that the D_1 deformation probably occurred coevally with the syn-tectonic calc-alkaline magmatic occurrences, those being dated from ca. 615 Ma until ca. 575–565 Ma. This upper 575–565 Ma limit for the D_1 age is an important issue and will be further discussed below.

5.1.2. The Upper Complex and the D_2 Deformation

The Upper Complex is dominated by ash-flow tuffs emplaced in three main flare-ups and exposed inside or outside caldera structures, and by plutonic intrusions, mostly granitic, that were coeval with this D_2-related deformation (Figure 12b). Deformation was very weak and characterised by a brittle regime mainly represented by fault zones and vein formation throughout the Jbel Saghro area. Faults are mostly characterised by ca. N070–090°E orientations for the dextral strike-slip ones [47] whereas the ca. NW–SE trending direction may correspond to conjugate strike slip faults. However and according to Soulaimani et al. [86,87] and Azizi Samir et al. [177], the ca. NW–SE trending direction also corresponds to normal faulting yielding tilted blocks with syn-sedimentation processes. Such sedimentary deposits are volcaniclastic. The huge volumes of ash-flow tuffs associated with lava flows and related intrusions is considered as evidence for ash-flow caldera such as in the Qal'at Mgouna or Oued Dar'a areas (Figures 2 and 12b). We cannot exclude the presence of other caldera structures elsewhere in the Eastern Anti-Atlas. Because the structural limits of these caldera structures preferentially trend WNW–ESE to NW–SE [29,47], i.e., perpendicular to the direction of extension, the caldera yields an elliptic shape and is interpreted to be structurally controlled [141].

Three main ignimbrite flare-ups have been defined in the Upper Complex formation. The first one may have been emplaced at ca. 575 Ma and consists of dacitic ash-flow tuffs with related granodiorite and monzogranites [29]. The second flare-up occurred probably around 565 Ma and is related to monzogranite and granodiorite intrusions as well as the huge rhyo-dacitic dyke swarm in the western part of the Saghro [29,48,78,107]. The third ignimbrite flare-up is related to rhyolitic ash-flow tuff and cogenetic monzo-to syenogranite emplaced around 555 Ma [29,51,74,106,107]. Finally, a late magmatic stage is composed of the alkali-syenogranite plutons and related rhyolite dykes (Figure 12c). Such late alkali magmas highlight the persistence of the magmatism even after the emplacement of caldera-related rocks although they are less abundant. No radiometric ages are currently available on the alkali granites but related dykes provide ages bracketed between 550 and 520 Ma at the transition between the Proterozoic and Phanerozoic aeon [51,74,107,108]. Note that most of the intrusives such as aplitic and rhyolite dykes display a change in their orientation (i.e., ~N020°E, Figure 9c). Also, most of the hydrothermal veins related to those dykes and alkali plutons have the same direction pattern (Figure 9c). As no clear direction of shearing is evidenced in the horizontal plane, it is herein suggested that an extensional tectonic setting may control and assist the emplacement of both magmatic and hydrothermal structures in the ca. 550–520 Ma interval. The D_2 event is controlled by a ca. NW–SE to WNW–ESE direction of shortening and a ca. NE–SW to NNE–SSW direction of extension. Such control may evolve later toward a ca. N–S shortening direction and a ca. E–W extensional direction during the early Cambrian stage. This would be consistent with what is observed during the Adoudounian rifting period [86,87,106].

5.1.3. About the Transition between the Two Complexes and the D_1 and D_2 Tectonics

In the Eastern Anti-Atlas, the transition between the Lower and Upper Complexes is characterised by a significant increase of the magmatic addition rate [178] mostly evidenced by the Ediacaran volcanic flare-ups and by a change in the tectonic regime. However, such a transition appears as diachronous whether we consider the start of the volcanic activity or the change in tectonic regime.

The key evidence highlighting such a transition is the existence of an angular unconformity between the Lower and Upper Complex units [29,47,74,78]. However, the age of the transition remains elusive and debated. If we consider the available ages earlier volcanics of the Upper Complex that lie above the unconformity, the transition might occur between 580 and 570 Ma taking into account the error bars of the radiometric ages. This has been well described in the Western Anti-Atlas on the Tizgui geological map [29,179]. In the Central Anti-Atlas, Blein et al. [78] also suggest that most of the regional deformation observed there was completed by ca. 580 Ma and followed by an important erosional phase prior to the deposition of the Upper Complex volcaniclastic sequences. The 575 Ma age, therefore, represents a mean value.

Dating the deformations and thus the change in the tectonic regime from D_1 to D_2 is matter of more confusion. Indeed, the transition between the two complexes is estimated at ca. 575 Ma with the incipient volcanic activity and the occurrence of a strong angular uncorformity. By contrast, the transition between the two deformation events would be a little more recent and would have occurred around 565 Ma. The age assigned to the D_1 deformation appears thus mostly dependent on the radiometric ages obtained on the syntectonic plutons, and the issue of what plutons are syntectonic or not in the Eastern Anti-Atlas is clearly to be better assessed from field data. Currently, numerous plutons emplaced between ca. 575 and 565 Ma have been interpreted as syntectonic as they develop a coherent and homogenous ductile deformation in contact aureoles [48,105,106,121,123]. Given the error bars on the ages, we can actually question on their belonging to the earlier Upper Complex structuration, or to the later stage of the Lower Complex and D_1 deformation. As a matter of fact, discussions do exist about the possible intrusive character of some of these plutons in the lower part of the Upper Complex (e.g., The Igoudrane, Taouzzakt and Ikniwn plutons, Figures 2 and 3), while they may display an erosive roof on which lies Upper Complex volcaniclastics (at least the upper part of the Upper Complex). In addition, we have shown above that magmatic mushes at the origin of plutons emplaced around 575 and 565 Ma may be at the origin of the former ignimbritic flare-ups.

In any case, we assume that between 575 and 565 Ma, syn-D_1 plutons have developed in the Lower Complex metagreywackes, both contact metamorphism and ductile deformation that we interpret as the ongoing tectono-magmatic evolution between the Lower and Upper Complex structuration as suggested by Tuduri et al. [48]. Possibly, the S_2 cleavage refraction that developed after the main first-order folding event may be related to this transitional stage. It also remains difficult to assess whether some plutons were intruded within folds (e.g., the Bou Teglimt granodiorite in core of the Imiter inlier anticline, Figure 3a) and thus after the folding event (i.e., plutons would belong to the earlier stage of the Upper Complex) or if their emplacement played a part in the anticline structuring (i.e., plutons would belong to the Lower Complex tectono-magmatic history). Consequently, taking the important dioritic and granodioritic plutonism as systematically belonging to the Lower Complex might be misleading. As well, it is not straightforward to math the change in the tectonic regime (D_1-D_2 transition) with the transition between the Lower and Upper Complexes.

Therefore, we herein suggest that the reported tectonic transition must have been an ongoing process through the Lower-Upper Complex transition, given the deformation features (cleavage, weak upright folding) observed in the volcaniclastic rocks of the lower part of the Upper Complex in the western Saghro and Central Anti-Atlas [29,78]. Indeed, Blein et al. [78] recall that rapid variations in thickness of the volcanic and volcaniclastic rocks of the Upper Complex suggest they were deposited during active tectonics and on highly variable basement (i.e., Lower Complex units) topography. Such variations in the topography may be due to the earlier transpressive stage but also to later extensional-transtensional tectonics. In the rest of the Jbel Saghro no clear evidence of deformation (except cleavage) has been described affecting the lower part of the Upper Complex rocks. Note that the "Série molassique du Dadès" described by Walsh et al. [29] in the northern Qal'at Mgouna area, as being bedded, deformed and weakly metamorphosed in lower greenschist facies corresponds to the tilted intra-caldera volcanic sequence which underwent propylitic hydrothermal alteration. This formation herein belongs to the Upper Complex.

The preservation of the same shortening direction and tectonic style (i.e., strike slip dominated) further suggests that D_2 is a continuation of D_1 even though D_1 was associated with transpressive tectonics and D_2 linked with transtension to extension. Eventually, the transition between the D_1 and the D_2 deformation regimes occurred, while the shortening direction (parallel to Z strain axis) remained roughly constant (i.e., NWSE to WNW–ESE). However, one can note a shift in the two other strain directions showing a decrease of the vertical extension that becomes horizontal. This explains the numerous extensional features developed during the D2 stage (i.e., calderas formation and multiple ore concentrations within open structures). We note that the transition from D_1 to D_2 must be achieved prior the emplacement of the Thagassa IRGD around 565 Ma [48]. This transition is supposed to be progressive and the earliest mineralisation stages, such as the ones emplaced in the Thaghassa area, are the witnesses of this transition.

Therefore, we assume that the D_1 deformation might affect the lower units of the Upper Complex. Future works may focuse on testing this assumption. The contrasting structural levels that exist between the Lower Complex and Upper Complex units may argue against such a continuum. However, the combination of exhumation processes along strike-slip fault systems and of denudation history, integrating erosion processes [180–182] provides the first elements of an answer. Moreover, ignimbrite flare-ups and caldera formation are assumed to have been occurred rapidly as catastrophic events, contributing unconformities between the volcaniclastic rocks of the Upper Complex and the Lower Complex units.

5.2. The Mineralising Model

This study demonstrates the strong spatial link that exists between ore deposits and magmatism in the Eastern Anti-Atlas. A common hypothesis for the source of the mineralisation is to involve fluid exsolutions from intrusions. Even though we cannot demonstrate this assumption for all the ore deposits, a progressive and continuous vein formation model that began in the magmatic stage, developed an intermediate stage and finally ended under hydrothermal conditions is well constrained at Thaghassa and Qal'at Mgouna. Such a model of ore formation thus involves a three-stage model as stated in Table 1. About the economic stages, even though they were formed late during the veining stage, they benefited from the existence of previously formed veins. This model again highlights the significant role of the magmatism and related structures for ore deposition and concentration [183].

Table 1. Synthetic table summarizing the magmatic-hydrothermal features of main ore deposits of the Saghro area.

	The Zone des Dykes Deposit	**The Qal'at MGouna District**		**The Thaghassa Deposit**	**The Imiter Deposit**
Stage I (strong magmatic affinities)	Not expressed	Granodiorite stock emplacement and fluid exsolution	Alkali-granite emplacement with quartz, K-feldspar, F-tourmaline, F-muscovite in miarolitic cavities and stockscheider (400 < T °C < 600) [1]	Aplite dyke emplacement (500 < T °C < 600 °C) [1]	Not expressed
Stage II (intermediate stage between magmatic and hydrothermal conditions)	Not expressed	K-feldspar and magnetite alteration (disseminated and in veinlet stockwork)	Strong alteration with quartz, F-tourmaline, F-Cl-micas, andalusite, F-Cl apatite, monazite (250 < T °C < 400) [1]	Quartz, K-feldspar, muscovite, apatite, tourmaline and apatite (T °C < 500) [1]	Not expressed
Stage III (hydrothermal)	Quartz, adularia veins with calcite, chlorite, sulfides and gold (210 < T °C < 280) [1]	Quartz stockwork with Cl-biotite, Cl-amphibole, muscovite, sulfides (Cu–Mo) and gold (160 < T °C < 460) [1]	Chlorite-rich breccias, thenAdularia, specularite, quartz veins with sulfides and "gold" (160 < T °C< 200) [1]	Striped quartz veins filled by quartz, sericite, sulfides and gold (300 < T °C < 450) [1]	Firstly, quartz-adularia veins with silver-rich sulfides and alloys (100 < T °C < 280) [1] and then dolomite-quartz veins with Ag-rich galena and sphalerite (60 < T °C < 110) [1]

[1] Temperatures have been estimated using selected geothermometers applied on micas [184], chlorites [185,186], arsenopyrites [187,188], activity diagrams generated for tourmaline, albite, andalusite, paragonite and kaolinite [189] and microthermometric data results [41,45,48,155,159,160,166,170–173]. See Tuduri [47] for details.

- The first stage shows strong magmatic influence. It is characterised by emplacement of porphyry stocks, aplite dykes and sills at high temperatures from 400 °C up to 600 °C. At Thaghassa, this stage was responsible for the partial melting of the metagreywackes in response to the Ikniwn granodiorite thermal effect and for the related genesis of leucocratic S-type haplogranitic sills. In the Qal'at Mgouna district, this stage was responsible for the formation of stockscheider and miarolitic cavities within sills and dykes.
- The second intermediate stage consists of magmatic-hydrothermal vein emplacement and associated pervasive alteration. The persistence of the magmatic character is shown by the occurrence of high-temperature alteration phases such as tourmaline, micas, andalusite, apatite, K-feldspar with quartz. In the Qal'at Mgouna district, at Isamlal, this stage can be compared with the classical potassic and magnetite alteration in some porphyry type systems [190]. It is also marked by the wide pervasive development of Al-silicate–Al-hydroxide–phosphate–muscovite–F-rich phlogopite and F-rich tourmaline alteration, related to the late Si-rich alkali granites. K-feldspar, apatite, white mica along vein rims are observed at the beginning of vein aperture at Thaghassa. Temperatures of formation are bracketed between 250 and 500 °C.
- The third stage is hydrothermal and formed at lower temperature ($60 < T\ (°C) < 300$) producing gangue minerals except for the Thaghassa and Isamlal deposits where high-temperature minerals were also formed (350–450 °C). This stage end with the emplacement of economic ore.

The conditions of vein formation vary depending on their location in the Lower or Upper Complex and are reflected by variations in mineralogy and internal texture. Such variations are basically due to different structural levels of formation. Indeed, the geometry of the mineralised structures is controlled by tectonics, hydrostatic pressure, effective vertical stress and volcano-related effects. The Thaghassa prospect, hosted by the Lower Complex metagreywakes, exhibits texture and mineralogy indicative of high-temperature conditions of formation. The Zone des Dykes vein system, entirely developed in Upper Complex ash-flow tuffs, shows internal textures consistent with low-temperature epithermal deposits. The Qal'at Mgouna deposits are developed at an intermediate structural level. Veins hosted by the Lower Complex rocks are related to high-temperature formation (i.e., the Isamlal porphyry Au(–Cu_Mo) deposit) whereas those formed at shallower levels reflect low-temperature conditions (Talat-n-Tabarought and Tawrirt-n-Cwalh districts). Tuduri et al. [154] suggest that high temperature systems emplaced at ca. 150–200 MPa, whereas the lower temperature systems were formed at a lower depth (20–50 MPa). The regional variations clearly document the transition from magmatic to hydrothermal conditions, i.e., from somewhat high temperature fluids (350 °C and higher) at Thaghassa and Isamlal, to lower temperature hydrothermal fluids (below 300 °C) at the Zone des Dykes and Imiter.

For all ore deposits described in this study, the Ag and Au economic concentrations (with Cu, Zn, Pb) correlate with ore-forming fluids with moderate to high salinity. This is consistent with transport by chloro-complexes and confirms the importance of brines in such ore formation. If brines are frequent in the formation of porphyry copper deposit [183,191] and probably IRGDs [64,68], their role in intermediate sulfidation epithermal systems remains a matter of debate. In large Mexican epithermal silver deposits of intermediate sulfidation state, Wilkinson et al. [26] suggested that the ore forming fluids, were injected into a geothermal circulation system in response to the ascent of a magmatic intrusion. Such hydrothermal diapirs would be sourced from a stratified hyper-saline brine reservoir, formed in response to incremental exsolution of magmatic fluid, and intense brine condensation at depth, with halite precipitation, being stored above the source magma reservoirs [26, 192,193]. By contrast, Essarraj et al. [40,41,49] suggested that the ore-forming fluids were related to deep-basinal sedimentary brines and that metals had no genetic relationship with Neoproterozoic magmatism, on the basis of numerous deposits they investigated in the Eastern and Central Anti-Atlas. They suggested that ore brines resulted from evaporatively concentrated seawater in Triassic basins producing hot basinal brines, comparable with conditions for Mississippi Valley-Type (MVT) deposits.

We here suggest that all ore deposits described above are related to the Ediacaran magmatic-hydrothermal complex emplaced from 575 to 530–520 Ma. The concept of stored hypersaline brines is emphasised following Scott et al. [193]. Nevertheless, while a magmatic origin of such stored brines is obvious, the origin for Ca-rich brines has yet to be defined. Though such Ca-rich brines may derive from magmatic processes, they are also widespread in the deeper parts of many sedimentary basins and involved in ore forming processes [194,195]. This is, pro parte, the reason why Essarraj et al. [40,41,49] support a deep-basinal sedimentary brine model in the Anti-Atlas. Surprisingly, they do not support an Ediacaran model for such a model but a more recent one that is Permo-Triasic in age. Nevertheless, prior and during the early stage of development of the SLIP that characterise the Upper Complex and the related ore deposits, periods that roughly belong to the Ediacaran Gaskiers glaciation on the West African Craton and around [196,197], would have occurred between 595 and 565 Ma in the Anti-Atlas [198]. Such evidence may also point to a possible contribution of natural cryogenic brines in the ore forming processes. Indeed, according to the Starinsky model of evolution of a marine-cryogenic basin [199], these brines usually are seawater-derived and also enriched in Mg, K, Na, Ca, Cl, SO_4 and Br, even if they may have been heavily modified by fluid–rock interactions and(or) dilution [200]. Future studies would have to address the possible role of Ediacaran glaciations on the ore-forming processes in the Anti-Atlas.

The age of the mineralisations in the Jbel Saghro remains poorly constrained due to the lack of absolute dating. Nevertheless, we can assume that the transtensional regime characteristic of the Upper Complex provided extensional structures for melt and fluid circulations that are favourable for magmatic-hydrothermal ore forming processes. This period of time (575–550 Ma and 550–520 Ma) was suitable for ore emplacement as suggested above. We thus assume that most of the mineralised systems may have been emplaced between ca. 575 and 520 Ma. Indeed, these ore deposits seem to have been emplaced when tectonic regime changes at the transition between the Lower and Upper Complexes and when the typical medium-K calc-alkaline arc magmatism became more abundant in between 580 and 570 Ma. Some porphyry Au(–Cu–Mo) deposit may have been emplaced earlier around 575 Ma. In the Sirwa mountains belonging to the Central Anti-Atlas, Cu–Mo ± Au mineralisations associated with high-K calc-alkaline intrusions are also assumed to have been formed between 575 and 560 Ma [59,201]. Similar ages are also suggested in the vicinity of Bouskour where Re/Os analyses on molybdenite related to a Cu-rich mineralised stage, yield a weighted average age of 574.9 ± 2.4 Ma [103]. Further, the Thaghassa deposit displays strong similarities with the earlier base metal assemblage observed at Imiter and Tiouit [43,45,47,48,51]. Indeed, in the Tiouit gold deposit, the ore body is closely associated with the Ikniwn granodiorite dated at 564 ± 6 [48]. At Imiter, $^{40}Ar/^{39}Ar$ dating on sericites related to the earlier base metal sulphide veins range from 577 ± 4 to 563 ± 5 Ma, in good agreement with the synchronous Taouzzakt granodiorite dated at 572 ± 5 Ma and the Thaghassa model of emplacement (U-Pb radiometric ages on zircon, [48,51]). The intermediate sulfidation epithermal Au(–Ag–Cu–Pb–Zn) deposit of the Zone des Dykes may have been emplaced during lull periods soon after the emplacement of the second ignimbrite flare-up and related huge dyke swarm in the western Saghro (around 560 Ma). Similarly, the huge intermediate sulfidation epithermal Ag(–Hg–Pb–Zn) deposit at Imiter may have been emplaced following the third ignimbrite flare-up around 550 Ma. This assumption adopts the age alreadyproposed for the Imiter mineralisation on the basis of absolute dating of felsic volcanism at 550 Ma [45,51,101]. Lastly, we suggest that the intermediate to low sulfidation epithermal Au–Ag–Te deposits were emplaced later when magmatism became less abundant, more silicic and alkaline between 550 and 530–520 Ma [74,107,108]. This is supported by the fact that some late rhyolitic dykes do not cross the Cambrian boundary while they cut across mineralised structures, at Qal'at Mgouna for example (Figure 9a)

5.3. Implication of the Tectonic Regime Changes for the Late Neoproterozoic—Early Cambrian Geodynamic Evolution and Ore Deposit Emplacement

In the light of our results, a geodynamic evolution model is proposed (Figure 13), showing the spatial and temporal distribution of metal deposits in the Eastern Anti-Atlas that may be reasonably extended to the whole Anti-Atlas. Considering the tectonic and metallogenetic framework at the scale of the Anti-Atlas regional scale, we suggest a first-order influence of subduction dynamics on the shift with time of metal concentrations and ore deposit types in the Anti-Atlas. In our scenario (Figure 13a,b) and according to Walsh et al. [29], the 615–575 Ma period is characterised by an Andean-type subduction of a wide continuous slab along the northern Gondwana margin (i.e., the currently northern side of South America and Africa). This long period of subduction (ca. 40 Myr) probably occurs because the large slab width (>2000 km) increases the viscous resistance of the mantle on the slab [202]. In that model, oceanic lithosphere *subducts* beneath the continental lithosphere that progressively becomes thicker due to the presence of the West African Craton. Suction between ocean and continent increases, favouring slab flattening and mantle wedge closure [203].

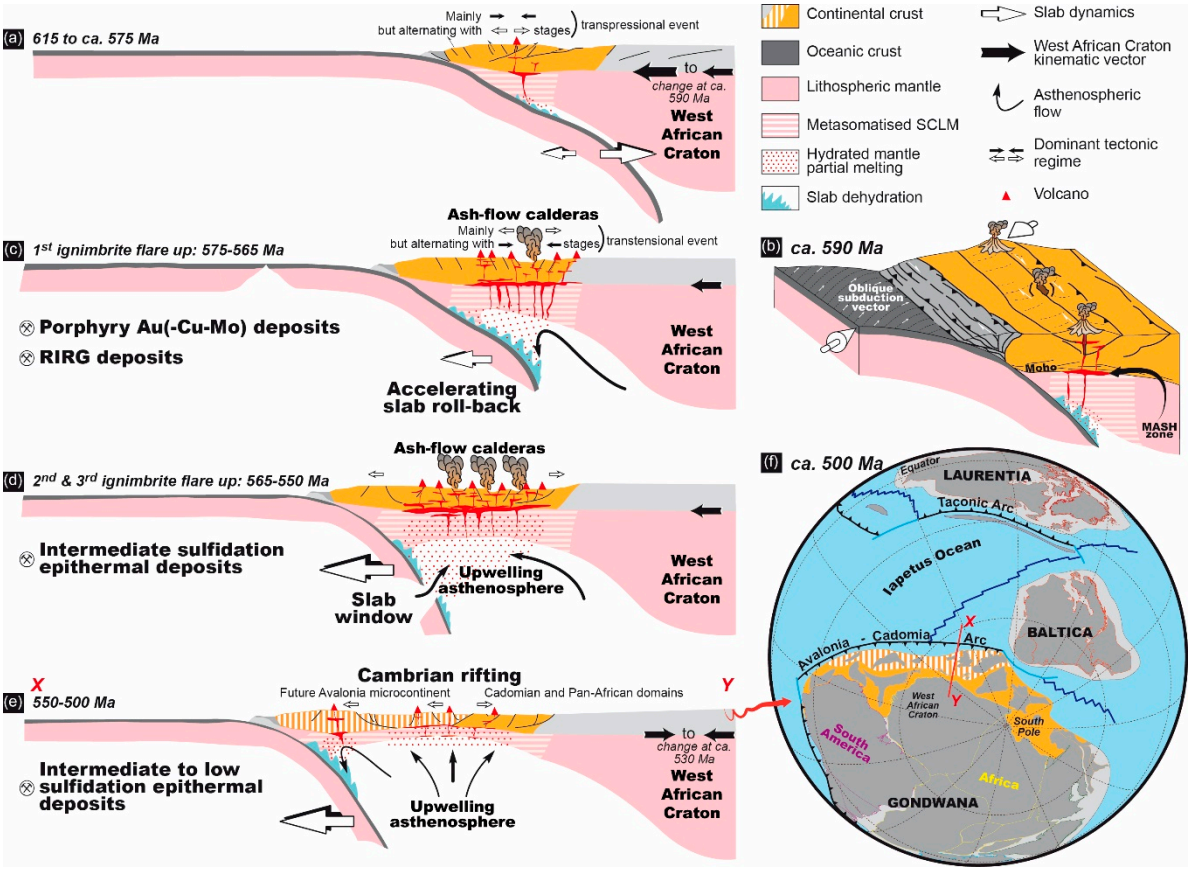

Figure 13. Compiled lithospheric-scale reconstructions (**a**–**e**) of the Pan-African/Cadomian belt systems from the West African Craton foreland to the Iapetus oceanic domain showing the possible progressive slab retreat since ca. 575 Ma to 500 Ma as suggested in text. Zones of partial melting in both the subcontinental lithospheric mantle (SCLM) and the lower crust, as well as the zones of storage and transfer of melts are shown in red. Kinematic vectors related to the West African Craton drifting are from Merdith et al. [204] using the GPlates software [205]. The palaeotectonic map reconstruction of Gondwana (**f**) has been realised using the GPlates software and the global plate models with kinematic continuity of Domeier [206].

Both slab flattening and probably relatively high convergence rate control the D_1 deformation in the overriding plate. A subduction vector (Figure 13b) oblique to the continental margin may explain

the overall transpression regime that characterises the Lower Complex. Indeed, the lack of nappes, fold nappes, mylonitic fabrics and metamorphic gradient preclude a continental collision setting in that period. Possibly, a volcanic arc accretion event may locally emphasize this deformation. Melt generation remains limited given the restricted size of the mantle wedge while their ascent may occur when regional or local extensional regime occurred (Figure 13a,b). Ore forming processes are limited in this setting as they depend on the generation and ascent of fertile melts. However, melts produced and stored at depth in the MASH (melting, assimilation, storage and homogenization) zone may become more fertile in the following stages.

From 575 Ma, the ongoing evolution of the flattened subduction of oceanic beneath cratonic lithospheres causes a dynamic push on the slab surface [203]. This occurs as the rate of wedge closure increases, pushing the slab backward and initiating slab roll-back and high-volume magmatic production (Figure 13c), ultimately leading to the first ignimbrite flare-up. Ongoing slab roll-back along with tectonic regimes becoming more extensional initiate the second, and then the third ignimbrite flare-ups (Figure 13d). Slab tearing and (or) breakoff provide important asthenospheric flow that probably catalyse partial melting of both the asthenospheric mantle wedge and subcontinental lithosphere mantle (SCLM). The latest alkali magmas are assumed to have been emplaced at an extensional stage related to the Adoudounian rift in the Western Anti-Atlas [87,106] that corresponds to a back-arc setting. Such ongoing extensional tectonics [206,207] will ultimately result in the opening of the future Rheic Ocean (Figure 13e,f).

A collision then post-collision scenario cannot be applied to the Anti-Atlas region between 615 and 520 Ma, since subduction do not cease in our model but progressively migrate towards lower latitudes (Figure 13). Eventually, such subduction dynamics determine the dominant stress regime in the overriding plate, which influences the metals mobilization in the MASH zone and, their ascent through the crust, and thus controls the distribution of resulting metal occurrences [208–212].

According to Tosdal and Richards [211], most of the mineralised structures are suggested to have formed during the D_2-related transtensive regime caused by shortening in a WNW–ESE direction and extension along the NNE–SSW direction (Figures 12c and 13c–e). In our interpretation, porphyry Au(–Cu–Mo) and intrusion-related gold deposits are emplaced earlier than the first and(or) second ignimbrite flare-ups (i.e., 575 and(or) 565 Ma). Intermediate sulfidation epithermal Au, Ag deposits may be emplaced during lull periods after the second and (or) the third flare-ups (i.e., 560 and(or) 550 Ma). Compressive structures are indicated in the Zone des Dykes and Imiter districts, as the result of likely a specific structures geometry with respect to the shortening direction. Intermediate to low sulfidation epithermal Au–Ag–Te deposits are emplaced late and in relation with the felsic alkaline magmatic stage (550–520 Ma).

We have stressed here the existence of a long period of magmatism, i.e., over a 95 Myr duration, which is characterised by an increase in produced magmatic volumes, probably in response to geodynamical controls, marked by a late magmatic paroxysm in the form of several ignimbrite flare-ups over a shorter duration of ca. 25 Myr. Such long-lived magmatic activity is paralleled by a tectonic progressive evolution from beginning within transpression conditions to transtension then extension, allowing the mineralisations to take place.

At the regional scale, we may question a possible diachronism of the magmatic activity between the western Bou Azzer and Siroua and the eastern Saghro inliers (Figure 2). Indeed, the main volcanic event occurred between 580 and 560 Ma in Bou Azzer, Siroua and western Saghro inliers. In the central and eastern Jbel Saghro area, volcanic rocks as reported are somewhat younger and mostly dated between 570 and 550 Ma from west to east [51,74]. This suggests that the main volcanic stage progresses toward the east along with the D_2 tectonic regime. If we compare with the Sierra Madre Occidental as a model of large silicic volcanic province [14,147,148,213], the widespread ash-flow tuff deposits of the Anti-Atlas domain should be emplaced as ignimbrite flare-ups and are correlated with progressive and diachronic formation toward the east of caldera collapse structures, broadly oriented E–W to NW–SE. This volcano-structural framework developed coevally with a transtensive tectonic

regime characterised by both NNE–SSW extension and WNW–ESE shortening. In terms of melting processes, the main controlling factor in the generation of such a SLIP is a crustal setting located along a long-lived active subduction zone that evolves into a post-subduction domain via slab-roll back processes. According to Bryan and Ferrari [14] and Ernst [12], a huge thermal pulse is at the origin of a large-scale crustal anataxis of fertile and hydrous lower-crustal materials as well as metasomatised subcontinental lithospheric mantle. Flare-up models are in part inherited from the late evolution of arc settings that underwent slab-roll back, slab-breakoff and slab-window [14,147,148,214], as propoded here and correlated with the D_1 and D_2 tectonic model (Figure 13). Because they represent transient events of high magmatic fluxes from the mantle [215], volcanic flare ups are considered here as highly potential for Ag(–Au) economic deposits emplacement.

6. Conclusions

We document in this paper a long-lived tectono-magmatic event that produced two main litho-structural units we refer to as the Lower and Uper Complexes, respectively. The Lower Complex is coeval with the main Pan-African D_1 deformation consisting of a transpressive regime responsible for folding, faulting and pluton emplacement under the effects of a NW–SE to WNW–ESE direction of shortening from 615 to 575 Ma. The Upper Complex is characterised by the emplacement of large volumes of ash-flow tuffs and volcanoclastic rocks and related intrusions. These were linked with the formation of ash-flow caldera structures which are uncommom examples of preserved Precambrian ash-flow calderas.

Ore deposits (porphyry, intermediate and low sulfidation epithermal deposit types, and IRGD) show strong spatial and temporal relationships with the emplacement of the widespread magmatic units belonging to the Upper Complex. For each ore deposit, fluid circulations associated with plutonic and/or volcanic systems can be invoked to be at the origin of the genesis of economic paragenesis. We suggest that magmatism of the Upper Complex and ore concentrations were both coeval with a D_2 deformation stage (575–540 Ma) and were controlled by the same transtensive tectonic regime under the effect of a nearly WNW–ESE shortening direction.

Despite an incomplete record by absolute datations, we infer that the Jbel Saghro was affected over a long period of time (i.e., 95 Myr) by successively magmatic, magmato-hydrothermal and hydrothermal events which formed a large mineralised province with substantial economic potential. Previous authors have already envisioned such a long period of magmatism and hydrothermalism in the area [29,47,74]. We further defend such a view and contend the Jbel Saghro province compares in this respect to numerous examples of large magmatic-related mineralised systems documented elsewere during the Archaean to Caenozoic times. It may be questioned whether the particular longevity of the magmatic activity in areas dominated by transpressive and transtensive tectonics could be related to the specific behaviour of ancient continental domains in which tectonics are dominated by vertical forces and are linked with especially huge magmatism [216–218]. This debate is currently open and our results illustrate one additional example of long-lived tectono-magmatic event that characterises the late Precambrian in this part or the African continent. Considering the large volume of ash-flow tuffs that crop out in the Western, Central and Eastern Anti-Atlas and their long-lived magmatic activity (575–550 Ma), we infer that the whole Anti-Atlas area (i.e., 700 km long) belongs to a continental silicic large igneous province as defined by Bryan and Ferrari [14], and Ernst [12], and emplaced in a subduction to post-subduction setting and that may be linked to a wide area including the Cadomian segments [28,206,207,219]. Anyway, our results offer further evidence that the majority of metal deposits in the Moroccan Anti-Atlas could be formed during the Neoproterozoic times coevally with the tectonic and magmatic evolutions in this period. They also demonstrate that structural geology can provide relevant constraints for debating the age and mode of formation of ore deposits, specifically in the context of a large silicic magmatic provinces.

Author Contributions: J.T., A.C., L.B. (Luc Barbanson), J.-L.B., M.L., A.E., L.B. (Lakhlifi Badra), C.E.-L., M.D. and S.S. took part in the field investigation; M.L., A.E. and L.M. supported the field investigation; J.T., A.C., L.B.

(Luc Barbanson), J.-L.B., C.E.-L., S.S., and M.D. interpreted the data and took part in the discussion; J.T., A.C., J.-L.B. and M.D. wrote the original draft; J.T. and A.C. reviewed and edited the paper.

Funding: This work has been undertaken with the help of the French-Moroccan programs "Action Intégrée No 222/STU/00".

Acknowledgments: The REMINEX exploration team and SMI mining company provided funds and logistics for field and laboratory studies. We particularly acknowledge El Hajj Bouiroukouten and the intern geologists of MANAGEM for their constant help and support. We are grateful to the Masters students from the BRGM Campus, University of Orléans, University of Lille and LaSalle Beauvais who were involved in the field for geological mapping exercises. Olivier Rouer and Gilles Drouet are warmly thanked for assistance and help with electronic microprobe analyses. The manuscript benefitted considerably from constructive reviews by four anonymous referees.

Conflicts of Interest: The authors declare no conflict of interest.

References

1. Dostal, J.; Caby, R.; Keppie, J.D.; Maza, M. Neoproterozoic magmatism in Southwestern Algeria (Sebkha el Melah inlier): A northerly extension of the Trans-Saharan orogen. *J. Afr. Earth Sci.* **2002**, *35*, 213–225. [CrossRef]
2. Ennih, N.; Liegeois, J.-P. The boundaries of the West African craton, with special reference to the basement of the Moroccan metacratonic Anti-Atlas belt. *Geol. Soc. Lond. Spec. Publ.* **2008**, *297*, 1–17. [CrossRef]
3. Liégeois, J.P.; Latouche, L.; Boughrara, M.; Navez, J.; Guiraud, M. The LATEA metacraton (Central Hoggar, Tuareg shield, Algeria): Behaviour of an old passive margin during the Pan-African orogeny. *J. Afr. Earth Sci.* **2003**, *37*, 161–190. [CrossRef]
4. Ouzegane, K.; Kienast, J.-R.; Bendaoud, A.; Drareni, A. A review of Archaean and Paleoproterozoic evolution of the In Ouzzal granulitic terrane (Western Hoggar, Algeria). *J. Afr. Earth Sci.* **2003**, *37*, 207–227. [CrossRef]
5. Thomas, R.J.; Fekkak, A.; Ennih, N.; Errami, E.; Loughlin, S.C.; Gresse, P.G.; Chevallier, L.P.; Liegeois, J.-P. A new lithostratigraphic framework for the Anti-Atlas Orogen, Morocco. *J. Afr. Earth Sci.* **2004**, *39*, 217–226. [CrossRef]
6. El Bahat, A.; Ikenne, M.; Söderlund, U.; Cousens, B.; Youbi, N.; Ernst, R.; Soulaimani, A.; El Janati, M.H.; Hafid, A. U–Pb baddeleyite ages and geochemistry of dolerite dykes in the Bas Drâa Inlier of the Anti-Atlas of Morocco: Newly identified 1380Ma event in the West African Craton. *Lithos* **2013**, *174*, 85–98. [CrossRef]
7. Ikenne, M.; Söderlund, U.; Ernst, R.E.; Pin, C.; Youbi, N.; El Aouli, E.H.; Hafid, A. A c. 1710 Ma mafic sill emplaced into a quartzite and calcareous series from Ighrem, Anti-Atlas—Morocco: Evidence that the Taghdout passive margin sedimentary group is nearly 1 Ga older than previously thought. *J. Afr. Earth Sci.* **2017**, *127*, 62–76. [CrossRef]
8. Youbi, N.; Kouyaté, D.; Söderlund, U.; Ernst, R.E.; Soulaimani, A.; Hafid, A.; Ikenne, M.; El Bahat, A.; Bertrand, H.; Rkha Chaham, K.; et al. The 1750Ma Magmatic Event of the West African Craton (Anti-Atlas, Morocco). *Precambrian Res.* **2013**, *236*, 106–123. [CrossRef]
9. Davies, J.H.F.L.; Marzoli, A.; Bertrand, H.; Youbi, N.; Ernesto, M.; Schaltegger, U. End-Triassic mass extinction started by intrusive CAMP activity. *Nat. Commun.* **2017**, *8*, 15596. [CrossRef]
10. Knight, K.B.; Nomade, S.; Renne, P.R.; Marzoli, A.; Bertrand, H.; Youbi, N. The Central Atlantic Magmatic Province at the Triassic-Jurassic boundary: Paleomagnetic and $^{40}Ar/^{39}Ar$ evidence from Morocco for brief, episodic volcanism. *Earth Planet. Sci. Lett.* **2004**, *228*, 143–160. [CrossRef]
11. Marzoli, A.; Callegaro, S.; Dal Corso, J.; Davies, J.H.F.L.; Chiaradia, M.; Youbi, N.; Bertrand, H.; Reisberg, L.; Merle, R.; Jourdan, F. The Central Atlantic Magmatic Province (CAMP): A Review. In *The Late Triassic World: Earth in a Time of Transition*; Tanner, L.H., Ed.; Springer International Publishing: Cham, Switzerland, 2018; pp. 91–125.
12. Ernst, R.E. *Large Igneous Provinces*; Cambridge University Press: Cambridge, UK, 2014.
13. Ernst, R.; Bleeker, W. Large igneous provinces (LIPs), giant dyke swarms, and mantle plumes: Significance for breakup events within Canada and adjacent regions from 2.5 Ga to the Present. *Can. J. Earth Sci.* **2010**, *47*, 695–739. [CrossRef]
14. Bryan, S.E.; Ferrari, L. Large igneous provinces and silicic large igneous provinces: Progress in our understanding over the last 25 years. *GSA Bull.* **2013**, *125*, 1053–1078. [CrossRef]

15. Chappell, B.W.; White, A.J.R. Two contrasting granite types: 25 years later. *Aust. J. Earth Sci.* **2001**, *48*, 489–499. [CrossRef]
16. Bonin, B. A-type granites and related rocks: Evolution of a concept, problems and prospects. *Lithos* **2007**, *97*, 1–29. [CrossRef]
17. Ernst, R.E.; Jowitt, S.M. Large Igneous Provinces (LIPs) and Metallogeny. In *Tectonics, Metallogeny, and Discovery: The North American Cordillera and Similar Accretionary Settings*; Colpron, M., Bissig, T., Rusk, B.G., Thompson, J.F.H., Eds.; Society of Economic Geologists: Littleton, CO, USA, 2013; Volume 17, pp. 17–51.
18. Arndt, N.T.; Lesher, C.M.; Czamanske, G.K. Mantle-derived magmas and magmatic Ni-Cu-(PGE) deposits. In *Economic Geology 100th Anniversary Volume*; Hedenquist, J.W., Thompson, J.F.H., Goldfarb, R.J., Richard, J.P., Eds.; Society of Economic Geologists: Littleton, CO, USA, 2005; pp. 5–23.
19. Barnes, S.J.; Holwell, D.A.; Le Vaillant, M. Magmatic Sulfide Ore Deposits. *Elements* **2017**, *13*, 89–95. [CrossRef]
20. Goodenough, K.M.; Schilling, J.; Jonsson, E.; Kalvig, P.; Charles, N.; Tuduri, J.; Deady, E.A.; Sadeghi, M.; Schiellerup, H.; Müller, A.; et al. Europe's rare earth element resource potential: An overview of REE metallogenetic provinces and their geodynamic setting. *Ore Geol. Rev.* **2016**, *72*, 838–856. [CrossRef]
21. Ernst, R.E.; Bell, K. Large igneous provinces (LIPs) and carbonatites. *Mineral. Petrol.* **2010**, *98*, 55–76. [CrossRef]
22. Rao, N.V.C.; Lehmann, B. Kimberlites, flood basalts and mantle plumes: New insights from the Deccan Large Igneous Province. *Earth-Sci. Rev.* **2011**, *107*, 315–324. [CrossRef]
23. Barton, M.D. 13.20—Iron Oxide(–Cu–Au–REE–P–Ag–U–Co) Systems A2—Holland, Heinrich, D. In *Treatise on Geochemistry (Second Edition)*; Turekian, K.K., Ed.; Elsevier: Oxford, UK, 2014; pp. 515–541.
24. Camprubí, A. Tectonic and Metallogenetic History of Mexico. In *Tectonics, Metallogeny, and Discovery: The North American Cordillera and Similar Accretionary Settings*; Colpron, M., Bissig, T., Rusk, B.G., Thompson, J.F.H., Eds.; Society of Economic Geologists: Littleton, CO, USA, 2013; Volume 17, pp. 201–243.
25. Camprubí, A.; Albinson, T. Epithermal deposits in México—Update of current knowledge, and an empirical reclassification. *Geol. Soc. Am. Spec. Pap.* **2007**, *422*, 377–415.
26. Wilkinson, J.J.; Simmons, S.F.; Stoffell, B. How metalliferous brines line Mexican epithermal veins with silver. *Sci. Rep.* **2013**, *3*, 2057. [CrossRef]
27. Ballèvre, M.; Le Goff, E.; Hébert, R. The tectonothermal evolution of the Cadomian belt of northern Brittany, France: A Neoproterozoic volcanic arc. *Tectonophysics* **2001**, *331*, 19–43. [CrossRef]
28. Linnemann, U.; Pereira, F.; Jeffries, T.E.; Drost, K.; Gerdes, A. The Cadomian Orogeny and the opening of the Rheic Ocean: The diacrony of geotectonic processes constrained by LA-ICP-MS U–Pb zircon dating (Ossa-Morena and Saxo-Thuringian Zones, Iberian and Bohemian Massifs). *Tectonophysics* **2008**, *461*, 21–43. [CrossRef]
29. Walsh, G.J.; Benziane, F.; Aleinikoff, J.N.; Harrison, R.W.; Yazidi, A.; Burton, W.C.; Quick, J.E.; Saadane, A. Neoproterozoic tectonic evolution of the Jebel Saghro and Bou Azzer—El Graara inliers, eastern and central Anti-Atlas, Morocco. *Precambrian Res.* **2012**, *216–219*, 23–62. [CrossRef]
30. Boyer, C.; Leblanc, M. Les appareils émissifs de la formation volcanique infracambriennes de Ouarzazate, Anti-Atlas (Maroc). *Comptes rendus hebdomadaires des séances de l'Académie des sciences* **1977**, *285*, 641–644.
31. Moume, W.; Youbi, N.; Marzoli, A.; Bertrand, H.; Gärtner, A.; Linnemann, U.; Gerdes, A.; Ernst, R.; Söderlund, U.; Hachimi Hind, E.; et al. The distribution of the Central Iapetus Magmatic Province (CIMP) into West African craton: U-Pb dating, geochemistry and petrology of Douar Eç-çour and Imiter mafic Dyke Swarms (High and Anti-Atlas, Morocco). In Proceedings of the 2nd Colloquium of the International Geoscience Programme (IGCP638), Casablanca, Morocco, 7–12 November 2017.
32. Puffer, J.H. A late Neoproterozoic eastern Laurentian superplume: Location, size, chemical composition, and environmental impact. *Am. J. Sci.* **2002**, *302*, 1–27. [CrossRef]
33. Barbey, P.; Oberli, F.; Burg, J.P.; Nachit, H.; Pons, J.; Meier, M. The Palaeoproterozoic in western Anti-Atlas (Morocco): A clarification. *J. Afr. Earth Sci.* **2004**, *39*, 239–245. [CrossRef]
34. Burkhard, M.; Caritg, S.; Helg, U.; Robert-Charrue, C.; Soulaimani, A. Tectonics of the Anti-Atlas of Morocco. *Comptes Rendus Geosci.* **2006**, *338*, 11–24. [CrossRef]
35. Missenard, Y.; Zeyen, H.; Frizon de Lamotte, D.; Leturmy, P.; Petit, C.; Sébrier, M.; Saddiqi, O. Crustal versus asthenospheric origin of relief of the Atlas Mountains of Morocco. *J. Geophys. Res. Solid Earth* **2006**, *111*, B03401. [CrossRef]

36. Bourque, H.; Barbanson, L.; Sizaret, S.; Branquet, Y.; Ramboz, C.; Ennaciri, A.; El Ghorfi, M.; Badra, L. A contribution to the synsedimentary versus epigenetic origin of the Cu mineralizations hosted by terminal Neoproterozoic to Cambrian formations of the Bou Azzer–El Graara inlier: New insights from the Jbel Laassel deposit (Anti Atlas, Morocco). *J. Afr. Earth Sci.* **2015**, *107*, 108–118. [CrossRef]
37. Pouit, G. Paléogéographie et répartition des minéralisations stratiformes de cuivre dans l'Anti-Atlas occidental (Maroc). *Chronique de la Recherche Minière* **1966**, *34*, 279–289.
38. Borisenko, A.S.; Lebedev, V.I.; Borovikov, A.A.; Pavlova, G.G.; Kalinin, Y.A.; Nevol'ko, P.A.; Maacha, L.; Kostin, A.V. Forming conditions and age of native silver deposits in Anti-Atlas (Morocco). *Dokl. Earth Sci.* **2014**, *456*, 663–666. [CrossRef]
39. Oberthur, T.; Melcher, F.; Henjes-Kunst, F.; Gerdes, A.; Stein, H.; Zimmerman, A.; El Ghorfi, M. Hercynian age of the cobalt-nickel-arsenide-(gold) ores, Bou Azzer, Anti-Atlas, Morocco: Re-Os, Sm-Nd, and U-Pb age determinations. *Econ. Geol.* **2009**, *104*, 1065–1079. [CrossRef]
40. Essarraj, S.; Boiron, M.-C.; Cathelineau, M.; Banks, D.A.; Benharref, M. Penetration of surface-evaporated brines into the Proterozoic basement and deposition of Co and Ag at Bou Azzer (Morocco): Evidence from fluid inclusions. *J. Afr. Earth Sci.* **2005**, *41*, 25–39. [CrossRef]
41. Essarraj, S.; Boiron, M.-C.; Cathelineau, M.; Tarantola, A.; Leisen, M.; Boulvais, P.; Maacha, L. Basinal Brines at the Origin of the Imiter Ag-Hg Deposit (Anti-Atlas, Morocco): Evidence from LA-ICP-MS Data on Fluid Inclusions, Halogen Signatures, and Stable Isotopes (H, C, O). *Econ. Geol.* **2016**, *111*, 1753–1781. [CrossRef]
42. Abia, E.H.; Nachit, H.; Marignac, C.; Ibhi, A.; Saadi, S.A. The polymetallic Au-Ag-bearing veins of Bou Madine (Jbel Ougnat, eastern Anti-Atlas, Morocco): Tectonic control and evolution of a Neoproterozoic epithermal deposit. *J. Afr. Earth Sci.* **2003**, *36*, 251–271. [CrossRef]
43. Al Ansari, A.E.; Sagon, J.P. Le gisement d'or de Tiouit (Jbel Saghro, Anti-Atlas, maroc). Un système mésothermal polyphasé à sulfures-or et hématite-or dans une granodiorite potassique d'âge Protérozoïque supérieur. *Chronique de la Recherche Minière* **1997**, *527*, 3–25.
44. Leblanc, M.; Lbouabi, M. Native silver mineralization along a rodingite tectonic contact between serpentinite and quartz diorite (Bou Azzer, Morocco). *Econ. Geol.* **1988**, *83*, 1379–1391. [CrossRef]
45. Levresse, G.; Cheilletz, A.; Gasquet, D.; Reisberg, L.; Deloule, E.; Marty, B.; Kyser, K. Osmium, sulphur, and helium isotopic results from the giant Neoproterozoic epithermal Imiter silver deposit, Morocco: Evidence for a mantle source. *Chem. Geol.* **2004**, *207*, 59–79. [CrossRef]
46. Marcoux, E.; Wadjinny, A. Le gisement Ag–Hg de Zgounder (Jebel Siroua, Anti-Atlas, Maroc): Un épithermal néoprotérozoïque de type Imiter. *Comptes Rendus Geosci.* **2005**, *337*, 1439–1446. [CrossRef]
47. Tuduri, J. Processus de formation et relations spatio-temporelles des minéralisations à or et argent en contexte volcanique Précambrien (Jbel Saghro, Anti-Atlas, Maroc). Implications sur les relations déformation-magmatisme-volcanisme-hydrothermalisme. Ph.D. Thesis, University of Orléans, Orléans, France, 2005.
48. Tuduri, J.; Chauvet, A.; Barbanson, L.; Labriki, M.; Dubois, M.; Trapy, P.-H.; Lahfid, A.; Poujol, M.; Melleton, J.; Badra, L.; et al. Structural control, magmatic-hydrothermal evolution and formation of hornfels-hosted, intrusion-related gold deposits: Insight from the Thaghassa deposit in Eastern Anti-Atlas, Morocco. *Ore Geol. Rev.* **2018**, *97*, 171–198. [CrossRef]
49. Essarraj, S.; Boiron, M.-C.; Cathelineau, M.; Banks, D.A.; El Boukhari, A.; Chouhaidi, M.Y. Brines related to Ag deposition in the Zgounder silver deposit (Anti-Atlas, Morocco). *Eur. J. Mineral.* **1998**, *10*, 1201–1214. [CrossRef]
50. Levresse, G.; Bouabdellah, M.; Gasquet, D.; Cheilletz, A. Basinal Brines at the Origin of the Imiter Ag-Hg Deposit (Anti-Atlas, Morocco): Evidence from LA-ICP-MS Data on Fluid Inclusions, Halogen Signatures, and Stable Isotopes (H, C, O)—A Discussion. *Econ. Geol.* **2017**, *112*, 1269–1272. [CrossRef]
51. Cheilletz, A.; Levresse, G.; Gasquet, D.; Azizi-Samir, M.R.; Zyadi, R.; Archibald, A.D.; Farrar, E. The giant Imiter silver deposit: Neoproterozoic epithermal mineralization in the Anti-Atlas, Morocco. *Miner. Depos.* **2002**, *37*, 772–781. [CrossRef]
52. Pelleter, E.; Cheilletz, A.; Gasquet, D.; Mouttaqi, A.; Annich, M.; Camus, Q.; Deloule, E.; Ouazzani, L.; Bounajma, H.; Ouchtouban, L. U/Pb Ages of Magmatism in the Zgounder Epithermal Ag–Hg Deposit, Sirwa Window, Anti-Atlas, Morocco. In *Mineral Deposits of North Africa*; Bouabdellah, M., Slack, J.F., Eds.; Springer International Publishing: Cham, Switzerland, 2016; pp. 143–165.

53. Ahmed, A.H.; Arai, S.; Ikenne, M. Mineralogy and Paragenesis of the Co-Ni Arsenide Ores of Bou Azzer, Anti-Atlas, Morocco. *Econ. Geol.* **2009**, *104*, 249–266. [CrossRef]
54. Ennaciri, A.; Barbanson, L.; Touray, J.C. Mineralized hydrothermal solution cavities in the Co-As Ait Ahmane mine (Bou Azzer, Morocco). *Miner. Depos.* **1995**, *30*, 75–77. [CrossRef]
55. Leblanc, M. Co-Ni arsenide deposits, with accessory gold, in ultramafic rocks from:Morocco. *Can. J. Earth Sci.* **1986**, *23*, 1592–1602. [CrossRef]
56. Thiéblemont, D.; Chêne, F.; Liégeois, J.-P.; Ouabadi, A.; Le Gall, B.; Maury, R.C.; Jalludin, M.; Ouattara Gbélé, C.; Tchaméni, R.; Fernandez-Alonso, M. *Geological Map of Africa at 1:10 Million Scale*, 35th International Geology Congress ed; CCGM-BRGM: Orléans, France, 2016.
57. Hollard, H.; Choubert, G.; Bronner, G.; Marchand, J.; Sougy, J. Carte géologique du Maroc, échelle: 1/1.000.000. *Notes et Mémoires du Service Géologique du Maroc* **1985**, *260*.
58. Mouttaqi, A.; Rjimati, E.; Maacha, A.; Michard, A.; Soulaimani, A.; Ibouh, H. Les principales mines du Maroc. *Notes et Mémoires du Service Géologique du Maroc* **2011**, *564*, 375.
59. Thomas, R.J.; Chevallier, L.P.; Gresse, P.G.; Harmer, R.E.; Eglington, B.M.; Armstrong, R.A.; de Beer, C.H.; Martini, J.E.J.; de Kock, G.S.; Macey, P.H.; et al. Precambrian evolution of the Sirwa Window, Anti-Atlas Orogen, Morocco. *Precambrian Res.* **2002**, *118*, 1–57. [CrossRef]
60. Goldfarb, R.J.; Groves, D.I. Orogenic gold: Common or evolving fluid and metal sources through time. *Lithos* **2015**, *233*, 2–26. [CrossRef]
61. Groves, D.I.; Santosh, M.; Goldfarb, R.J.; Zhang, L. Structural geometry of orogenic gold deposits: Implications for exploration of world-class and giant deposits. *Geosci. Front.* **2018**, *9*, 1163–1177. [CrossRef]
62. Hart, C.J. Reduced intrusion-related gold systems. In *Mineral Deposits of Canada: A Synthesis of Major Deposit Types, District Metallogeny, the Evolution of Geological Provinces, and Exploration Methods*; Special Publication; Geological Association of Canada, Mineral Deposits Division: St. John's, NL, Canada, 2007; pp. 95–112.
63. Kontak, D.; O'Reilly, G.; MacDonald, M.; Horne, R.; Smith, P. Gold in the Meguma Terrane, Southern Nova Scotia: Is There a Continuum between Mesothermal Lode Gold and Intrusion-related Gold Systems? In Proceedings of the 49th Annual Meeting of the GAC-MAC, St. Catharines, ON, Canada, 12–14 May2004; p. 128.
64. Lang, J.R.; Baker, T. Intrusion-related gold systems: The present level of understanding. *Miner. Depos.* **2001**, *36*, 477–489. [CrossRef]
65. Walshe, J.; Neumayr, P.; Cooke, D. Two boxes we don't need: Orogenic and intrusion-related gold systems. In Proceedings of the STOMP 2005: Structure, Tectonics and Ore Mineralisation Processes, Townsville, Australia, 29 August–2 September 2005; EGRU: Townsville, Australia, 2005; p. 143.
66. Boiron, M.-C.; Cathelineau, M.; Banks, D.A.; Fourcade, S.; Vallance, J. Mixing of metamorphic and surficial fluids during the uplift of the Hercynian upper crust: Consequences for gold deposition. *Chem. Geol.* **2003**, *194*, 119–141. [CrossRef]
67. Vallance, J.; Cathelineau, M.; Boiron, M.C.; Fourcade, S.; Shepherd, T.J.; Naden, J. Fluid-rock interactions and the role of late Hercynian aplite intrusion in the genesis of the Castromil gold deposit, northern Portugal. *Chem. Geol.* **2003**, *194*, 201–224. [CrossRef]
68. Baker, T.; Lang, J.R. Fluid inclusion characteristics of intrusion-related gold mineralization, Tombstone–Tungsten magmatic belt, Yukon Territory, Canada. *Mineral. Depos.* **2001**, *36*, 563–582. [CrossRef]
69. Chauvet, A.; Volland-Tuduri, N.; Lerouge, C.; Bouchot, V.; Monié, P.; Charonnat, X.; Faure, M. Geochronological and geochemical characterization of magmatic-hydrothermal events within the Southern Variscan external domain (Cévennes area, France). *Int. J. Earth Sci.* **2012**, *101*, 69–86. [CrossRef]
70. Mustard, R.; Ulrich, T.; Kamenetsky, V.S.; Mernagh, T. Gold and metal enrichment in natural granitic melts during fractional crystallization. *Geology* **2006**, *34*, 85–88. [CrossRef]
71. Gouiza, M.; Charton, R.; Bertotti, G.; Andriessen, P.; Storms, J.E.A. Post-Variscan evolution of the Anti-Atlas belt of Morocco constrained from low-temperature geochronology. *Int. J. Earth Sci.* **2017**, *106*, 593–616. [CrossRef]
72. Teixell, A.; Ayarza, P.; Zeyen, H.; Fernàndez, M.; Arboleya, M.-L. Effects of mantle upwelling in a compressional setting: The Atlas Mountains of Morocco. *Terra Nova* **2005**, *17*, 456–461. [CrossRef]
73. Choubert, G. Histoire géologique du Précambrien de l'Anti-Atlas de l'Archéen à l'aurore des temps primaires. *Notes et Mémoires du Service Géologique du Maroc* **1963**, *162*, 352.

74. Gasquet, D.; Levresse, G.; Cheilletz, A.; Azizi-Samir, M.R.; Mouttaqi, A. Contribution to a geodynamic reconstruction of the Anti-Atlas (Morocco) during Pan-African times with the emphasis on inversion tectonics and metallogenic activity at the Precambrian-Cambrian transition. *Precambrian Res.* **2005**, *140*, 157–182. [CrossRef]
75. Hefferan, K.; Soulaimani, A.; Samson, S.D.; Admou, H.; Inglis, J.; Saquaque, A.; Latifa, C.; Heywood, N. A reconsideration of Pan African orogenic cycle in the Anti-Atlas Mountains, Morocco. *J. Afr. Earth Sci.* **2014**, *98*, 34–46. [CrossRef]
76. Leblanc, M.; Lancelot, J.R. Interprétation géodynamique du domaine panafricain (Précambrien terminal) de l'Anti-Atlas (Maroc) à partir de données géologiques et géochronologiques. *Can. J. Earth Sci.* **1980**, *17*, 142–155. [CrossRef]
77. Saquaque, A.; Benharref, M.; Abia, H.; Mrini, Z.; Reuber, I.; Karson, J.A. Evidence for a Panafrican volcanic arc and wrench fault tectonics in Jbel Saghro, Morocco. *Geol. Rundsch.* **1992**, *81*, 1–13. [CrossRef]
78. Blein, O.; Baudin, T.; Chèvremont, P.; Soulaimani, A.; Admou, H.; Gasquet, P.; Cocherie, A.; Egal, E.; Youbi, N.; Razin, P.; et al. Geochronological constraints on the polycyclic magmatism in the Bou Azzer-El Graara inlier (Central Anti-Atlas Morocco). *J. Afr. Earth Sci.* **2014**, *99*, 287–306. [CrossRef]
79. El Hadi, H.; Simancas, J.F.; Martínez-Poyatos, D.; Azor, A.; Tahiri, A.; Montero, P.; Fanning, C.M.; Bea, F.; González-Lodeiro, F. Structural and geochronological constraints on the evolution of the Bou Azzer Neoproterozoic ophiolite (Anti-Atlas, Morocco). *Precambrian Res.* **2010**, *182*, 1–14. [CrossRef]
80. Inglis, J.D.; D'Lemos, R.S.; Samson, S.D.; Admou, H. Geochronological constraints on late Precambrian intrusions, metamorphism, and tectonism in the Anti-Atlas mountains. *J. Geol.* **2005**, *113*, 439–450. [CrossRef]
81. Inglis, J.D.; MacLean, J.S.; Samson, S.D.; D'Lemos, R.S.; Admou, H.; Hefferan, K. A precise U-Pb zircon age for the BleIda granodiorite, Anti-Atlas, Morocco: Implications for the timing of deformation and terrane assembly in the eastern Anti-Atlas. *J. Afr. Earth Sci.* **2004**, *39*, 277. [CrossRef]
82. Saquaque, A.; Admou, H.; Karson, J.; Hefferan, K.; Reuber, I. Precambrian accretionary tectonics in the Bou Azzer-El Graara region, Anti-Atlas, Morocco. *Geology* **1989**, *17*, 1107–1110. [CrossRef]
83. Gasquet, D.; Ennih, N.; Liégeois, J.-P.; Soulaimani, A.; Michard, A. The Pan-African Belt. In *Continental Evolution: The Geology of Morocco*; Michard, A., Saddiqi, O., Chalouan, A., Frizon de Lamotte, D., Eds.; Springer-Verlag: Berlin/Heidelberg, Germany, 2008; pp. 33–64.
84. Álvaro, J.J.; Benziane, F.; Thomas, R.; Walsh, G.J.; Yazidi, A. Neoproterozoic–Cambrian stratigraphic framework of the Anti-Atlas and Ouzellagh promontory (High Atlas), Morocco. *J. Afr. Earth Sci.* **2014**, *98*, 19–33. [CrossRef]
85. Choubert, G. In Essai d'application de la notion d'Infracambrien aux formations anciennes de l'Anti-Atlas (Maroc). In Proceedings of the 19th International Geological Congress, Alger, Algeria, 8–15 September 1952; pp. 33–71.
86. Soulaimani, A.; Michard, A.; Ouanaimi, H.; Baidder, L.; Raddi, Y.; Saddiqi, O.; Rjimati, E.C. Late Ediacaran–Cambrian structures and their reactivation during the Variscan and Alpine cycles in the Anti-Atlas (Morocco). *J. Afr. Earth Sci.* **2014**, *98*, 94–112. [CrossRef]
87. Soulaimani, A.; Bouabdelli, M.; Piqué, A. The Upper Neoproterozoic-Lower Cambrian continental extension in the Anti-Atlas (Morocco). *Bulletin de la Société Géologique de France* **2003**, *174*, 83–92. [CrossRef]
88. Chèvremont, P.; Blein, O.; Razin, P.; Baudin, T.; Barbanson, L.; Gasquet, D.; Soulaimani, A.; Admou, H.; Youbi, N.; Bouabdelli, M.; et al. Carte géologique du Maroc (1/50 000), feuille de Bou Azer. *Notes et Mémoires du Service Géologique du Maroc* **2013**, *535bis*, 153.
89. Ducrot, J.; Lancelot, J.R. Problème de la limite Précambrien–Cambrien: Étude radiochronologique par la méthode U–Pb sur zircons du volcan du Jbel Boho (Anti-Atlas marocain). *Can. J. Earth Sci.* **1977**, *14*, 2771–2777. [CrossRef]
90. Maloof, A.C.; Schrag, D.P.; Crowley, J.L.; Bowring, S.A. An expanded record of Early Cambrian carbon cycling from the Anti-Atlas Margin, Morocco. *Can. J. Earth Sci.* **2005**, *42*, 2195–2216. [CrossRef]
91. Fekkak, A.; Pouclet, A.; Ouguir, H.; Ouazzani, H.; Badra, L.; Gasquet, D. Géochimie et signification géotectonique des volcanites du Cryogénien inférieur du Saghro (Anti-Atlas oriental, Maroc). *Geodin. Acta* **2001**, *13*, 1–13.
92. Ouguir, H.; Macaudière, J.; Dagallier, G. Le Protérozoïque supérieur d'Imiter, Saghro oriental, Maroc: Un contexte géodynamique d'arrière arc. *J. Afr. Earth Sci.* **1996**, *22*, 173–189. [CrossRef]

93. Baidder, L.; Raddi, Y.; Tahiri, M.; Michard, A. Devonian extension of the Pan-African crust north of the West African craton, and its bearing on the Variscan foreland deformation: Evidence from eastern Anti-Atlas (Morocco). *Geol. Soc. Lond. Spec. Publ.* **2008**, *297*, 453–465. [CrossRef]
94. Malusà, M.G.; Polino, R.; Feroni, A.C.; Ellero, A.; Ottria, G.; Baidder, L.; Musumeci, G. Post-Variscan tectonics in eastern Anti-Atlas (Morocco). *Terra Nova* **2007**, *19*, 481–489. [CrossRef]
95. Michard, A.; Soulaimani, A.; Hoepffner, C.; Ouanaimi, H.; Baidder, L.; Rjimati, E.C.; Saddiqi, O. The South-Western Branch of the Variscan Belt: Evidence from Morocco. *Tectonophysics* **2010**, *492*, 1–24. [CrossRef]
96. Frizon de Lamotte, D.; Tavakoli-Shirazi, S.; Leturmy, P.; Averbuch, O.; Mouchot, N.; Raulin, C.; Leparmentier, F.; Blanpied, C.; Ringenbach, J.-C. Evidence for Late Devonian vertical movements and extensional deformation in northern Africa and Arabia: Integration in the geodynamics of the Devonian world. *Tectonics* **2013**, *32*, 107–122. [CrossRef]
97. Alvaro, J.J.; Macouin, M.; Ezzouhairi, H.; Charif, A.; Ayad, N.A.; Ribeiro, M.L.; Ader, M. Late Neoproterozoic carbonate productivity in a rifting context: The Adoudou Formation and its associated bimodal volcanism onlapping the western Saghro inlier, Morocco. *Geol. Soc. Lond. Spec. Publ.* **2008**, *297*, 285–302. [CrossRef]
98. Álvaro, J.J. Late Ediacaran syn-rift/post-rift transition and related fault-driven hydrothermal systems in the Anti-Atlas Mountains, Morocco. *Basin Res.* **2013**, *25*, 348–360. [CrossRef]
99. Sebti, S.; Saddiqi, O.; El Haimer, F.Z.; Michard, A.; Ruiz, G.; Bousquet, R.; Baidder, L.; Frizon de Lamotte, D. Vertical movements at the fringe of the West African Craton: First zircon fission track datings from the Anti-Atlas Precambrian basement, Morocco. *Comptes Rendus Geosci.* **2009**, *341*, 71–77. [CrossRef]
100. Caritg, S.; Burkhard, M.; Ducommun, R.; Helg, U.; Kopp, L.; Sue, C. Fold interference patterns in the Late Palaeozoic Anti-Atlas belt of Morocco. *Terra Nova* **2004**, *16*, 27–37.
101. Levresse, G.; Bouabdellah, M.; Cheilletz, A.; Gasquet, D.; Maacha, L.; Tritlla, J.; Banks, D.; Moulay Rachid, A.S. Degassing as the Main Ore-Forming Process at the Giant Imiter Ag–Hg Vein Deposit in the Anti-Atlas Mountains, Morocco. In *Mineral Deposits of North Africa*; Bouabdellah, M., Slack, J.F., Eds.; Springer International Publishing: Cham, Switzerland, 2016; pp. 85–106.
102. Tuduri, J.; Chauvet, A.; Ennaciri, A.; Barbanson, L. Modèle de formation du gisement d'argent d'Imiter (Anti-Atlas oriental, Maroc). Nouveaux apports de l'analyse structurale et minéralogique. *Comptes Rendus Geosci.* **2006**, *338*, 253–261. [CrossRef]
103. Bouabdellah, M.; Maacha, L.; Jébrak, M.; Zouhair, M. Re/Os Age Determination, Lead and Sulphur Isotope Constraints on the Origin of the Bouskour Cu–Pb–Zn Vein-Type Deposit (Eastern Anti-Atlas, Morocco) and Its Relationship to Neoproterozoic Granitic Magmatism. In *Mineral Deposits of North Africa*; Bouabdellah, M., Slack, F.J., Eds.; Springer International Publishing: Cham, Switzerland, 2016; pp. 277–290.
104. Hindermeyer, J.; Choubert, G.; Destombes, J.; Gauthier, H. Carte géologique de l'Anti-Atlas oriental: Feuille Dadès et Jbel Saghro 1/200 000. *Notes et Mémoires du Service Géologique du Maroc* **1977**, *161*.
105. Baidada, B.; Ikenne, M.; Barbey, P.; Soulaimani, A.; Cousens, B.; Haissen, F.; Ilmen, S.; Alansari, A. SHRIMP U–Pb zircon geochronology of the granitoids of the Imiter Inlier: Constraints on the Pan-African events in the Saghro massif, Anti-Atlas (Morocco). *J. Afr. Earth Sci.* **2018**. [CrossRef]
106. De Wall, H.; Kober, B.; Errami, E.; Ennih, N.; Greiling, R.O. Age de mise en place et contexte géologique des granitoïdes de la boutonnière d'Imiter (Saghro oriental, Anti-Atlas, Maroc). In Proceedings of the 2ème Colloque International 3MA (Magmatisme, Métamorphisme & Minéralisations Associées), Marrakech, Maroc, 10–12 May 2001; p. 19.
107. O'Connor, E.; Barnes, R.; Beddoe-Stephens, B.; Fletcher, T.; Gillespie, M.; Hawkins, M.; Loughlin, S.; Smith, M.; Smith, R.; Waters, C. *Geology of the Drâa, Kerdous, and Boumalne districts, Anti-Atlas, Morocco*; British Geological Survey: Nottingham, UK, 2010; p. 310.
108. Schiavo, A.; Taj Eddine, K.; Algouti, A.; Benvenuti, M.; Dal Piaz, G.V.; Eddebi, A.; El Boukhari, A.; Laftouhi, N.; Massironi, M.; Ounaimi, H.; et al. Carte géologique du Maroc au 1/50000, feuille Imtir. *Notes et Mémoires du Service Géologique du Maroc* **2007**, *518*.
109. Charlot, R.; Choubert, G.; Faure-Muret, A.; Tisserant, D. Etude géochronologique du Précambrien de l'Anti-Atlas (Maroc). *Notes et Mémoires du Service Géologique du Maroc* **1970**, *30*, 99–134.
110. Choubert, G. Sur le Précambrien marocain. *Comptes rendus hebdomadaires des séances de l'Académie des sciences* **1945**, *221*, 249–251.

111. Hindermeyer, J. Le Précambrien I et le Précambrien II du Saghro. *Comptes rendus hebdomadaires des séances de l'Académie des sciences* **1953**, *237*, 921–923.
112. Hindermeyer, J. Le Précambrien III du Saghro. *Comptes rendus hebdomadaires des séances de l'Académie des sciences* **1953**, *237*, 1024–1026.
113. Derré, C.; Lécolle, M. Altérations hydrothermales dans le Protérozoïque supérieur du Saghro (Anti-Atlas oriental). Relations avec les minéralisations. *Chronique de la Recherche Minière* **1999**, *536–537*, 39–61.
114. Fekkak, A.; Boualoul, M.; Badra, L.; Amenzou, M.; Saquaque, A.; El-Amrani, I.E. Origine et contexte géotectonique des dépôts détritiques du Groupe Néoprotérozoïque inférieur de Kelaat Mgouna (Anti-Atlas Oriental, Maroc). *J. Afr. Earth Sci.* **2000**, *30*, 295–311. [CrossRef]
115. Fekkak, A.; Pouclet, A.; Badra, L. The Pre-Panafrican rifting of Saghro (Anti-Atlas, Morocco): Exemple of the middle Neoproterozoic Basin of Boumalne. *Bulletin de la Société Géologique de France* **2002**, *173*, 25–35. [CrossRef]
116. Fekkak, A.; Pouclet, A.; Benharref, M. The Middle Neoproterozoic Sidi Flah Group (Anti-Atlas, Morocco): Synrift deposition in a Pan-African continent/ocean transition zone. *J. Afr. Earth Sci.* **2003**, *37*, 73–87. [CrossRef]
117. Fekkak, A.; Pouclet, A.; Ouguir, H.; Badra, L.; Gasquet, D. The Kelaat Mgouna early Neoproterozoic Group (Saghro, Anti-Atlas, Morocco): Witness of an initial stage of the pre-Pan-African extension. *Bulletin de la Société Géologique de France* **1999**, *170*, 789–797.
118. Marini, F.; Ouguir, H. Un nouveau jalon dans l'histoire de la distension pré-panafricaine au Maroc: Le Précambrien II des boutonnières du Jbel Saghro nord-oriental (Anti-Atlas, Maroc). *Comptes Rendus de l'Académie des Sciences Série II Mécanique-physique Chimie, Sciences de l'univers, Sciences de la Terre* **1990**, *310*, 577–582.
119. Errami, E.; Bonin, B.; Laduron, D.; Lasri, L. Petrology and geodynamic significance of the post-collisional Pan-African magmatism in the Eastern Saghro area (Anti-Atlas, Morocco). *J. Afr. Earth Sci.* **2009**, *55*, 105–124. [CrossRef]
120. Liégeois, J.-P.; Fekkak, A.; Bruguier, O.; Errami, E.; Ennih, N. The Lower Ediacaran (630–610 Ma) Saghro group: An orogenic transpressive basin development during the early metacratonic evolution of the Anti-Atlas (Morocco). In Proceedings of the IGCP485 4th Meeting, Algiers, Algeria, 2 September 2006; p. 57.
121. Ighid, L.; Saquaque, A.; Reuber, I. Plutons syn-cinématiques et la déformation panafricaine majeure dans le Saghro oriental (boutonnière d'Imiter, Anti-Atlas, Maroc). *Comptes Rendus de l'Académie des Sciences Série II Mécanique-physique Chimie, Sciences de l'univers Sciences de la Terre* **1989**, *309*, 615–620.
122. El Baghdadi, M.; El Boukhari, A.; Jouider, A.; Benyoucef, A.; Nadem, S. Calc-alkaline arc I-type granitoid associated with S-type granite in the Pan-African belt of eastern Anti-Atlas (Saghro and Ougnat, South Morocco). *Gondwana Res.* **2003**, *6*, 557–572. [CrossRef]
123. Errami, E.; Olivier, P. The Iknioun granodiorite, tectonic marker of Ediacaran SE-directed tangential movements in the Eastern Anti-Atlas, Morocco. *J. Afr. Earth Sci.* **2012**, *69*, 1–12. [CrossRef]
124. Karl, A.; de Wall, H.; Rieger, M.; Schmitt, T.; Errami, E.; Kober, B.; Greiling, R.O. Petrography and geochemistry of the Bou Teglimt, Taouzzakt and Igoudrane intrusions in the Eastern Saghro (Anti Atlas, Morocco). In *Magmatic evolution of a Neoproterozoic island-arc: Syn- to post-orogenic igneous activity in the Anti-Atlas (Morocco)*; de Wall, H., Greiling, R.O., Eds.; Forschungszentrum Jülich, International Cooperation, Scientific Series: Jülich, Germany, 2001; Volume 45, pp. 243–253.
125. Ouguir, H.; Macaudière, J.; Dagallier, G.; Qadrouci, A.; Leistel, J.-M. Cadre structural du gîte Ag-Hg d'Imiter (Anti-Atlas, Maroc); implication métallogénique. *Bulletin de la Société Géologique de France* **1994**, *165*, 233–248.
126. Massironi, M.; Moratti, G.; Algouti, A.; Benvenuti, M.; Dal Piaz, G.V.; Eddebi, A.; El Boukhari, A.; Laftouhi, N.; Ounaimi, H.; Schiavo, A.; et al. Carte géologique du Maroc au 1/50000, feuille Boumalne. *Notes et Mémoires du Service Géologique du Maroc* **2007**, *521*.
127. Leistel, J.-M.; Qadrouci, A. Le gisement argentifère d'Imiter (Protérozoïque supérieur de l'Anti-Atlas, Maroc). Contrôles des mineralisations, hypothèses génétiques et perspectives pour l'exploration. *Chronique de la Recherche Minière* **1991**, *502*, 5–22.
128. Benkirane, Y. Les minéralisations à W (Sn, Mo, Au, Bi, Ag, Cu, Pb, Zn) du granite de Taourirt-Tamellalt dans leur cadre géologique, la boutonnière protérozoïque du SE de Boumalne du Dadès (Saghro oriental, Anti-Atlas, Maroc). In *3ème Cycle*; Université de Paris VI: Paris, France, 1987.

129. Lécolle, M.; Derré, C.; Nerci, K. The Proterozoic sulphide alteration pipe of Sidi Flah and its host series. New data for the geotectonic evolution of the Pan-African Belt in the eastern Anti-Atlas (Morocco). *Ore Geol. Rev.* **1991**, *6*, 501–536. [CrossRef]
130. Benziane, F. Lithostratigraphie et évolution géodynamique de l'anti-Atlas (Maroc) du paléoprotérozoïque au néoprotérozoïque: Exemples de la boutonnière de Tagragra Tata et du Jebel Saghro. In *3ème Cycle*; Université de Chambéry: Chambéry, France, 2007.
131. Bajja, A. Volcanisme syn à post orogénique du Néoprotérozoïque de l'Anti-Atlas: Implications pétrogénétiques et géodynamiques. Ph.D. Thesis, Université Chouaib Doukkali, El Jadida, Maroc, 1998.
132. Benharref, M. Le Précambrien de la boutonnière d'El Kelaa des M'Gouna (Saghro, Anti-Atlas, Maroc). Pétrographie et structures de l'ensemble. Implications lithostratigraphiques et géodynamiques. In *3ème Cycle*; Université Cadi Ayyad: Marrakech, Maroc, 1991.
133. Bouladon, J.; Jouravsky, G. Les ignimbrites du Précambrien III de Tiouine et du sud marocain. *Notes et Mémoires du Service Géologique du Maroc* **1954**, *120*, 37–59.
134. Fauvelet, E.; Hindermeyer, J. Note préliminaire sur les granites associés à des coulées rhyolitiques au Sud de Ouarzazate (Anti-Atlas central) et dans le Sarho. *C. R. Hebd. Seances Acad. Sci.* **1952**, *234*, 2626–2628.
135. Mifdal, A.; Peucat, J. Datation U-Pb et Rb-Sr du volcanisme acide de l'Anti-Atlas marocain et du socle sous-jacent dans la région de Ouarzazate. Apport au problème de la limite Précambrien-Cambrien. *Sci. Géol. Bull.* **1985**, *38*, 185–200.
136. Acocella, V. Understanding caldera structure and development: An overview of analogue models compared to natural calderas. *Earth-Sci. Rev.* **2007**, *85*, 125–160. [CrossRef]
137. Lipman, P.W. The roots of ash flow calderas in western north america: Windows into the tops of granitic batholiths. *J. Geophys. Res. Solid Earth* **1984**, *89*, 8801–8841. [CrossRef]
138. Lipman, P.W. Subsidence of ash-flow calderas: Relation to caldera size and magma-chamber geometry. *Bull. Volcanol.* **1997**, *59*, 198–218. [CrossRef]
139. Williams, H. Calderas and their origin. University of California publications. *Bull. Dep. Geol. Sci.* **1941**, *25*, 239–346.
140. Acocella, V.; Korme, T.; Salvini, F.; Funiciello, R. Elliptic calderas in the Ethiopian Rift: Control of pre-existing structures. *J. Volcanol. Geotherm. Res.* **2003**, *119*, 189–203. [CrossRef]
141. Holohan, E.P.; Troll, V.R.; Walter, T.R.; Münn, S.; McDonnell, S.; Shipton, Z.K. Elliptical calderas in active tectonic settings: An experimental approach. *J. Volcanol. Geotherm. Res.* **2005**, *144*, 119–136. [CrossRef]
142. Ross, C.S.; Smith, R.L. Ash-flow tuffs: Their origin, geologic relations and identification. *Geol. Surv. Prof. Pap.* **1961**, *366*, 81.
143. Smith, R.L. Ash flows. *Geol. Soc. Am. Bull.* **1960**, *71*, 795–842. [CrossRef]
144. Smith, R.L.; Bailey, R.A. Resurgent cauldrons. *Geol. Soc. Am. Mem.* **1968**, *116*, 613–662.
145. Bellier, O.; Sébrier, M. Relationship between tectonism and volcanism along the Great Sumatran Fault Zone deduced by image analyses. *Tectonophysics* **1994**, *233*, 215–231. [CrossRef]
146. Chesner, C.A.; Rose, W.I. Stratigraphy of the Toba Tuffs and the evolution of the Toba Caldera Complex, Sumatra, Indonesia. *Bull. Volcanol.* **1991**, *53*, 343–356. [CrossRef]
147. Ferrari, L.; Valencia-Moreno, M.; Bryan, S. Magmatism and tectonics of the Sierra Madre Occidental and its relation with the evolution of the western margin of North America. *Geol. Soc. Am. Spec. Pap.* **2007**, *422*, 1–39.
148. Ferrari, L.; Lopez-Martinez, M.; Rosas-Elguera, J. Ignimbrite flare-up and deformation in the southern Sierra Madre Occidental, western Mexico: Implications for the late subduction history of the Farallon plate. *Tectonics* **2002**, *21*. [CrossRef]
149. Lécuyer, F.; Bellier, O.; Gourgaud, A.; Vincent, P.M. Tectonique active du Nord-Est de Sulawesi(Indonésie) et contrôle structural de la caldeira de Tondano. *Comptes Rendus de l'Academie des Sciences Ser. IIA Earth Planet. Sci.* **1997**, *325*, 607–613. [CrossRef]
150. Van Wyk de Vries, B.; Merle, O. Extension induced by volcanic loading in regional strike-slip zones. *Geology* **1998**, *26*, 983–986. [CrossRef]

151. Tuduri, J.; Chauvet, A.; Barbanson, L.; Labriki, M.; Badra, L. In Atypical gold mineralization within the Neoproterozoic of Morocco. Structural and mineralogical constraints from the Thaghassa prospect (Boumalne inlier, Jbel Saghro, Eastern Anti-Atlas). In Proceedings of the Mineral Exploration and Sustainable Development, Athens, Greece, 24–28 August 2003; Eliopoulos, D.G., Ed.; Millpress: Athens, Greece; pp. 537–540.
152. Goldstein, R.H.; Reynolds, T.J. *Systematics of Fluid Inclusions in Diagenetic Minerals*; Society for Sedimentary Geology: Broken Arrow, OK, USA, 1994; Volume 31, p. 199.
153. Lécolle, M.; Derré, C.; Rjimati, E.C.; Fonteilles, M.; Azza, A.; Benanni, A. Une altération hydrothermale peralumineuse à silicates, phosphates et rutile dans le Protérozoïque supérieur du Saghro (Anti-Atlas, Maroc). Genèse et implications métallogéniques. *Comptes Rendus de l'Académie des Sciences Série II Mécanique-physique Chimie Sciences de l'univers Sciences de la Terre* **1993**, *316*, 123–130.
154. Tuduri, J.; Dubois, M.; Try, E.; Chauvet, A.; Barbanson, L.; Ennaciri, A. The porphyry to epithermal transition in atypical late Neoproterozoic REE-Au-Ag-Te occurrences. *Acta Mineral.-Petrogr. Abstr. Ser.* **2010**, *6*, 288.
155. Delapierre, A. Etude de la minéralisation aurifère d'Isamlal (Jbel Saghro, Anti-Atlas, Maroc). In *Mem. Diplôme*; Université de Lausanne: Lausanne, Switzerland, 2000; p. 128.
156. Leloix, C. Etude des minéralisations aurifères épithermales d'Isamlal. District de Kelaat M'Gouna (Anti-Atlas, Maroc). In *Rapport Reminex*; Université d'Orléans: Orléans, France, 1999; p. 44.
157. Sizaret, S. Etude des minéralisations aurifères d'Isamlal (district de Kelâa M'Gouna, Anti-Atlas, Maroc). Master's Thesis, Université d'Orléans, Orléans, France, 1999.
158. Gaspard, E. Etude du prospect d'Isamlal (Anti-Atlas Oriental- Maroc): Caractérisation d'un porphyre à Au-Cu-Mo. Master's Thesis, Université d'Orléans—ENAG, Orléans, France, 2014.
159. Try, E.; Dubois, M.; Tuduri, J.; Ventalon, S.; Potdevin, J.-L.; Chauvet, A.; Barbanson, L. The transition between porphyric and epithermal styles: Insights from F.I. of the Kelâa M'Gouna prospect, Morocco. In Proceedings of the ECROFI-XX 20th Biennial Conferences, Granada, Spain, 21–27 September 2009; Volume 20, pp. 261–262.
160. Tomczyk, C. Âge de mise en place et modèle génétique du stockwerk du prospect à Au-Ag-Te de Kelâa M'Gouna (Maroc). Master's Thesis, University of Lille, Lille, France, 2010.
161. Dong, G.; Morrison, G.; Jaireth, S. Quartz textures in epithermal veins, Queensland; classification, origin and implication. *Econ. Geol.* **1995**, *90*, 1841–1856. [CrossRef]
162. Etoh, J.; Izawa, E.; Watanabe, K.; Taguchi, S.; Sekine, R. Bladed quartz and its relationship to gold mineralization in the Hishikari low-sulfidation epithermal gold deposit, Japan. *Econ. Geol.* **2002**, *97*, 1841–1851. [CrossRef]
163. André-Mayer, A.-S.; Leroy, J.L.; Bailly, L.; Chauvet, A.; Marcoux, E.; Grancea, L.; Llosa, F.; Rosas, J. Boiling and vertical mineralization zoning: A case study from the Apacheta low-sulfidation epithermal gold-silver deposit, southern Peru. *Mineral. Depos.* **2002**, *37*, 452–464. [CrossRef]
164. Chauvet, A.; Bailly, L.; André, A.-S.; Monié, P.; Cassard, D.; Tajada, F.; Vargas, J.; Tuduri, J. Internal vein texture and vein evolution of the epithermal Shila-Paula district, southern Peru. *Mineral. Depos.* **2006**, *41*, 387–410. [CrossRef]
165. Simmons, S.F.; Christenson, B.W. Origins of calcite in a boiling geothermal system. *Am. J. Sci.* **1994**, *294*, 361–400. [CrossRef]
166. Saule, A. La Zones des Dykes, Anti-Atlas Marocain: Caractérisation des fluides minéralisateurs et du gisement. Master's Thesis, Institut National Polytechnique de Lorraine, Nancy, France, 2012.
167. Albinson, T.; Norman, D.I.; Cole, D.; Chomiak, B. Controls on Formation of Low-Sulfidation Epithermal Deposits in Mexico: Constraints from Fluid Inclusion and Stable Isotope Data. In *New Mines and Discoveries in Mexico and Central America*; Society of Economic Geologists: Littleton, CO, USA, 2001; Volume 8, pp. 1–32.
168. Guillou, J.-J.; Monthel, J.; Picot, P.; Pillard, F.; Protas, J.; Samana, J.-C. L'imitérite, Ag_2HgS_2, nouvelle espèce minérale; propriétés et structure cristalline. *Bull. Mineral.* **1985**, *108*, 457–464.
169. Guillou, J.-J.; Monthel, J.; Samama, J.-C.; Tijani, A. Morphologie et chronologie relative des associations minérales du gisement mercuro-argentifère d'Imiter (Anti-Atlas—Maroc). *Notes et Mémoires du Service Géologique du Maroc* **1988**, *44*, 215–228.
170. Levresse, G. Contribution à l'établissement d'un modèle génétique des gisements d'Imiter (Ag-Hg), Bou Madine (Pb-Zn-Cu-Ag-Au), Bou Azzer (Co, Ni, As, Au, Ag) dans l'Anti-Atlas marocain. In *3ème Cycle*; Institut National Polytechnique de Lorraine: Nancy, France, 2001.

171. Baroudi, Z.; Beraaouz, E.H.; Rahimi, A.; Chouhaidi, M.Y. Minéralisations polymétalliques argentifères d'Imiter (Jbel Saghro, Maroc): Minéralogie, évolution des fluides minéralisateurs et mécanismes de dépôt. *Chronique de la Recherche Minière* **1999**, *536–537*, 91–111.
172. Hulin, C.; Dubois, M.; Tuduri, J.; Chauvet, A.; Boulvais, P.; Gaouzi, A.; Mouhajir, M.; Essalhi, M.; Outhounjite, S. New fluid inclusions and oxygen isotope data to constrain a formation model for the Imiter Ag world class deposit (Anti-Atlas, Morocco). In Proceedings of the ECROFI XXII 22nd Biennial Conferences, Antalya, Turkey, 4–9 June 2013; pp. 78–79.
173. Hulin, C.; Dubois, M.; Tuduri, J.; Chauvet, A.; Boulvais, P.; Gaouzi, A.; Mouhajir, M.; Essalhi, M.; Outhounjite, S. A fluid inclusion and stable isotope study of the world class Imiter silver deposit (Morocco). In Proceedings of the 24ème Réunion des Sciences de la Terre, Pau, France, 27–31 October 2014; p. 373.
174. Tuduri, J.; Pourret, O.; Chauvet, A.; Barbanson, L.; Gaouzi, A.; Ennaciri, A. Rare earth elements as proxies of supergene alteration processes from the giant Imiter silver deposit (Morocco). In *Let's Talk Ore Deposits, Proceeding of the Eleventh Biennial SGA Meeting*; Barra, F., Reich, M., Campos, E., Tornos, F., Eds.; Ediciones Universidad Católica del Norte: Antofagasta, Chile, 2011; Volume 2, pp. 826–828.
175. Tuduri, J.; Pourret, O.; Boulvais, P.; Chauvet, A.; Barbanson, L.; Gaouzzi, A.; Hulin, C.; Dubois, M. A reassessment of fluid-mineral relations in the world-class Imiter silver deposit (Anti-Atlas, Morocco). In Proceedings of the SEG 2012 Conference, Lima, Peru, 23–26 September 2012; Society of Economic Geologists: Lima, Peru, 2012.
176. Graybeal, F.T.; Vikre, P. A review of silver-rich mineral deposits and their metallogeny. In *SEG Special Publication: The Challenge of Finding New Mineral Resources: Global Metallogeny, Innovative Exploration, and New Discoveries*; Goldfarb, R.J., Marsh, E.E., Monecke, T., Eds.; Society of Economic Geologists: Littleton, CO, USA, 2010; Volume 15, pp. 85–117.
177. Azizi Samir, M.R.; Ferrandini, J.; Tane, J.L. Tectonique et volcanisme tardi-Pan Africains (580-560 M.a.) dans l'Anti-Atlas Central (Maroc): Interpretation geodynamique a l'echelle du NW de l'Afrique. *J. Afr. Earth Sci.* **1990**, *10*, 549–563. [CrossRef]
178. Ducea, M.N.; Paterson, S.R.; DeCelles, P.G. High-Volume Magmatic Events in Subduction Systems. *Elements* **2015**, *11*, 99–104. [CrossRef]
179. Harrison, R.W.; Yazidi, A.; Benziane, F.; Quick, J.E.; El Fahssi, A.; Stone, B.D.; Yazidi, M.; Saadane, A.; Walsh, G.J.; Aleinikoff, J.N.; et al. Carte géologique au 1/50 000, Feuille Tizgui. *Notes et Mémoires du Service Géologique du Maroc* **2008**, *470*, 131.
180. McQuarrie, N.; Barnes, J.B.; Ehlers, T.A. Geometric, kinematic, and erosional history of the central Andean Plateau, Bolivia (15–17° S). *Tectonics* **2008**, *27*, TC3007. [CrossRef]
181. Till, A.B.; Roeske, S.; Sample, J.C.; Foster, D.A. *Exhumation Associated with Continental Strike-Slip Fault Systems*; The Geological Society of America: Boulder, CO, USA, 2007; Volume 434, p. 264.
182. Willett, S.D.; Brandon, M.T. On steady states in mountain belts. *Geology* **2002**, *30*, 175–178. [CrossRef]
183. Hedenquist, J.W.; Lowenstern, J.B. The role of magmas in the formation of hydrothermal ore deposits. *Nature* **1994**, *370*, 519–527. [CrossRef]
184. Monier, G.; Robert, J.L. Muscovite solid solutions in the system K_2O, MgO, FeO, AL_2O_3, SiO_2, H_2O: An experimental study at 2 kbar P_{H2O} and comparison with natural Li-free white micas. *Mineral. Mag.* **1986**, *50*, 257–266. [CrossRef]
185. Cathelineau, M.; Nieva, D. A chlorite solid solution geothermometer: The Los Azufres (Mexico) geothermal system. *Contrib. Mineral. Petrol.* **1985**, *91*, 235–244. [CrossRef]
186. Kranidiotis, P.; MacLean, W.H. Systematics of chlorite alteration at the Phelps Dodge massive sulfide deposit, Matagami, Quebec. *Econ. Geol.* **1987**, *82*, 1898–1911. [CrossRef]
187. Kretschmar, U.; Scott, S.D. Phase relations involving arsenopyrite in the system Fe-As-S and their application. *Can. Mineral.* **1976**, *14*, 364–386.
188. Sundblad, K.; Zachrisson, E.; Smeds, S.A.; Berglund, S.; Aalinder, C. Sphalerite geobarometry and arsenopyrite geothermometry applied to metamorphosed sulfide ores in the Swedish Caledonides. *Econ. Geol.* **1984**, *79*, 1660–1668. [CrossRef]
189. Lynch, G.; Ortega, J. Hydrothermal alteration and tourmaline-albite equilibria at the Coxheat porphyry Cu-Mo-Au deposit, Nova Scotia. *Can. Mineral.* **1997**, *35*, 79–94.
190. Sillitoe, R.H. Porphyry Copper Systems. *Econ. Geol.* **2010**, *105*, 3–41. [CrossRef]

191. Kouzmanov, K.; Pokrovski, G.S. Hydrothermal controls on metal distribution in porphyry Cu (-Mo-Au) systems. In *Geology and Genesis of Major Copper Deposits and Districts of the World: A Tribute to Richard H. Sillitoe*; Hedenquist, J.W., Harris, M., Camus, F., Eds.; Special Publications of the Society of Economic Geologists: Littleton, CO, USA, 2012; Volume 16, pp. 573–618.
192. Rottier, B.; Kouzmanov, K.; Casanova, V.; Wälle, M.; Fontboté, L. Cyclic Dilution of Magmatic Metal-Rich Hypersaline Fluids by Magmatic Low-Salinity Fluid: A Major Process Generating the Giant Epithermal Polymetallic Deposit of Cerro de Pasco, Peru. *Econ. Geol.* **2018**, *113*, 825–856. [CrossRef]
193. Scott, S.; Driesner, T.; Weis, P. Boiling and condensation of saline geothermal fluids above magmatic intrusions. *Geophys. Res. Lett.* **2017**, *44*, 1696–1705. [CrossRef]
194. Letsch, D.; Large, S.J.E.; Buechi, M.W.; Winkler, W.; von Quadt, A. Ediacaran glaciations of the west African Craton—Evidence from Morocco. *Precambrian Res.* **2018**, *310*, 17–38. [CrossRef]
195. Pinneker, Y.V.; Lomonosov, I.S. Concentrated brines of Siberian Platform and their counterparts in Asia, Europe, Africa and America. *Int. Geol. Rev.* **1968**, *10*, 431–442. [CrossRef]
196. Richard, A.; Pettke, T.; Cathelineau, M.; Boiron, M.-C.; Mercadier, J.; Cuney, M.; Derome, D. Brine–rock interaction in the Athabasca basement (McArthur River U deposit, Canada): Consequences for fluid chemistry and uranium uptake. *Terra Nova* **2010**, *22*, 303–308. [CrossRef]
197. Linnemann, U.; Pidal, A.P.; Hofmann, M.; Drost, K.; Quesada, C.; Gerdes, A.; Marko, L.; Gärtner, A.; Zieger, J.; Ulrich, J.; et al. A ~565 Ma old glaciation in the Ediacaran of peri-Gondwanan West Africa. *Int. J. Earth Sci.* **2018**, *107*, 885–911. [CrossRef]
198. Vernhet, E.; Youbi, N.; Chellai, E.H.; Villeneuve, M.; El Archi, A. The Bou-Azzer glaciation: Evidence for an Ediacaran glaciation on the West African Craton (Anti-Atlas, Morocco). *Precambrian Res.* **2012**, 196–197. [CrossRef]
199. Starinsky, A.; Katz, A. The formation of natural cryogenic brines. *Geochim. Cosmochim. Acta* **2003**, *67*, 1475–1484. [CrossRef]
200. Toner, J.D.; Catling, D.C.; Sletten, R.S. The geochemistry of Don Juan Pond: Evidence for a deep groundwater flow system in Wright Valley, Antarctica. *Earth Planet. Sci. Lett.* **2017**, *474*, 190–197. [CrossRef]
201. Belkacim, S.; Ikenne, M.; Souhassou, M.; Elbasbas, A.; Toummite, A. The Cu-Mo±Au mineralizations associated to the High-K calc-alkaline granitoids from Tifnoute valley (Siroua massif, anti-atlas, Morocco): An arc-Type porphyry in the late neoproterozoic series. *J. Environ. Earth Sci.* **2014**, *4*, 90–106.
202. Loiselet, C.; Husson, L.; Braun, J. From longitudinal slab curvature to slab rheology. *Geology* **2009**, *37*, 747–750. [CrossRef]
203. Manea, V.C.; Pérez-Gussinyé, M.; Manea, M. Chilean flat slab subduction controlled by overriding plate thickness and trench rollback. *Geology* **2012**, *40*, 35–38. [CrossRef]
204. Merdith, A.S.; Collins, A.S.; Williams, S.E.; Pisarevsky, S.; Foden, J.D.; Archibald, D.B.; Blades, M.L.; Alessio, B.L.; Armistead, S.; Plavsa, D.; et al. A full-plate global reconstruction of the Neoproterozoic. *Gondwana Res.* **2017**, *50*, 84–134. [CrossRef]
205. Boyden, J.A.; Müller, R.D.; Gurnis, M.; Torsvik, T.H.; Clark, J.A.; Turner, M.; Ivey-Law, H.; Watson, R.J.; Cannon, J.S. Next-generation plate-tectonic reconstructions using GPlates. In *Geoinformatics: Cyberinfrastructure for the Solid Earth Sciences*; Keller, G.R., Baru, C., Eds.; Cambridge University Press: Cambridge, UK, 2011; pp. 95–113.
206. Domeier, M. A plate tectonic scenario for the Iapetus and Rheic oceans. *Gondwana Res.* **2016**, *36*, 275–295. [CrossRef]
207. Torsvik, T.H.; Cocks, L.R.M. Gondwana from top to base in space and time. *Gondwana Res.* **2013**, *24*, 999–1030. [CrossRef]
208. Richards, J.P. Postsubduction porphyry Cu-Au and epithermal Au deposits: Products of remelting of subduction-modified lithosphere. *Geology* **2009**, *37*, 247–250. [CrossRef]
209. Richards, J.P. Magmatic to hydrothermal metal fluxes in convergent and collided margins. *Ore Geol. Rev.* **2011**, *40*, 1–26. [CrossRef]
210. Sillitoe, R.H.; Hedenquist, J.W. Linkages between volcanotectonic settings, ore-fluid compositions and epithermal precious metal deposits. In *Volcanic, Geothermal and Ore-Forming Fluids; Rulers and Witnesses of Processes within the Earth*; Simmons, S.F., Graham, I., Eds.; Society of Economic Geologist Special Publication: Littleton, CO, USA, 2003; Volume 10, pp. 315–343.

211. Tosdal, R.; Richards, J. Magmatic and structural controls on the development of porphyry Cu±Mo±Au deposits. *Rev. Econ. Geol.* **2001**, *14*, 157–181.
212. Menant, A.; Jolivet, L.; Tuduri, J.; Loiselet, C.; Bertrand, G.; Guillou-Frottier, L. 3D subduction dynamics: A first-order parameter of the transition from copper- to gold-rich deposits in the eastern Mediterranean region. *Ore Geol. Rev.* **2018**, *94*, 118–135. [CrossRef]
213. Bryan, S.E.; Orozco-Esquivel, T.; Ferrari, L.; López-Martínez, M. Pulling apart the Mid to Late Cenozoic magmatic record of the Gulf of California: Is there a Comondú Arc? *Geol. Soc. Lond. Spec. Publ.* **2013**, *385*. [CrossRef]
214. Thorkelson, D.J.; Breitsprecher, K. Partial melting of slab window margins: Genesis of adakitic and non-adakitic magmas. *Lithos* **2005**, *79*, 25–41. [CrossRef]
215. de Silva, S. Arc magmatism, calderas, and supervolcanoes. *Geology* **2008**, *36*, 671–672. [CrossRef]
216. Chauvet, A.; Alves Da Silva, F.C.; Faure, M.; Guerrot, C. Structural evolution of the Paleoproterozoic Rio Itapicuru granite-greenstone belt (Bahia, Brazil): The role of synkinematic plutons in the regional tectonics. *Precambrian Res.* **1997**, *84*, 139–162. [CrossRef]
217. Hickman, A.H. Two contrasting granite-greenstone terranes in the Pilbara Craton, Australia: Evidence for vertical and horizontal tectonic regimes prior to 2900 Ma. *Precambrian Res.* **2004**, *131*, 153–172. [CrossRef]
218. Van Kranendonk, M.J.; Collins, W.J.; Hickman, A.; Pawley, M.J. Critical tests of vertical vs. horizontal tectonic models for the Archaean East Pilbara Granite-Greenstone Terrane, Pilbara Craton, Western Australia. *Precambrian Res.* **2004**, *131*, 173–211. [CrossRef]
219. Nance, R.D.; Murphy, J.B.; Strachan, R.A.; Keppie, J.D.; Gutiérrez-Alonso, G.; Fernández-Suárez, J.; Quesada, C.; Linnemann, U.; D'lemos, R.; Pisarevsky, S.A. Neoproterozoic-early Palaeozoic tectonostratigraphy and palaeogeography of the peri-Gondwanan terranes: Amazonian v. West African connections. *Geol. Soc. Lond. Spec. Publ.* **2008**, *297*, 345–383. [CrossRef]